EFFECT OF FORGING PRESSURE ON THE MICROSTRUCTURE OF LINEAR FRICTION WELDED INCONEL 738 SUPERALLOY

By

MARK YAO AMEGADZIE

A thesis submitted to the Faculty of Graduate Studies of

The University of Manitoba

in partial fulfillment of the requirements for the degree of

Master of Science

Department of Mechanical and Manufacturing Engineering

University of Manitoba

Winnipeg

ACKNOLEDGEMENTS

I would like to thank my supervisor Dr. M. C. Chaturvedi for providing me with this privilege to work on an interesting project as this. I am also grateful for his indomitable contributions to making this research a success. I am grateful to my co-supervisor Dr. O. A. Ojo, for his timely guidance, consistent intellectual contributions and close supervision throughout my program.

I am grateful to NSERC for financial support. I appreciate the technical assistance of M. Guerin and E. Daalgard of the Aerospace Manufacturing Technology Centre of the Institute for Aerospace Research, National Research Council (NRC), Montréal, Canada. I am grateful to Mike Boswick for his technical assistance. I will like to thank my colleagues and friends – Richard Buckson, Lawrence Osoba, Oyedele Ola Temitope, Kwadwo Owusu Poku, Jonathan Mawuli Tsikata and Nana Baafour Kwakye for their support in diverse ways. I am also grateful to my parents for bringing me up in a modest manner.

I give my greatest and profound gratitude to God for life, good health, wisdom and understanding.

ABSTRACT

Inconel 738, which is a nickel base superalloy used for hot section components of aircraft and industrial turbines is difficult to fabricate and repair by fusion welding due to its susceptibility to heat affected zone (HAZ) intergranular cracking. Crack-free joining of the difficult-to-weld alloy is currently achieved by using linear friction welding (LFW). Nevertheless, oxidation along the joint during LFW is a major problem. Information about the effect of process parameters on the microstructural evolution of linear friction welded nickel base alloys is very limited. In this work, the effect of forging pressure on the microstructure of linear friction welded Inconel 738 was studied. The results as elucidated in this work showed that increased forging pressure caused strain-induced rapid solidification of metastable liquid, which resulted in complete elimination of deleterious liquid phase oxides in bonded material contrasting the generally accepted view that assumes extrusion of solid state oxides during LFW.

Table of Contents

List of Tables

List of Figures

Copyright Permissions

Figure 2-1: Source – "Welding Metallurgy" (2nd Edition) Reprinted with permission from the Global Rights Department, John Wiley & Sons, Inc. (April 30, 2012)

Figure 2-2: Source – "Welding Metallurgy" (2nd Edition) Reprinted with permission from the Global Rights Department, John Wiley & Sons, Inc. (April 30, 2012)

Figure 2-3: Source – "Welding Metallurgy" (2nd Edition) Reprinted with permission from the Global Rights Department, John Wiley & Sons, Inc. (April 30, 2012)

Figure 2-4: Source – "Welding Metallurgy" (2nd Edition) Reprinted with permission from the Global Rights Department, John Wiley & Sons, Inc. (April 30, 2012)

Figure 2-5: Source – "Welding Metallurgy" (2nd Edition) Reprinted with permission from the Global Rights Department, John Wiley & Sons, Inc. (April 30, 2012)

Figure 2-6: Source – "Welding Metallurgy" (2nd Edition) Reprinted with permission from the Global Rights Department, John Wiley & Sons, Inc. (April 30, 2012)

Figure 2-7: Source – "Welding Metallurgy" (2nd Edition) Reprinted with permission from the Global Rights Department, John Wiley & Sons, Inc. (April 30, 2012)

Figure 2-8: Source – "Welding Metallurgy" (2nd Edition) Reprinted with permission from the Global Rights Department, John Wiley & Sons, Inc. (April 30, 2012)

Figure 2-9: Source – "Welding Metallurgy" (2nd Edition) Reprinted with permission from the Global Rights Department, John Wiley & Sons, Inc. (April 30, 2012)

Figure 2-10: Source – "Welding Metallurgy" (2nd Edition) Reprinted with permission from the Global Rights Department, John Wiley & Sons, Inc. (April 30, 2012)

Figure 2-11: Source – Welding Journal. Reprinted with permission.

Figure 2-12: Source – Welding Journal. Reprinted with permission.

Figure 2-14: Source – Welding Journal. Reprinted with permission (July 06, 2012).

Figure 2-15: Source – "Robotic Friction Stir Welding" Reprinted with permission from Emerald Group Publishing Limited (April 20, 2012).

Figure 2-17: Source – Mater. Sci. and Eng. A. Reprinted with permission from Elsevier (April 17, 2012).

Figure 2-18: Source – "Industrial Robot-An International Journal" Reprinted with permission from Emerald Group Publishing Limited (April 20, 2012).

Chapter 1

Introduction

Superalloys remain crucial in high temperature applications because they possess desirable properties which make them useful at elevated temperatures. Generally, superalloys are classified into three main groups; namely Cobalt, Nickel and Iron base superalloys. IN 738 is a nickel base superalloy that derives its strength mainly from the precipitation of the ordered intermetallic Ni_3(Al, Ti), γ' phase. IN 738 is used in the manufacture of hot section components in aero and land based gas turbine engines due to their high temperature strength and hot corrosion resistance. The operating environment of service components made from IN 738 in gas turbine engines is extremely hostile, and this can lead to degradation of the components. When the components are damaged, they are either repaired or replaced.

It is prudent to repair service damaged components than replace them since the cost of repair is relatively lower than the cost of replacement. Welding has proven to be an economical way of joining which is used in the fabrication and repair of these components. IN 738 which contains a substantial amount of Al and Ti (> 6wt %) is difficult to weld by conventional methods due to its propensity to heat affected zone (HAZ) intergranular cracking. The cause of this type of cracking is attributed to liquation of second phase particles, subsequent wetting of the grain boundaries by liquid and eventually de-cohesion along one of the solid-liquid interfaces under the influence of on-cooling tensile stresses [2, 3]. In the quest to achieve crack free welding of IN 738, linear friction welding, which was presumed to be a solid state process with the potential for

joining aerospace components, was used to produce welds of nickel base alloys devoid of cracks [4-7]. Linear friction welding is a self-regulating process that uses heat generated by the reciprocating motion of two parts against each other in plasticizing and subsequently joining them under the influence of an axial compressive forging force during the last stage of the process. The weld joint integrity of most linear friction welds is significantly affected by the welding parameters used which include; the forge pressure, amplitude and frequency. The prospects for joining nickel base alloys with this new technology is promising but there is limited information available on the effect of welding parameters on microstructural changes induced during the linear friction welding process. This research was initiated to study the effect of forge pressure on the microstructure of linear friction welded IN 738.

Optical, scanning electron and electron probe microscopy techniques were used to study the microstructure of the pre-weld, welded and Gleeble simulated samples. Mechanical testing was also performed by taking hardness measurements across the weld joint regions. The results of this work showed that increased forging pressure resulted in a reduction in the amount of re-solidified γ-γ' eutectic products, which could detrimentally affect the mechanical properties of the material. Similarly, increased forging pressure resulted in the reduction of deleterious oxides along the weld line that could jeopardize the weld integrity of the linear friction welded specimens. Information obtained from this research will be useful in optimizing the forge pressure during the linear friction welding process to produce weld joints with desirable mechanical properties.

Chapter 2

Literature Review

2.1 Introduction

In this chapter, the physical metallurgy of IN 738 will be discussed. This will be followed by a discussion on the effect of alloying elements on the microstructure of IN 738. Subsequent to this, will be a discussion on conventional fusion welding processes and the defects associated with them. Cracking due to occurrence of liquation during conventional welding processes will also be discussed, and a discussion on friction welding processes will be presented.

2.2 Physical Metallurgy of IN 738

Inconel 738 is a nickel base superalloy strengthened through both solid solution and precipitation hardening. It possesses excellent creep-rupture strength and hot corrosion resistance at high temperatures. Inconel 738 consists of an fcc (face centered cubic) austenitic solid solution matrix, usually referred to as gamma phase, with an intermetallic phase called gamma prime embedded in it [9]. IN 738 derives its strength from the precipitation of the ordered $L1_2$ intermetallic (gamma prime phase). Two types of the alloy exist; the high carbon version, normally designated as IN 738C, and the low carbon version designated as IN 738LC. The high carbon version (IN 738C) contains about 0.15-0.20 wt% of carbon while the low carbon version (IN 738LC) contains carbon in the range of 0.09-0.13wt% [10]. IN 738LC also contains a lower zirconium content which improves its castability. In order to prevent micropores from forming during ingot

solidification, hot isostatic pressure, which involves the application of isostatic pressure, is applied in an inert (argon) atmosphere at high temperature. The alloy is subjected to a standard solution heat treatment (SHT) at 1120^{o}C for 2 hours and air cooled. This is followed directly by a standard aging treatment at 845^{o}C for 24 hours, and then air cooled. The melting range of IN 738 is between 1230^{o}C and 1315^{o}C whereas its density is 8.11 gm/cm^{3}.

2.2.1 Microstructure of Cast IN 738

The microstructure of IN 738LC consists of microconstituents embedded in the austenitic gamma matrix. These microconstituents include; MC carbides, sulphocarbides, borides, gamma prime phase and other solidification microconstituents. A discussion on these microconstituents and the gamma matrix is presented next.

2.2.1.1 The Gamma Matrix

This is a continuous phase of nickel base austenite which contains a significant amount of solid solution strengtheners such as chromium, molybdenum, tungsten, cobalt, iron, titanium, and aluminium [11]. These solid solution strengtheners differ from nickel by 1 to 13% in atomic diameter. Tungsten, molybdenum, and chromium are strong solution strengtheners whereas titanium, aluminium and cobalt are considered weak solid solution strengtheners [12]. Aluminium, in addition to being a precipitation strengthener, is a potent solid solution strengthener. High temperature creep is dominant at 0.6Tm (Tm is melting temperature of the alloy) where creep strength of the gamma matrix is diffusion dependent. Slow diffusing elements such as molybdenum and tungsten are effective in

reducing high temperature strength. Cobalt makes cross slip more difficult by decreasing the stacking fault energy which causes the dissociation of dislocations into partial dislocations [11]. The high tolerance of nickel for alloying elements without phase instability makes the alloy resistant to severe high temperatures due to the nearly filled third electron shell. Cr when added in a particular minimum amount will form protective Cr_2O_3 scales having low cation vacancy content which barricades the diffusion of metallic elements outward, and restricts the diffusion of oxygen, nitrogen, sulphur and harmful elements inward. Table 2-1 shows the proportion by weight % of alloying elements added to IN 738C and IN 738LC.

2.2.1.2 The Gamma Prime (γ') Phase

This is a unique intermetallic phase that can be precipitated in austenitic nickel superalloys by precipitation-hardening heat treatments [11]. The γ' phase is the principal high-temperature strengthening phase of the alloy. The γ' formed in IN 738 is of the type A_3B where A is predominantly nickel and B, aluminium and titanium. It is represented as Ni_3(Al, Ti). The composition of γ' in IN 738 has been suggested to be [13].

$$(Ni_{.922}Co_{.058}Cr_{.017}Mo_{.002}W_{.002})\ (Al_{.518}Ti_{.352}Ta_{.046}Nb_{.410}W_{.014}Cr_{.020})$$

IN 738 is strengthened through resistance offered to dislocation movement by γ' precipitates in the alloy. The morphology of γ' is determined by the lattice mismatch between the γ and γ'. They occur as spheres at 0-0.2% lattice mismatch, as cubes at mismatches of 0.5-1.0%, and plates at mismatches above 1.25%.

Table 2-1: Nominal composition of cast IN 738C and IN 738LC

Element	IN 738LC (wt %)	IN 738C (wt %)
Carbon	0.11	0.17
Cobalt	8.5	8.5
Chromium	16.00	16.00
Molybdenum	1.75	1.75
Tungsten	2.60	2.60
Tantalum	1.75	1.75
Niobium	0.90	0.90
Aluminium	3.40	3.40
Titanium	3.40	3.40
Boron	0.01	0.01
Zirconium	0.05	0.1
Iron	LAP	LAP
Manganese	LAP	LAP
Silicon	LAP	LAP
Sulphur	LAP	LAP
Nickel	Balance (61)	Balance (61)

LAP means low as possible.

The long range order exhibited by γ' is responsible for the formation of anti-phase boundary (APB) faults by the passage of dislocation through it. This results in APB strengthening by dislocation- γ' precipitate interaction anytime the alloy is strained under shear.

2.2.1.3 Carbides

Carbides generally form at grain boundaries in nickel alloys. The common carbides peculiar to IN 738 include MC and $M_{23}C_6$ carbides. Carbides form when the carbon content in the alloy exceeds 0.05% [13]. MC carbides have the general formula MC, where "M" represents metallic elements such as titanium, tantalum, niobium, or tungsten. MC carbides are stable carbides that form below the temperature where solidification begins. Their tendency to dissolve in the solid phase during solution heat treatment is low. MC carbides occur as irregular discontinuous blocky particles, despite that plate-like and regular types have been observed [12]. They are heterogeneously distributed throughout the alloy in-between and within grains, with much prevalence in the interdendritic regions with almost no orientation in the alloy. MC carbides are formed from the reaction of carbon with titanium, tantalum and niobium. Other reactions between some alloying elements and carbon in IN 738 can result in producing other types of carbides typically $M_{23}C_6$ and M_6C carbides.

In $M_{23}C_6$, M usually represents chromium but this element can be replaced by tungsten, molybdenum, or cobalt. They form during heat treatments and in service within the temperature range of 760^{o}C to 980^{o}C. These carbides can form either from the

degeneration of MC carbides or from soluble carbon in the alloy matrix. $M_{23}C_6$ carbides are dominantly believed to be formed by the following reaction:

$$MC + \gamma \longrightarrow M_{23}C_6 + \gamma' \ldots\ldots\ldots\ldots\ldots\ldots\ldots\ldots\ldots (1)$$

$M_{23}C_6$ carbides are usually located on the grain boundaries where they provide the beneficial effect of inhibiting grain boundary sliding. Similarly, the gamma prime generated by reaction (1) engloves the carbides and the grain boundary in a relatively, creep resistant layer. On the other hand, gamma prime particles located on the grain boundaries can play a key role in blocking the growth of $M_{23}C_6$ cells. Cellular $M_{23}C_6$ can de-cohere at their interface or fracture thereby initiating fracture which eventually leads to rupture failure. The formation of $M_{23}C_6$ depletes chromium from the matrix. This increases the solubility of gamma prime near the grain boundary normally characterized by leaving denuded zones.

M_6C carbides are similar to $M_{23}C_6$ carbides but form at temperatures in the range of 815^{o}C to 980^{o}C when the molybdenum and tungsten contents of the base alloy are high, in excess of about 6 to 8%. They have a complex cubic structure. M_6C carbides can be formed by the reaction of MC carbides with the matrix as illustrated in the equation below:

$$MC + \gamma \longrightarrow M_6C + \gamma' \ldots\ldots\ldots\ldots\ldots\ldots\ldots\ldots\ldots (2)$$

Carbides can degrade the mechanical properties of the alloy when they precipitate as continuous grain-boundary films. They may also render the alloy unstable during service by tying up essential elements that would otherwise promote stability of the alloy.

2.2.1.4 Gamma-Gamma Prime (γ- γ') Eutectic

The γ- γ' eutectic forms at temperatures approaching the equilibrium solidus of the alloy where continuous solute enrichment occurs due to supersaturation of interdendritic liquid with γ' forming elements. The γ- γ' eutectic reaction temperature in IN 738 has been reported to occur towards the end of solidification at about 1198^{o}C [20] and 1230^{o}C [21]. Rosenthal et al have observed the γ- γ' eutectic reaction to have occurred over a range of temperatures [22].

2.2.1.5 Borides and Sulphocarbides

Borides are hard refractory particles located at grain boundaries with shapes varying from blocky to "half moon" in appearance. The concentration of boron varies from 50-500ppm and it has a tendency to segregate at the grain boundaries and act as a grain boundary strengthener during creep deformation. Borides are beneficial as they block the onset of grain boundary tearing under creep rupture loading. The types of borides observed in superalloys are of the form M_3B_2, with a tetragonal unit cell [14]. Zhang et al have also discovered another type of boride of the form M_5B_3 that formed in superalloys [15]. Sulphur is generally present in trace elements in superalloys. However, sulphur has been ascertained to severely segregate to grain boundaries in superalloys [16]. Elements such as Ti, Zr, Nb, Hf, and La which have low solubilities in the γ matrix but high affinity for sulphur tie up sulphur by forming several sulphur-rich intermetallic phases referred to as sulphocarbides [17]. Other researchers have also identified borides and sulphocarbides in IN 738. Ojo et al identified some intermetallic phases near the γ- γ' eutectic phase which they called terminal solidification products. These boride phases were identified through

EDS analysis to be Cr-Mo rich particles, Ni-Ti rich particles and Ni-Zr rich particles [17]. Similarly, Hoffelner et al, by x-ray diffraction analysis, identified M_3B_2 type and M_2SC sulphocarbides in IN 738 after a series of heat treatments [18].

2.3 Welding Processes

Welding can be defined as a process for joining metals and other materials by means of heat, pressure or both, with or without a filler metal to produce a joint through fusion or re-crystallization across the interface [30]. Welding is categorized into two groups. They are fusion welding and solid state welding processes. Fusion welding refers to welding processes that use a filler metal to achieve coalescence without applying pressure. Some examples of fusion welding processes include oxyacetylene welding, Gas Tungsten Arc Welding (GTAW), Submerged Arc Welding, Resistance Welding (RW), Electron Beam Welding (EBW) and Laser Welding. On the other hand, solid state welding refers to welding processes that do not involve melting of material at the joint, and coalescence of parts achieved through the application of pressure alone or pressure and heat. Examples of solid state joining processes include friction welding and diffusion bonding processes. A discussion on conventional fusion welding is presented next.

2.3.1 Shielded Metal Arc Welding

Shielded Metal Arc Welding (SMAW) is a process which melts and joins metals by heating the parts to be joined with an arc between a coated metal electrode and the work piece. The electrode used is sometimes coated with a flux that assists in creating the arc and also providing the shielding gas and slag covering that protects the weld from

contamination (figure 2-1).The electrode core contains the filler metal that is deposited in the form of beads during welding. The type of current (alternating current, AC or direct current, DC) used during this process is dependent on the type of electrode. The power employed during welding is measured practically in terms of current. The amperage needed to weld depends on the electrode diameter, the size and thickness of the pieces to be welded, and the position of the welding. Welding in the horizontal or flat position is preferred to welding in the vertical or overhead position. Generally optimum weld results are achieved by maintaining a short arc, moving the electrode at a uniform speed, and feeding the electrode downwards at a constant speed as it melts.

2.3.2 Oxyacetylene Welding

Oxyacetylene welding is a versatile gas welding process that uses a flame generated by a reaction between a fuel gas and oxygen to melt and join metals. The oxyacetylene flame burns at about $3316^{o}C$, and is the only flame that is hot enough to melt almost all commercial metals. Due to high heat input in oxyacetylene welding, the heat affected zone produced is quite large coupled with a relatively high distortion. The cost of the equipment is relatively cheaper than other types of welding processes. Since there is limited power protection, oxyacetylene welding is not suitable for welding reactive metals such as zirconium and titanium. Oxyacetylene welding can be performed with or without the use of a filler metal. Figure 2-2 is a schematic diagram showing the oxyacetylene welding process.

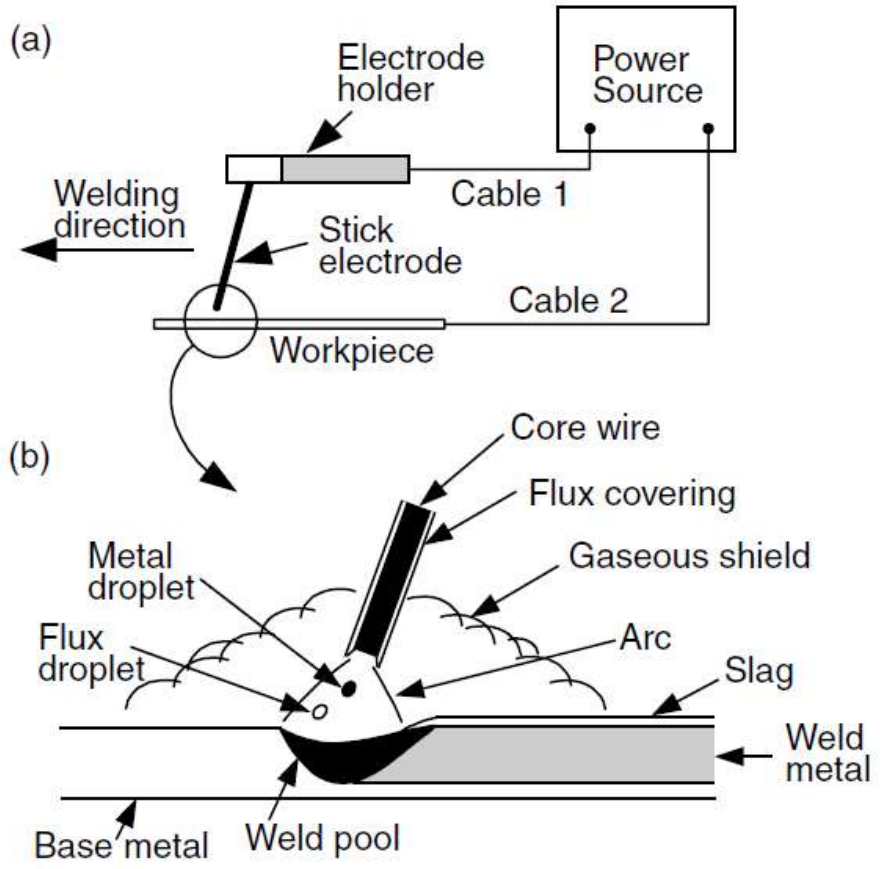

Figure 2-1: Shielded metal arc welding: a) overall process, b) welding area enlarged.

Source: "Welding Metallurgy" (2nd Ed) by Sindo Kuo [115]. Reprinted with permission from the Global Rights Departmeunt, John Wiley & Sons, Inc. (April 30, 2012)

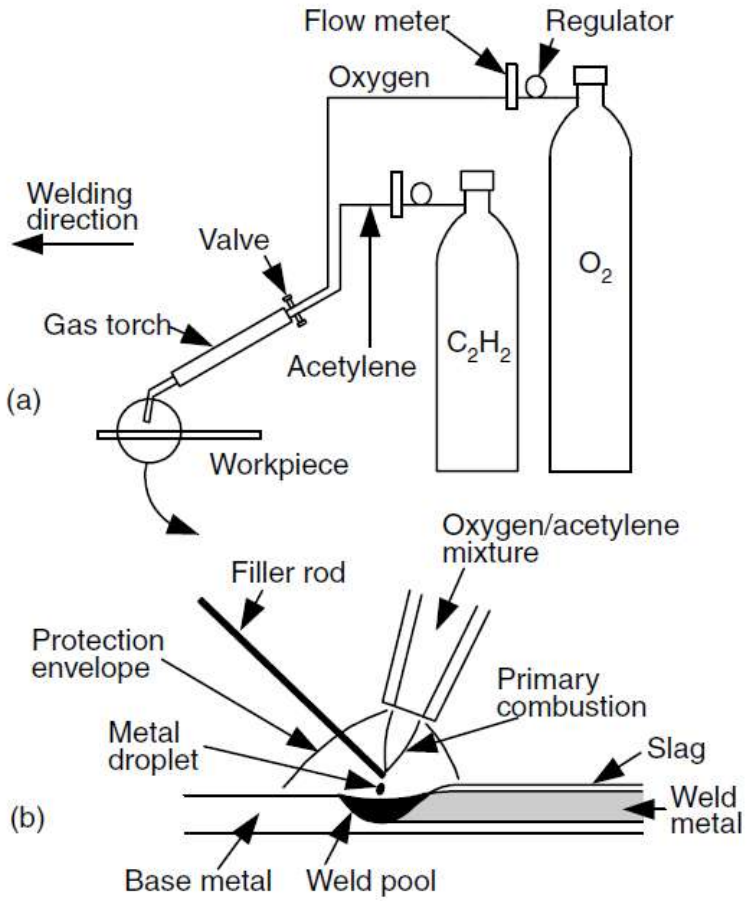

Figure 2-2: Oxyacetylene welding: a) overall process, b) welding area enlarged.

Source: "Welding Metallurgy" (2nd Ed) by Sindo Kuo [115]. Reprinted with permission from the Global Rights Department, John Wiley & Sons, Inc. (April 30, 2012)

2.3.3 Gas Tungsten Arc Welding (GTAW)

Gas tungsten arc welding process is also known as the tungsten inert gas (TIG) welding process. TIG welding is an arc welding process that produces an arc between a non-consumable electrode and the part to be welded. The molten weld metal, tungsten electrode, and the heat affected zone are shielded from atmospheric contamination by a blanket of inert gas fed through the GTAW torch. Argon, a chemically inactive gas is used during this welding process. In addition, the inert gas used is usually odourless and transparent thus providing maximum visibility of the arc to the welder. Hydrogen gas is sometimes added to enhance the maximum speed. The TIG process can produce temperatures up to 1927^{o}C. A filler metal may be added manually if required. No sputter or slag is produced during the process as this helps to produce sound welds. Figure 2-3 is a diagram illustrating the TIG process. The concentrated arc produced, permits pin point control of heat input to the work piece which usually results in a narrow heat affected zone. GTAW is used to weld stainless steel, nickel alloys such as Monel and Inconel, titanium, aluminium, magnesium, copper, brass, bronze and even gold. GTAW is also used to weld dissimilar metals to one another such as copper to brass and stainless to mild steel.

2.3.4 Submerged Arc Welding

In 1936, Union Carbide commercially introduced the submerged arc welding process under the name Unionmelt Welding. The process was developed to produce longitudinal welds on line pipe for gas transportation, but soon saw use in the manufacture of ships

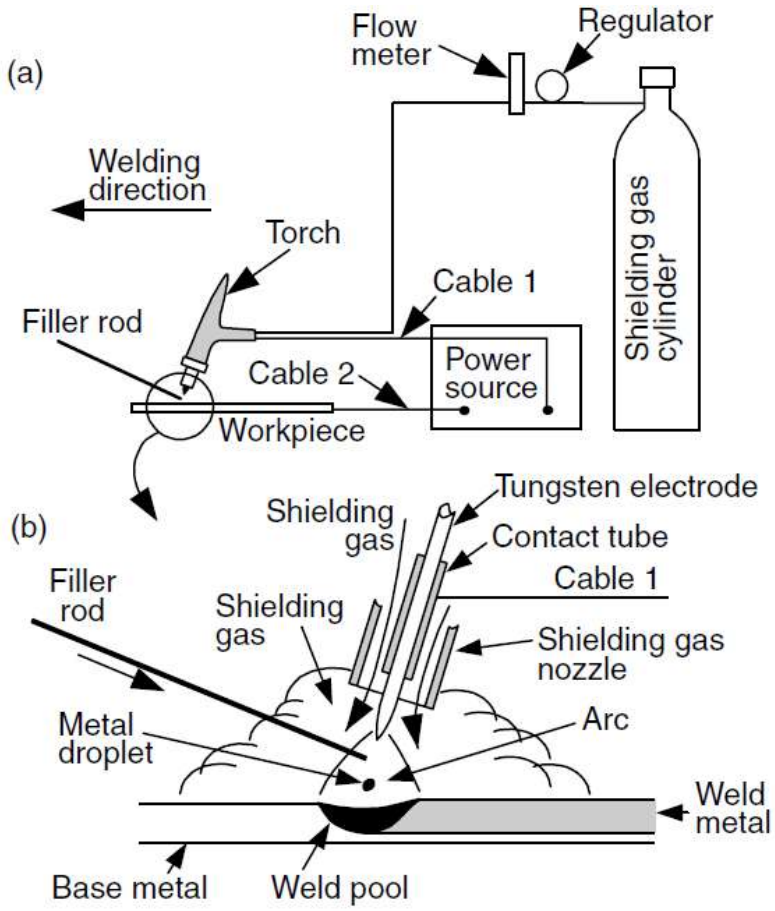

Figure 2-3: Gas tungsten arc welding: a) overall process, b) welding area enlarged.

Source: "Welding Metallurgy" (2nd Ed) by Sindo Kuo [115]. Reprinted with permission from the Global Rights Department, John Wiley & Sons, Inc. (April 30, 2012)

and other military applications [23]. Submerged arc welding process is also referred to as Sub Arc Welding (SAW). Submerged arc welding achieves coalescence of metals by heating the work pieces with an arc between a bare metal electrode and the work. Heat during submerged arc welding is produced when an electric current is passed in-between the welding wire and the work piece. The tip of the welding wire, arc, and weld joint are covered by a layer of granular flux. The heat generated by the arc melts the wire, the base metal and the flux. The flux shields the molten pool from atmospheric contamination, cleans impurities from the weld metal, and shapes the weld bead. Figure 2-4 shows a schematic of the SAW process. As already mentioned, the welding zone is completely covered by a blanket of granular flux such that the arc becomes invisible to the welder. This precludes the use of an eye shield during welding. The filler metal used during welding may be obtained from the electrode or from a supplemental source. The deepest penetration in a single pass of the electrode is about 1 ½ inches. Submerged arc welding process lends itself to automation as this improves productivity in most cases.

2.3.5 Gas Metal Arc Welding (GMAW)

This welding process is also referred to as Metal Inert Gas (MIG) Welding process. GMAW is a welding process that achieves coalescence of metals by heating them to their melting point with an electric arc. The arc produced is shielded from the atmosphere between a continuous, consumable electrode wire and the metal being welded. A constant voltage, direct current power source is most commonly used with GMAW. Meanwhile, constant current systems, as well as alternating current can be used. This process was originally developed for welding aluminium and other non-ferrous materials in the 1940s.

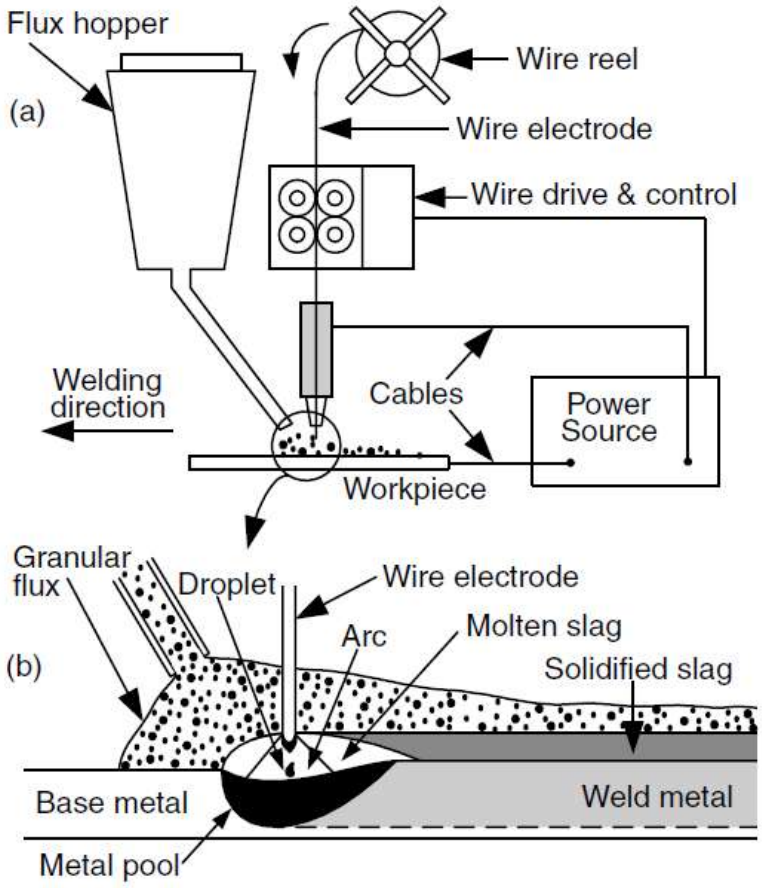

Figure 2-4: Submerged arc welding: a) overall process, b) welding area enlarged.

Source: "Welding Metallurgy" (2nd Ed) by Sindo Kuo [115]. Reprinted with permission from the Global Rights Department, John Wiley & Sons, Inc. (April 30, 2012)

However, GMAW was soon applied to steels because it reduced welding time per comparison to other welding processes. GMAW is a relatively fast process due to the continuous feed electrode supply that is used. GMAW is the most common industrial welding process, preferred for its versatility, speed and the relative ease with which it can be subjected to robotic automation. There is less distortion during welding because of the higher arc travel speeds during welding. The equipment used for this process is relatively sophisticated compared to other welding processes (figure 2-5).

2.3.6 Arc Spot Welding

This process uses the same equipment as that used in for Gas Metal Arc Welding. However, an automatic control system has been added to the Arc Spot Welding process. The function of the control system is to regulate the "arc on" time and the "arc of" time in cycles. It also controls the wire stick out or burn-back of the filler wire as the arc is extinguished. One beneficial effect of the control unit is that it removes the majority of human error encountered during the welding operation, hence duplicates the weld characteristics consistently [24]. Arc spot welding is used to join sheet material or plate up to ½ inch thick without having to drill or perform other costly operations. Furthermore, thin materials can be welded to heavy plates, or heavy plates to thin materials with minimum problems. Plasma arc welding (PAW) achieves coalescence through melting and joining metals by heating them with a constricted arc established between electrode and the metals. PAW is also similar to GTAW, but an orifice as well as shielding gas is used. The sonic speed of the gas as it passes through the constricted

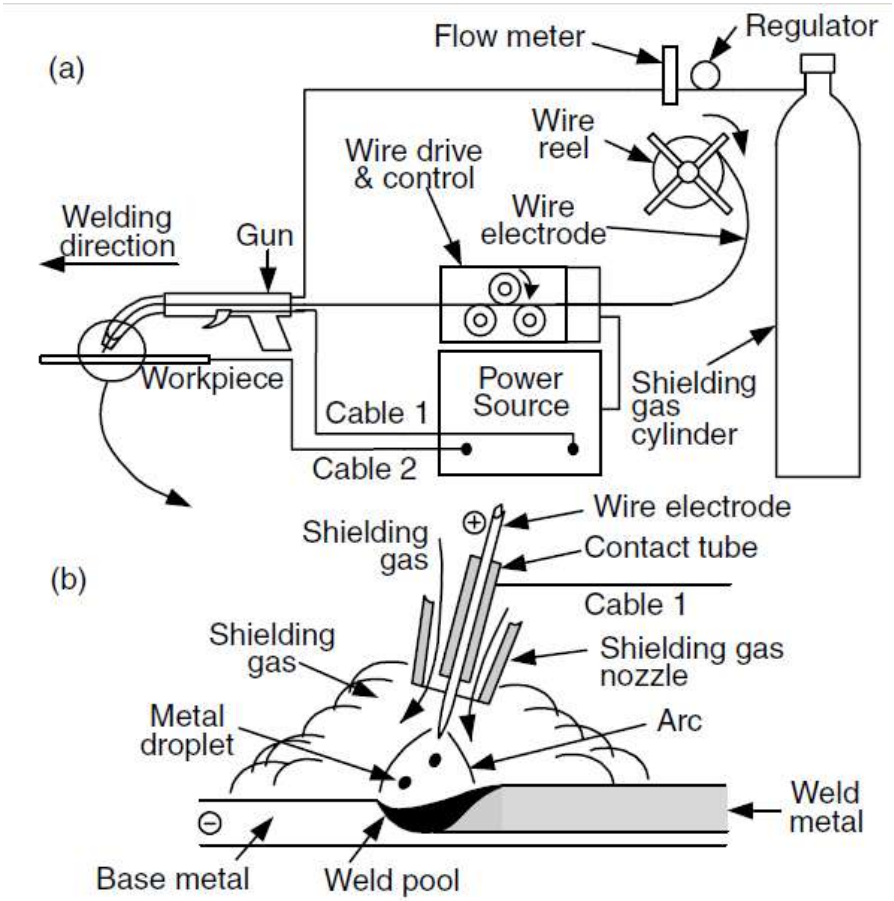

Figure 2-5: Gas metal arc welding: a) overall process, b) welding area enlarged.

Source: "Welding Metallurgy" (2nd Ed) by Sindo Kuo [115]. Reprinted with permission from the Global Rights Department, John Wiley & Sons, Inc. (April 30, 2012)

orifice generates temperatures of about 17000^{o}C. A less constricted slow moving cool gas provides shielding to the arc and the molten metal. In most cases, argon is used as the plasma, and helium is used as the shielding gas. In some cases argon is used for both the plasma and the shielding gas. The plasma arc welding process can be used to weld most metals and their alloys. Initial cost of the equipment is high but may be compensated for by the high arc temperatures that permit fast travel speeds thereby reducing the cost per weld. Moreover, with proper combinations of welding current, orifice gas flow and travel speed, render the possibility of making a keyhole. Keyholing signifies full penetration and it permits the use of remarkably higher welding speeds [115]. Figure 2-6 shows a diagram of the plasma arc welding process.

2.3.7 Electron Beam Welding

Electron beam welding is a welding process that achieves coalescence by bombarding the joint with an intense beam of high-voltage electrons to melt and join the work pieces to be welded. The cathode of the electron gun consists of a negatively charged filament, which, when heated up to its thermionic temperature emits electrons (figure 2-7a). The electrons are accelerated by the electric field between a negatively bias electrode and the anode. As the electrons pass through the keyhole in the anode, they are focused by an electromagnetic coil to a point at the surface of the material to be welded. The accelerating voltage and beam current usually employed during this process vary over ranges of 30-175kV and 50-1000mA, respectively. A very high intensity electron beam can vapourize the metal and form a vapour hole, that is, the keyhole as shown in figure

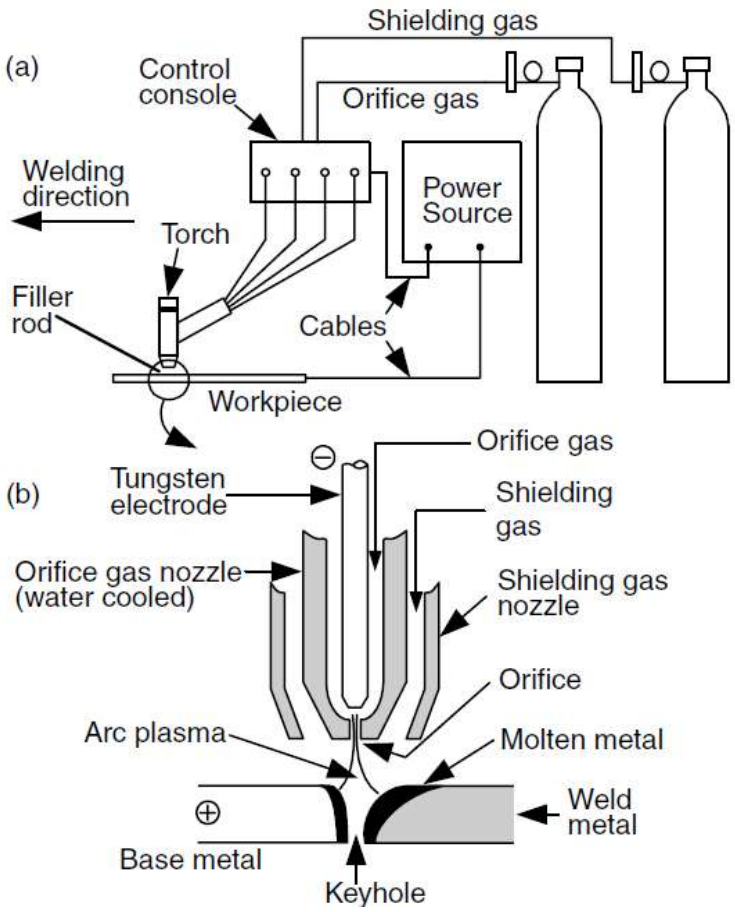

Figure 2-6: Plasma arc welding: (a) overall process; (b) welding area enlarged and shown with keyholing.

Source: "Welding Metallurgy" (2nd Ed) by Sindo Kuo [115]. Reprinted with permission from the Global Rights Department, John Wiley & Sons, Inc. (April 30, 2012)

2-7b, which makes it suitable for welding thick plates. Joints which require multiple-pass arc welding, can be welded in a single pass weld at high welding speed. This reduces the total heat input per unit length of the weld unlike in arc welding, thereby resulting in a very narrow heat-affected zone and minimum distortion. This joining method also permits welding of refractory and reactive metals in vacuum which are susceptible to contamination in air. The process lends itself to automation as this reduces the welding time and increases productivity. Furthermore, automatic control over the movement of the energy from its source to the work piece improves weld quality and speed. The initial cost of equipment and installation is high due to high vacuum (10^{-3} – 10^{-6} torr) requirements.

2.3.8 Laser Beam Welding

Lasers are classed into three categories, namely: solid state (ruby, neodymium, yttrium, aluminium, garnet), gas (helium-neon, carbon dioxide, argon), and injection (gallium arsenide, indium, antimonide). This implies that in laser welding, the laser beam is produced either as a gas laser or solid state laser. The laser beam produced is focused by optical mirrors or lenses to a small spot size to produce a controlled high power density, which melts the metal and vapourizes part of the metal in deep penetration welds (figure 2-8). The vapourized metal prevents the remaining energy from being reflected by the metal; and if the metal to be joined has excellent thermal diffusive property, then the greater will be the penetration. To produce sound laser welds, highly reflective surface conditions are not desirable since the beam is capable of vapourizing or melting holes in

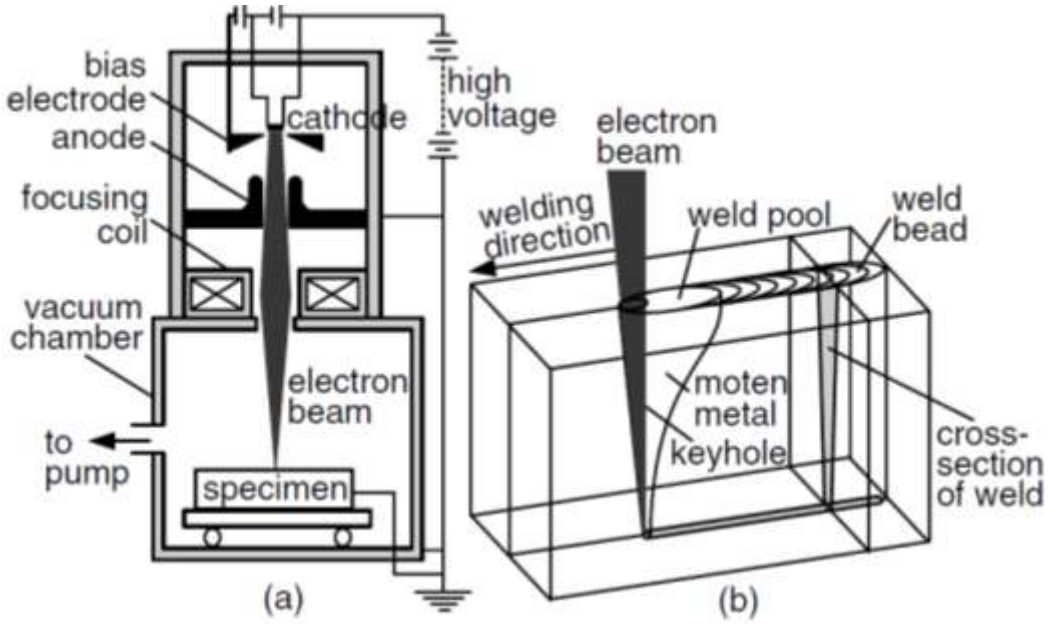

Figure 2-7: Electron beam welding: (a) overall process; (b) welding area enlarged

Source: "Welding Metallurgy" (2nd Ed) by Sindo Kuo [115]. Reprinted with permission from the Global Rights Department, John Wiley & Sons, Inc. (April 30, 2012)

opaque materials. On the other hand, the beam passes freely through transparent materials without affecting them. Equipment cost of this process is also relatively high.

2.3.9 Flux Cored Arc Welding (FCAW)

Flux cored arc welding is a welding process that uses a consumable tubular electrode containing a flux to join metals. The main purpose of the flux is to prevent oxidation during welding. Since flux cored welding uses a consumable electrode, it can be performed in all positions. This process is similar to MIG but differs in the sense that shielding is provided from the flux core and this enables sound welding operations in windy environments. In addition, deeper penetration of welds is also achieved using this process.

2.4 Fusion Welding Defects

Conventional fusion welding processes are prone to several types of defects such as gas porosities, inclusions, incomplete fusion, cracks and fissures etc. Discontinuities produced by local rupture are usually referred to as cracks or fissures. Several types of cracks exist and they include; (a) longitudinal cracks in the base metal parallel to the welding direction; (b) transverse cracks in the base metal perpendicular to the welding direction; (c) microcracks or macrocracks in the metal; (d) centerline longitudinal weld-metal cracks; (e) crater cracks; and (f) start cracks or bridging cracks. A combination of a strong weld metal and weak, low-ductility base metal results in longitudinal cracks while transverse cracks occur as a result of external contamination or a base metal with poor ductility. Contamination or impurities in the weld metal can lower the weldability by causing weld-metal microfissuring. Concave beads or an extremely deep, narrow weld

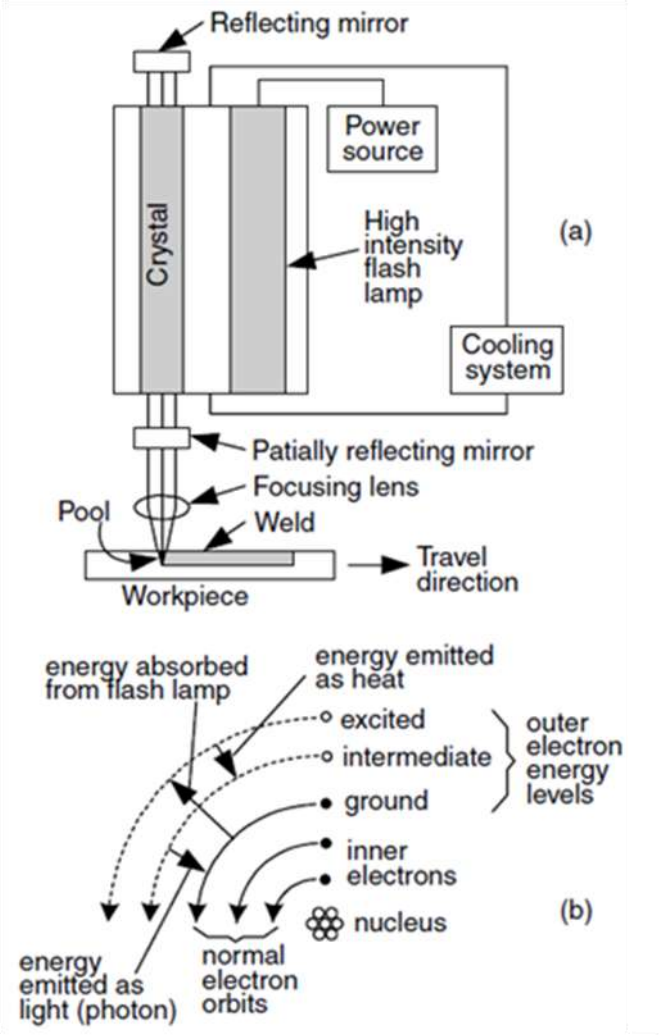

Figure 2-8: Laser beam welding: (a) overall process; (b) welding area enlarged

Source: "Welding Metallurgy" (2nd Ed) by Sindo Kuo [115]. Reprinted with permission from the Global Rights Department, John Wiley & Sons, Inc. (April 30, 2012)

bead will result in centerline longitudinal cracking. Crater cracking is caused by an arc extinguished over a relatively large weld pool. Cracks may also occur in the form of bridges. Bridging cracks are apparent in severely stressed joints where good penetration was not attained at the crack initiation point. Base metal cracking can be reduced through lower heat input and depositing small beads to generate lower residual stresses.

Gas pockets or voids indicate gas porosities in the weld metal. Gas porosity in the weld bead can be attributed to moisture, incorrect amperage or a long arc length and improper shielding. Inclusions refer to oxides, slag, or any non-metallic solids entrapped between the weld and the parent metal or between adjacent weld beads. Reactions between gas and metal or slag and metal can result in the production of gas porosity and inclusions in the weld metal and consequently affect the weld metal properties.

Incomplete fusion is a two dimensional flaw that occurs due to insufficient heat absorbed by the underlying metal from the weld. This causes incomplete melting at the interfaces of the weld and the base metal upon successive passes. Improper penetration is another type of defect which occurs when the metal is unable to penetrate to the bottom of the weld joint. Other weld defects include (i) Overlap: a protrusion of the weld metal beyond the toe, face or root of the weld (ii) Undercut: a groove melted into the base metal adjacent to the toe, cap or root of the weld metal and left unfilled by the weld metal; (iii) shrinkage voids: a cavity formed due to shrinkage during solidification; (iv) Arc Strikes: occurs by localized re-melting of metal surface, caused by inadvertent contact between an electrode and the metal surface; (v) underfill: a depression on the face of the weld or root surface extending below the surface of the adjacent base metal.

2.5 Solidification Cracking

Since fusion welding involves solidification of the weld metal, cracking observed during solidification of casts and ingots can occur in weld deposits of fusion welds during cooling. It is prevalent between columnar grains that form on solidification of the weld metal or at the weld centerline. Solidification cracking occurs during the terminal stage of solidification, when the tensile stresses developed across adjacent grains exceed the strength of the almost completely solidified weld metal [25-27]. The weld metal contracts during solidification due to both solidification shrinkage and thermal contraction. Despite that the base metal contracts too, its extent of contraction is less than that of the weld metal. This is because the base metal does not melt and does not get heated as much as the weld metal. Therefore, contraction of the solidifying metal can be opposed by the base metal, especially if the work piece is constrained and cannot contract freely. As a consequence tensile stresses develop in the weld metal such that at a certain point, the semi-solid material will no longer contain the thermal shrinkage strains associated with weld solidification and cooling. In order to offset the accumulating strains, cracks form at potential sites such as interdendritic regions and solidification grain boundaries, where the tendency of wetting is most rare. The factors influencing solidification cracking will be discussed next.

2.5.1 Factors Influencing Solidification Crack Susceptibility

(i) Solidification temperature range: the solid-liquid region produced during solidification is dependent on the freezing or solidification temperature regime. A wider solidification temperature range produces a larger solid-liquid region that is weak and prone to

solidification cracking. Undesirable impurities such as sulphur and phosphorous can result in larger solid-liquid region.

(ii) Amount and distribution of liquid at the terminal stage of solidification: A metal is most susceptible to cracking if its composition ranges between that of its pure form and highly alloyed state. This is illustrated in figure 2-9. A pure metal is devoid of eutectics at the grain boundaries therefore it is not susceptible to solidification cracking. On the other hand, the eutectic liquid between the grain boundaries of a highly alloyed metal is just high enough to promote incipient healing of cracks. A metal with composition in between its pure and highly alloyed state will have certain amount of liquid between its grains sufficient to form a thin continuous film rendering the material susceptible to cracking without excess liquid to promote healing of the cracks.

(iii) Surface tension of grain boundary liquid: a higher surface tension of the grain boundary liquid will result in large dihedral angle of the liquid. Figure 2-10 shows the effect of grain boundary liquid morphology on crack susceptibility. The susceptibility of an alloy to cracking decreases with increasing dihedral angle. When the surface tension between the grain boundary liquid and solid grains is extremely low, a continuous liquid film will form between the grains and the susceptibility to solidification cracking becomes high. On the contrary, if the surface tension is high, the liquid phase that would have formed will be globular and will not wet the grain boundary thereby decreasing the alloy's susceptibility to solidification cracking.

(iv) Ductility of weld metal: the lower the ductility of the solidifying weld metal, the higher the tendency for it to crack during solidification.

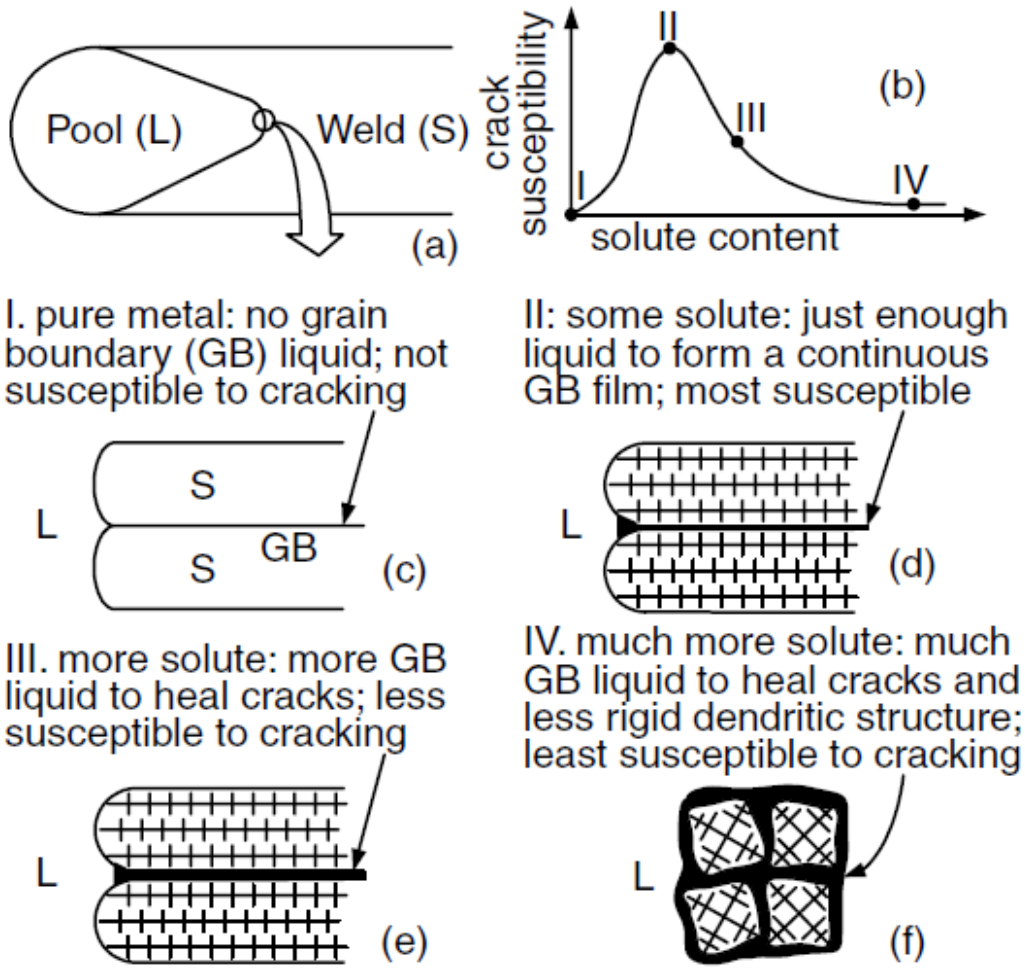

Figure 2-9: Effect of composition on crack susceptibility (a) weld (b) crack susceptibility curve (c) pure metal (d) low solute (e) more solute (f) much more solute.

Source: "Welding Metallurgy" (2nd Ed) by Sindo Kuo [115]. Reprinted with permission from the Global Rights Department, John Wiley & Sons, Inc. (April 30, 2012)

(v) Grain morphology of weld metal: fine equiaxed grains are less susceptible to solidification cracking than coarse columnar grains [29]. This is attributed to the fact that equiaxed grains are more ductile hence can deform to accommodate contraction strains more easily than columnar grains. In addition, fine-grained materials have a high grain boundary area and this reduces the concentration of low-melting point segregates at the grain boundaries. The extent of liquid feeding and healing of incipient cracks is also more effective in fine grained materials. All these are metallurgical factors affecting solidification cracking.

Mechanical factors on the other hand can also affect solidification cracking. They include joint geometry and residual stresses. Despite that the metallurgical factors previously discussed play a considerable role during cracking, cracking will not occur without the presence of tensile stresses. During the welding thermal cycle, residual stresses are introduced into the weld metal. The source of these stresses may be attributed to solidification shrinkage or thermal contraction of the weld metal. The controlling factor of the severity of these stresses is dependent on the resistance offered by the welded joint. Higher restraints at the weld joint produce larger stresses in the weld metal. The mechanism of solidification cracking will be discussed next.

2.5.2 Mechanism of Solidification Cracking

Generally, it is known that solidification cracking occurs at the terminal stage of weld pool solidification when tensile stresses developed across the adjacent grains exceed the strength of the nearly solidified weld metal. Due to solidification shrinkage during solidification, the weld metal contracts to a larger extent than the base metal since the

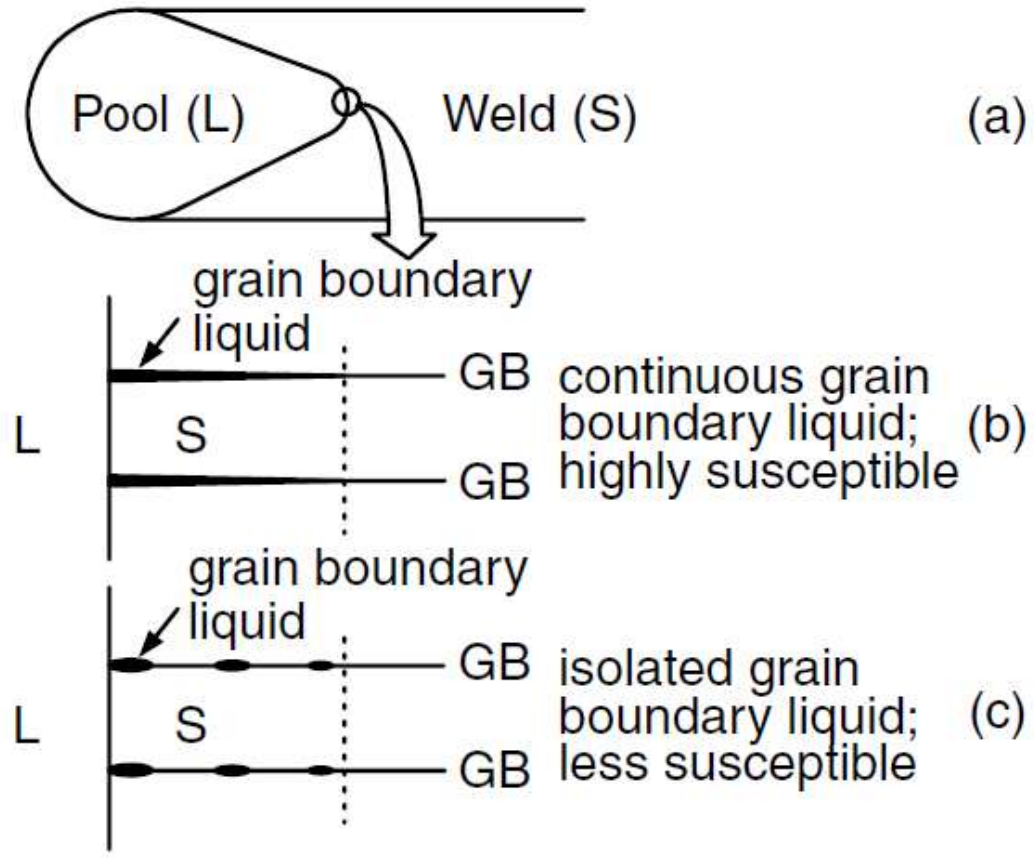

Figure 2- 10: Effect of grain boundary liquid morphology on crack susceptibility: (a) weld (b) continuous (c) isolated.

Source: "Welding Metallurgy" (2nd Ed) by Sindo Kuo [115]. Reprinted with permission from the Global Rights Department, John Wiley & Sons, Inc. (April 30, 2012)

base metal does not melt and as a result experiences lower temperatures than the weld metal. Nevertheless, the base metal can oppose the contraction of the solidifying weld metal more especially if the weld metal is unable to contract freely. This leads to the development of tensile stresses in the weld metal such that a point is reached where the semi-solid material can no longer withstand the thermal shrinkage strains of the weld during solidification and cooling. These accumulated strains are offset by cracks developing at potential sites which were wetted such as solidification grain boundaries and interdendritic regions [30]. Solidification cracking is a complex phenomenon that involves interplay between metallurgical and mechanical components. The primary metallurgical components include the amount and distribution of liquid at grain boundaries and interdendritic regions during the terminal stage of solidification, the solidification temperature range, ductility and grain morphology of the solidifying weld metal. A metal with composition between its pure and highly alloyed form is highly susceptible to solidification cracking than if it were either pure or highly alloyed. This is because in its pure form, solidification cracking will not occur since the metal is devoid of any low-melting point eutectic. However, in its highly alloyed form, the amount of eutectic liquid produced between grains is so high that it will cause healing of incipient cracks. The amount of liquid that would have been produced in the metal lying in-between the composition levels may not be sufficient to heal the cracks. On the contrary, this type of liquid may be thin enough to form a continuous liquid between grains thereby satisfying the conditions for solidification cracking to occur. A wide solidification temperature range, which may be induced by the presence of impurities or alloying elements, produces a corresponding larger solid-liquid region that renders the weld metal

extremely susceptible to solidification cracking. Furthermore, the metal becomes more prone to solidification cracking if it is less ductile. Fine equiaxed grains are more ductile than coarse columnar grains. This makes equiaxed grains less prone to solidification cracking than coarse columnar grains. Also, healing of incipient cracks is more effective in equiaxed grains than in columnar grains since liquid feeding is also relatively high in equiaxed grains than in columnar grains. Comparatively, the grain boundary area of equiaxed grains is large and hence reduces the concentration of low melting point segregates at grain boundaries.

The mechanical components include weld joint design, thickness and size of the parts to be joined, thermal strains caused by the uneven expansion and contraction of the weld and heat affected zone. A necessary requirement for solidification cracking to occur is the persistence of tensile stresses on adjacent grains during solidification. Residual stresses are also induced in the weld metal due to solidification shrinkage or thermal contraction or both. Thicker plates offer higher restraint which results in a correspondingly larger amount of residual stresses.

2.6 Heat Affected Zone Liquation Cracking

Liquid present in the heat affected zone (HAZ) on grain boundaries during fusion welding can penetrate the grain boundaries and spread along them to form a continuous thin film. There is the tendency for cracks to form along wetted grain boundaries when tensile stresses overcome the local strength of these boundaries. This type of cracking is usually referred to as heat affected zone (HAZ) liquation cracking or microfissuring or hot cracking [32]. When tensile stresses are imposed on the liquated grain boundaries

they open up or crack while compressive stresses close the liquation cracks. Grain boundary liquation can occur by supersolidus melting or non-equilibrium sub-solidus melting. Non-equilibrium sub-solidus melting is considered more detrimental since it can extend the temperature range within which a weldment will remain liquid thereby increase the alloy's susceptibility to HAZ liquation cracking [33]. Sub-solidus melting can occur by mainly two mechanisms. They include:

A. Constitutional liquation of second phase particles.

B. Segregation of melting point suppressants on the grain boundaries during pre-weld heat treatment, thermal processing and solidification.

The theory of constitutional liquation will be discussed next.

2.7 Constitutional Liquation

Constitutional liquation theory was first proposed by Pepe and Savage in 1967 where they observed liquation of titanium sulphide particles in 18-Ni maraging steels [34]. Since then, this theory has been used to explain the occurrence of non-equilibrium sub-solidus melting in different alloys, for example, M_6C in Hasteloy X [35], M_3B_2 in Udimet 700 [36], Cr_7C_3 and Ti(CN) in Inconel 600 [37], MC carbide and MNP Phosphides in Incoloy 903 [38], NbC and Laves phase in Inconel 718 [39], and MC carbide in Allvac 718Plus® [40]. The phenomenon of constitutional liquation is illustrated by the constitutional phase diagram of figure 2-11 [34]. An alloy of nominal composition C_o can be considered heated progressively from T1. The alloy of composition C_o consists of the intermetallic compound A_xB_y distributed within the α matrix. As the temperature is increased at an infinitely slow rate which corresponds to the equilibrium condition, the

solubility of B in the α matrix increases as the temperature is increased gradually until it reaches T2 where complete dissolution occurs transforming the A_xB_y intermetallic into a single phase solid solution of composition C_o. Further heating to temperatures below T5 will cause no transformation in phase but instead induce grain growth and equilibrium grain boundary segregation. At T5, that is the equilibrium solidus of the alloy, melting starts to produce the first infinitesimal liquid which corresponds to the point c. Hence the two phase alloy under equilibrium condition is converted to a single phase alloy until melting first occurs at the equilibrium solidus of the alloy. However, the dissolution character of the intermetallic phase during rapid heating thus under non-equilibrium condition is absolutely different from the observed behaviour under equilibrium conditions. Dissolution of A_xB_y intermetallic requires that it dissociates and further accommodates the excess component of B, which becomes liberated as excess solute in the immediate surrounding matrix. Hence the rate of dissolution of A_xB_y occurs at a finite rate which may be limited by either or both the dissociation step or accommodation process step. An increase in the heating rate will cause the system to reach a critical heating rate at which there is not enough time to raise the temperature to the equilibrium solidus to completely dissolve the A_xB_y intermetallic. At this critical heating rate including all heating rates above it, the dissociation and diffusion process steps will occur at a finite rate. The equilibrium structure for an alloy of this composition as a function of temperature is represented by the vertical line emerging from the composition C_o in figure 2-11. This implies that any departures from an equilibrium structure, such as due to rapid heating will result in redistribution of solute since the system will be striving to remain in equilibrium. Considering a spherical precipitate and a heating rate above the

critical heating rate, the anticipated changes in the domain of A_xB_y during heating to temperatures T3, Te and T4, respectively is illustrated in figures 2-12a to 2-12c. Upon heating to T3, the intermetallic compound A_xB_y starts dissociating since it is unstable with respect to a single phase solid solution of composition C_o. The intermetallic shrinks somewhat from its original shape or size to a smaller size or shape as depicted by the dashed and solid lines respectively in figure 2-12a. Liberated B atoms should diffuse into the adjacent α matrix. On the other hand, it can be seen from figure 2-11 that A_xB_y must be in contact with the matrix of composition m if they must all co-exist. Therefore, it is imperative that the concentration builds up in the α matrix such that a maximum concentration 'm' exists at the A_xB_y-phase interface and decrease toward the original matrix composition 'o' at the interior of the α phase. To maintain material balance, the area of the double cross hatched section of figure 2-12 must be equal to the single cross-hatched section. The concentration gradient produced in this manner is dependent on the following:

1. Heating Rate: the faster the heating rate, the steeper would be the concentration gradient.

2. Solute Diffusivity: the faster the diffusivity of solutes, the shallower would be the concentration gradient.

3. Accommodation Attribute: the relative ease with which the solute atoms are accommodated by each successive single phase region in the diffusion couple.

Heating from T3 to Te (eutectic temperature) leads to further dissociation of the intermtallic. This implies that the particle size continues to decrease as shown in figure 2-12, where the dashed and solid lines represent the location of A_xB_y interface at T3 and

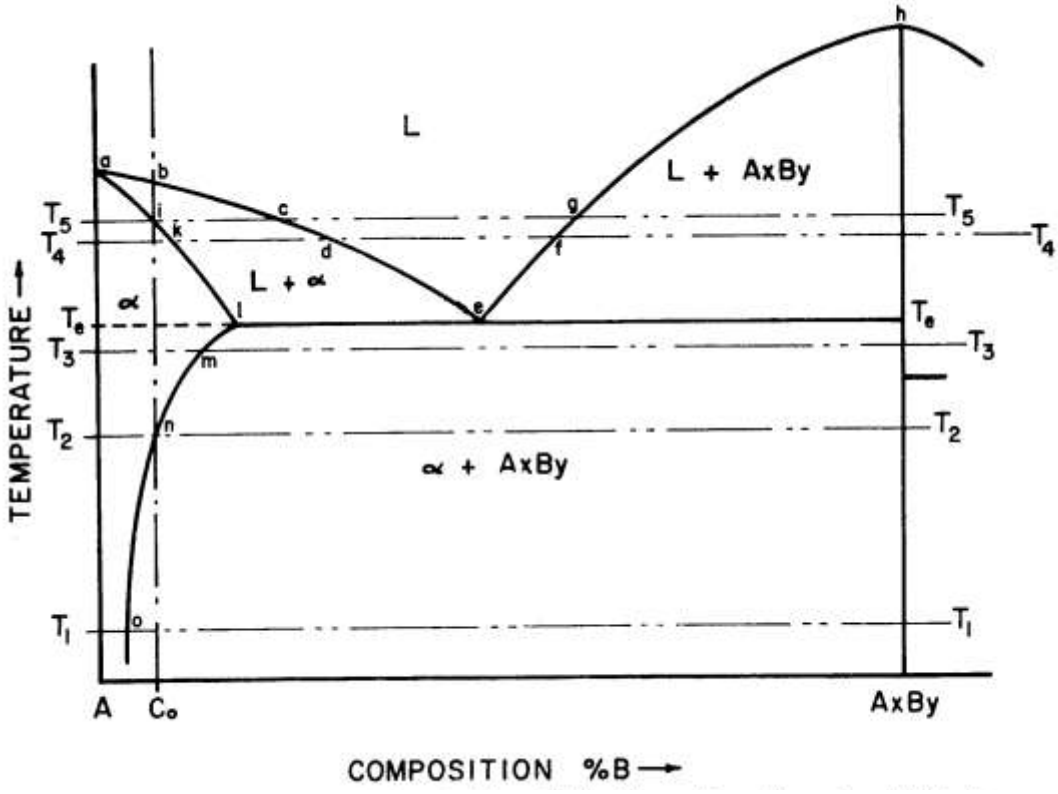

Figure 2-11: Schematic diagram of a portion of a hypothetical constitutional diagram for an alloy system exhibiting the behavior necessary for constitutional liquation.

Source: Welding Journal [34]. Reprinted with permission.

Te, respectively. At the eutectic temperature, Te, the composition corresponding to point 'e' will permit the formation of the first single phase liquid to form on the undissociated interface of A_xB_y, which implies that the undissociated portion of the intermetallic is surrounded by a liquid phase of composition 'e', which in turn, should be surrounded by the α matrix. Figure 2-12b shows the distribution of solute atoms in the three phases coexisting at the eutectic temperature Te. Further heating to T4 will allow additional time for the dissociation of the intermetallic A_xB_y. The expected distribution of solute upon reaching T4 is represented in figure 2-12c. On heating above Te, the equilibrium solubility of 'B' atoms in α phase decreases along the solidus "akl". Hence, as the temperature rises above Te, the concentrations of solid solution and liquid film in contact with each other should correspond to 'k' and 'd' respectively. At T4, each remaining undissolved particle of A_xB_y should be surrounded by liquid film of composition ranging from 'f' at the A_xB_y interface to 'd' at the interface with the α matrix. This results in localized melting under rapid heating or non-equilibrium conditions at temperatures ranging from Te to T5. The phenomenon by which this occurs is termed constitutional liquation. Henceforth, constitutional liquation occurs under rapid heating conditions to produce liquid pools at temperatures below the equilibrium solidus of the alloy.

2.7.1 Grain Boundary Segregation

Another mechanism by which non-equilibrium grain boundary melting can occur in metals is grain boundary segregation. It occurs by solute or impurity element segregation to grain boundaries which can reduce the melting temperature of boundary areas relative to the surrounding matrix. A prerequisite for liquation to occur by this manner is the

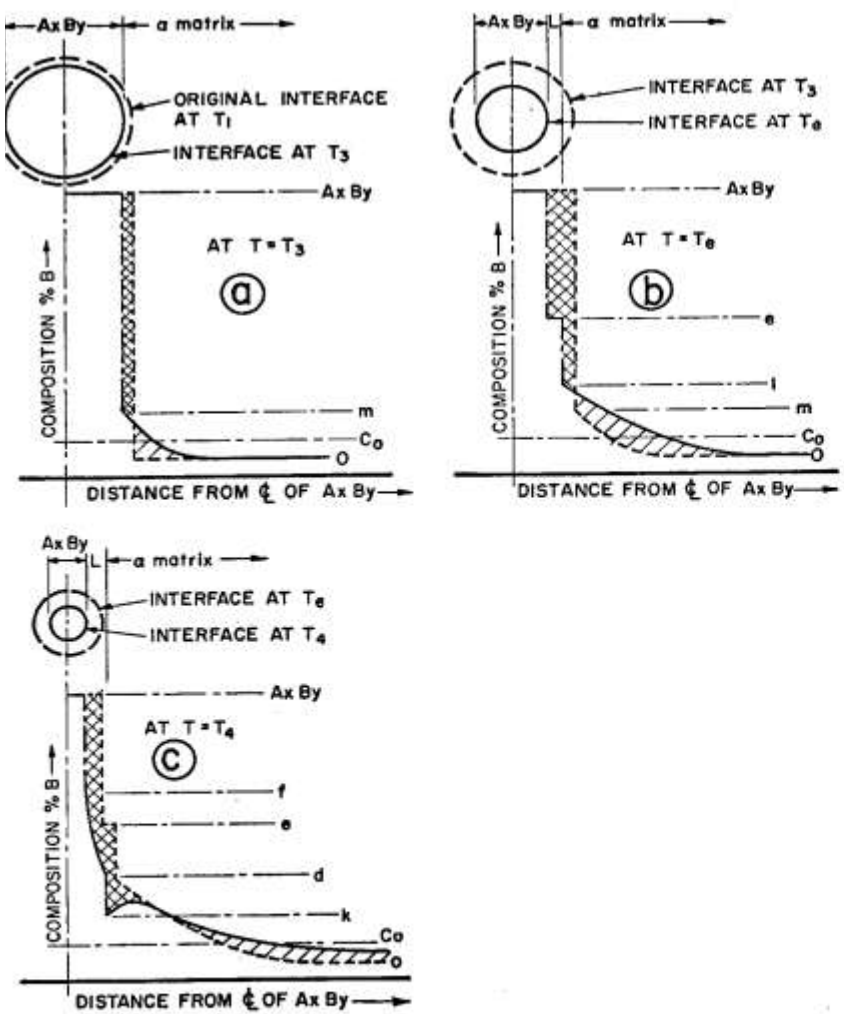

Figure 2-12: Schematic representation of the concentration gradients at various temperatures during formation of constitutional liquation.

Source: Welding Journal [34]. Reprinted with permission.

precedence of grain boundary segregation to the occurrence of liquation. At a certain temperature above the reduced melting temperature of the grain boundary material, non-equilibrium sub-solidus melting occurs [41]. Segregation of impurities to grain boundaries prior to welding may occur during thermal processes such as casting, heat treatment and hot forming. The phenomenon is diffusion controlled and can occur by two mechanisms, namely, equilibrium segregation [44-47] and non-equilibrium segregation [48-52]. Equilibrium segregation becomes apparent when a material is held at a sufficiently high temperature to allow considerable diffusion of solute atoms from inside the grain matrix to the grain boundary. This leads to a reduction in the interfacial free energy at the grain boundary. Equilibrium segregation increases with decreasing temperature as well as increasing initial solute concentration in the matrix. On the other hand, impurity atoms can also segregate to loosely packed sites such as free surfaces, phase boundaries, stacking faults and precipitate/matrix interface. Atoms involved in equilibrium segregation are confined to a few atomic layers at the grain boundary and the total amount is usually of the order of a few monolayers.

Non-equilibrium segregation occurs during cooling from elevated temperature. This form of segregation is dependent on the concentration gradient that forms between grain interiors and grain boundaries. Supersaturation of vacancy concentration occurs in the matrix with the grain boundaries acting as sinks for vacancies during cooling to lower temperatures. Annihilation of vacancies at the grain boundaries produces a concentration gradient of vacancy-solute complexes which in turn drive the complexes to diffuse from the grain within the diffusion range into the grain boundaries. The driving force for this process is the decrease in free energy which is associated with the annihilation of excess

vacancies produced at the grain boundaries. The extent of non-equilibrium segregation is dependent on the starting temperature, cooling rate, bulk concentration of solutes and the binding energy between solute atoms and vacancies [53-55]. High cooling rates limit the time available for diffusion of complexes to grain boundaries hence the rate of segregation is reduced. However, if the cooling rate is very slow such that a concentration gradient is produced between the grain boundary and grain interior, reverse diffusion of segregated solute atoms to grain interiors may occur, hence segregation is eliminated [56]. Increasing the thermal heat treatment temperature will increase the equilibrium concentration of vacancies which in turn increases segregation simultaneously.

A study on the effect of non-equilibrium and equilibrium segregation of solutes and how they influence the weldability of nickel-based superalloys was performed by Chen et al [56]. It was observed that liquid wettability of grain boundaries could be influenced by either non-equilibrium or equilibrium segregation of solutes. Solutes present in the grain boundary liquid were found to reduce the solidification range of the liquid and assist in HAZ microfissuring.

2.8 History and Development of the Friction Welding Process

In 1956, scientific study began on friction welding and it was subsequently established that metal rods could be joined to produce high quality butt joints [57]. Due to this, other researchers including Vill in the U.S.S.R began detailed studies with the aim of understanding the scientific mechanism behind friction welding [58]. Later in 1960, the process was introduced to the USA. The Caterpillar Tractor Company in 1962 invented a modified version of the process which was referred to as inertia friction welding or

flywheel friction welding which uses rotating flywheel to store the energy required for welding. Similarly, the Russian based process on the other hand was termed ‘continuous drive friction welding’ or ‘conventional’ friction welding. In the early part of the 1960’s, The Welding Institute (TWI) in Cambridge, UK, started contributing to friction welding through developing continuous-drive-type machines. TWI afterwards developed the linear friction welding process which had the capability of joining non-rotational symmetric parts together. Friction stir welding was developed by TWI in 1991 and patented accordingly. Following these historic trends, academic and industrial institutions have been involved in carrying out research on using friction welding to join a wide range of materials, namely, composites, aluminium, titanium, superalloys, etc.

Generally, friction welding is described as a process that generates the heat required for joining by converting mechanical energy to thermal energy at the interface without applying any form of heat from an outside source to the parts being joined together [59]. Normally, two surfaces rubbing against each other under the influence of an axial compressive force are involved in the process. This produces frictional heat at the interface and as a consequence, raises rapidly the temperature of the work piece over a short axial distance to values approaching, but below, the equilibrium melting range. The system is brought to a halt when sufficient plasticity of the material has been attained. A compressive pressure is then applied while the heated zone is still plastic within the plastic temperature range.

In conventional welding processes, melting and re-solidification leads to liquation cracking in the fusion and heat affected zones due to existing tensile stresses. Nickel base superalloys particularly those containing a substantial amount of aluminium and titanium

such as IN 738 are susceptible to intergranular microcracking during fusion welding processes. This is attributed to the constitutional liquation of phases present in the alloy which is responsible for weakening and embrittling the grain boundaries. Contrary to fusion welding processes, the friction welding processes are devoid of weld cracks, presumably due to them being solid state processes.

2.8.1 Inertia Friction Welding

In inertia friction welding, a pre-determined amount of kinetic energy is stored in a rotating flywheel which is entirely converted into frictional welding heat without the use of clutches, brakes, time or distance [60]. Figure 2-13 shows a schematic diagram of the inertia friction welding process. One of the two work pieces to be welded is held in a chuck while the other one is clamped in a non-rotating fixture. A flywheel and the chuck are mounted in a rotating spindle, which is driven to a desired speed. This speed which corresponds to a specific speed is dialed into the machine. The drive motor is disengaged when the appropriate speed is reached, thereby establishing a free-wheeling system. The non-rotating part is then pushed against the free-rotating work piece under an applied force. Meanwhile, the kinetic energy stored in the rotating flywheel is rapidly converted to frictional heat at the abutting surface as the axial pressure is applied. The flywheel is brought to a halt due to the interfacial friction which is also responsible for softening the material, causing plastic flow and upset. Process variables such as the weld time, the torque between the pieces and the upset are dependent on the welding process with the exception of the axial force which is in actual fact an external variable contributing to the inertia welding process. Figure 2-14 shows some characteristics of the joining process.

Figure 2-13: A schematic of an inertia welder

Source: Inertial Friction Welding, Manufacturing Technology, Inc. [60].

Based on the shape of the friction torque curve, the process is divided into three stages, viz, the pre-heat, heat and upset stage, respectively. During stage 1, wearing of surfaces occur due to interlocking and breaking of asperities. This causes a rapid increase in torque to a peak where the whole surface area is brought into real contact. The interfacial frictional heat generated causes the material to soften hence initiating plastic flow. Plastic flow on the other hand is confined to a relatively thin layer on the surface without considerably reaching into the bulk of the material. Due to the preponderance of thermal softening over strain hardening, the last part of stage 1 is characterized by a drop in the curve of the torque. Friction torque remains somewhat unchanged in stage 2, thus indicating a balancing effect between strain hardening and thermal softening. Here, both faying surfaces and the material behind are sufficiently plasticized to warrant the forging of the two work pieces together. Upon reaching the third stage, the temperature gradient across the interface decreases and the narrow deformation zone expands rapidly. Stage 3 is mainly characterized by torsional forging and gradual stiffening of the material leading to a rise in torque to another peak. The upset increases continuously whiles the material flushes out of the widening heat affected zone, from the center of the interface, via a spiral path to the outside of the periphery. At the beginning part of stage 1, the surface speed starts at some initial value as required for a specific work piece, and decreases following the parabolic curve to zero, to a time where the weld is complete. The end of stage 3 is signified by the complete cessation of the rotating wheel and the rigidity of the material.

Inertia friction welding has been utilized in the aerospace industry to successfully join nickel-base superalloys [60-63]. Stainless steels, which have been considered to be non-

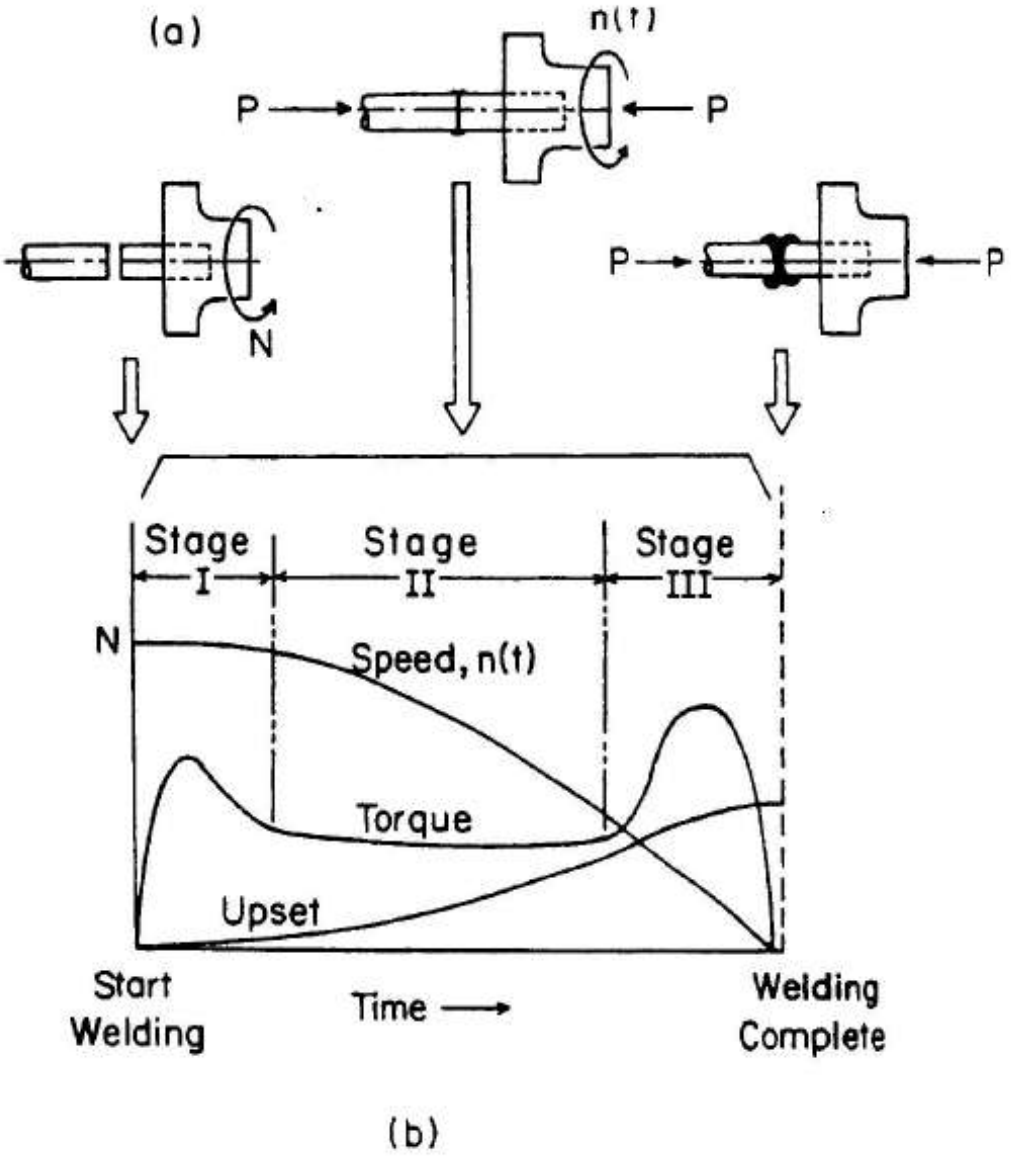

Figure 2 - 14: Some characteristics of flywheel friction welding process

Source: Welding Journal [140]. Reprinted with permission (July 06, 2012).

weldable by fusion methods have also been joined using inertia friction welding [65]. Present day applications of inertia friction welding can be found mainly in the earthmoving and automotive industry coupled with the demands of high production, consistency in part quality, low part costs and maintenance [64].

2.8.2 Continuous Drive Friction Welding

In this type of welding, one of the work pieces is rotated at a constant speed while the other is held stationary (figure 2-15a). At a certain time range during welding, an axial pressure is applied to both pieces in order to push them against each other. The material at the interface softens as a result of the frictional heat generated by the rubbing action of the work pieces hence causing a radial outflow of the upset collar. Rubbing continues at the interface of the work pieces until a certain axial shortening (or upset or burn-off) of the work pieces is produced [66]. The rotating work piece is stopped rapidly within a certain breaking time as the clutch is separated from the drive. Finally, the axial pressure also known as the forged pressure may be increased or maintained for a short period of time after terminating the rotation for the weld metal to cool under pressure.

Generally, the welding cycle is divided into two main stages, namely; the friction stage and forging stage. However, the frictioning phase is subdivided into four phases. These stages and phases were identified by Duffin and Bahrani who hypothesized the theory for the mechanics of continuous drive friction welding [67]. The variation of the speed of rotation, torque, axial force and axial shortening with time is shown in figure 2-15 [67]. The phases involved in the frictioning stage together with the forging stage will be discussed next.

Frictioning Stage

Phase I: Here, contact is established between the rotating and the stationary work piece as a result of the sliding motion between them. Metallic wedges form as a result of strong adhesion junctions at the areas of real contact [69]. There exists stronger adhesion between the surfaces at some junctions than the metal on both sides hence shear takes place at a short distance from the interface. Due to the non-uniformity of the rubbing speed across the interfaces, different sizes of metal fragments are transferred between both interfaces at interchangeable rates. This is accompanied by a corresponding increase in speed from zero at the center to a maximum at the periphery. The interaction at the interfaces causes the resisting torque to increase. Furthermore, the temperature at the interface also increases due to the continual action of rubbing between surfaces, wedge formation and transfer of fragments. The transferred fragments together with the wedges finally coalesce with each other at elevated temperatures to form the plasticized layer. The formed plasticised layer decreases the resisting torque signifying the end of phase 1.

Phase II: This is the transition phase where the metallic wedges and the transferred wedges are converted into the plastic layer. The resisting torque drops to an equilibrium value as a result of the spread of the plasticised layer across the surface. The temperature of the plasticised layer has been suggested to be about 100^{o}C to 300^{o}C below the bulk melting temperature of the alloy. The start of the axial shortening and the formation of the weld collar or flash are the main factors characterizing phase II. Heat is transferred to the material adjacent to the plasticised layer by conduction.

Phase III: Prior to the beginning of phase III, the material is fully plastic but not uniform in thickness across the section. This is because of the inconsistence in the applied

(a)

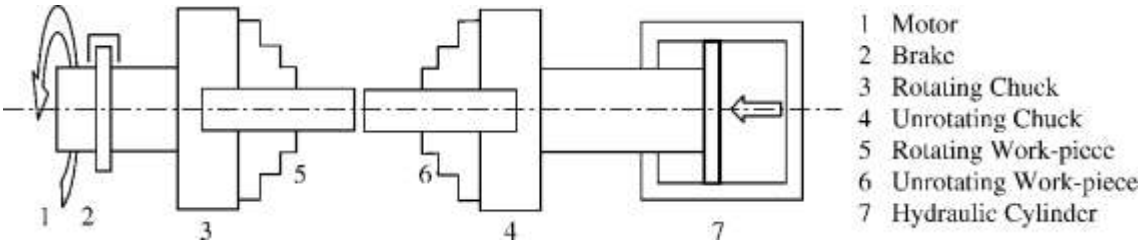

(b)

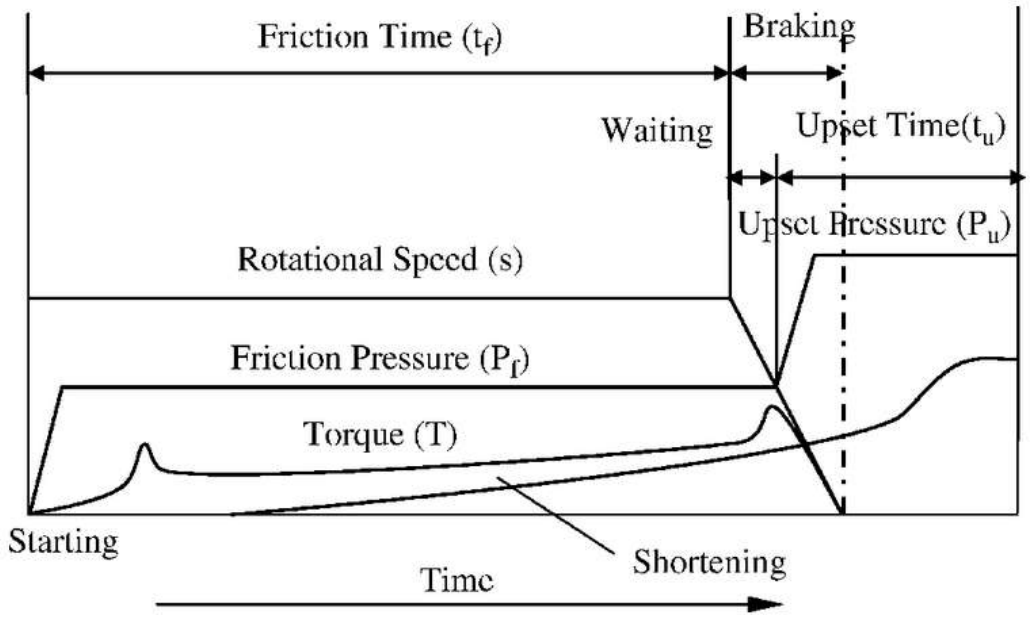

Figure 2- 15: (a) Layout of continuous drive friction welding (b) parameters on continuous drive friction welding.

Source: "Assembly Automation" by Kuscu et al [135]. Reprinted with permission from the Rights Assistant from Emerald (April 20, 2012).

pressure and rubbing speed. However, the rate of axial shortening and the torque remain essentially constant. The properties of the material being welded influence to a considerable extent the shape, location and dimension of the plasticised layer.

Phase IV: In this phase, deceleration occurs. As the rotation speed decreases, the plasticised area moves outward in a radial manner. The resisting torque ascends until the terminal peak torque value is reached, and then decreases to zero as the speed also decreases to zero. This marks the end of stage IV as the material at the interface is ready to be fused into the weld.

Forging Stage: In this stage, the welding parameters can be optimised to produce good welds such that the forged pressure applied will be the same as the friction pressure used. On the other hand, there may be instances where a continuous plasticized layer may not form due to the parameter settings and the friction pressure utilized during welding. Ideally, a sound joint is produced when the forged pressure is relatively higher than the friction pressure. The function of the forged pressure is to effectively spread the plasticized layer across the interface whiles sealing any holes and at the same time deforming the material in the heat affected zone. Successful welds of dissimilar nickel alloys [71], of aluminium alloys and steels [69, 70], steels [72-74] and titanium alloys [75] have been produced using continuous drive friction welding.

2.8.3 Linear Friction Welding

This form of joining was first patented in 1929 despite that the description of the process at that time was not explicit. Discussion about the concept of linear friction welding was

then documented in the 1960's but this was debatable because of the problem of generating linear reciprocation motion [98]. The next group of people to mention the process in a patent was The Caterpillar Tractor Company [99]. Since then many researchers began work on investigating ways to improve the efficiency of the linear friction welding process.

Linear friction welding was introduced with the aim of extending the current application of inertia friction welding to non-axisymmetric components [97]. Linear friction welding is also used as a substitute to inertia and electron beam welding, which are not recommended for joining metals used in some critical service conditions, such as fatigue [98]. Generally, due to the high cost of the linear friction welding equipment, its usage is currently confined to aeroengine applications where it has proven to be a cost effective process. However, efforts are being made to extend the usage of the process to other industrial sectors.

Linear friction welding is a process that achieves coalescence of parts through frictional heat generated by the linear reciprocation motion of two work pieces in contact with each other (figure 2-16). A forging pressure is applied to achieve coalescence at the terminal stage of the joining process after the faying surfaces of the parts to be joined together have become plasticised. This process was previously perceived to be an exclusive solid state process until recent studies showed that liquation can actually occur during linear friction welding process [100]. The linear friction welding process has four distinct phases (figure 2-17) and the major operational changes that occur during these phases will be discussed next.

Phase I: The two materials are brought into contact under pressure. Heat is generated from solid friction as the two surfaces rest on the asperities and rub against each other. Due to asperity wear, the true contact area increases considerably throughout this phase. No axial shortening of the specimens occur at this stage. If the rubbing speed is too low for a given axial force, the frictional heat generated will be inadequate to compensate for conduction and radiation losses. This results in insufficient thermal softening and subsequently prevents the start of the next stage. On the contrary, if the parameters are selected such that there is sufficient thermal softening of the material, a plasticised layer will begin to form at the interface to warrant the start of the next phase.

Phase II: As the material is softened due to sufficient heat being generated, wear particles begin to be expelled from the heat interface. The real contact area is assumed to be 100% and the heat affected zone expands. Moreover, the soft plasticized layer formed between the two materials is no longer able to support the axial load and this leads to stage 3 of the process.

Phase III: Here, axial shortening begins as a result of material being expelled from the interface. A plastic zone is developed as heat is generated through the breaking and reforming of bonds. The local stresses existing within the plasticized layer together with the assistance of the oscillatory movement extrudes the material from the interface into the flash. More material will be extruded from one part of the interface away from the centerline if the temperature increases excessively in that part such that a thicker plasticised layer is formed in that part. This may result in rotation of the interface from the original plane which could have been caused by an initial misalignment of the parts being joined.

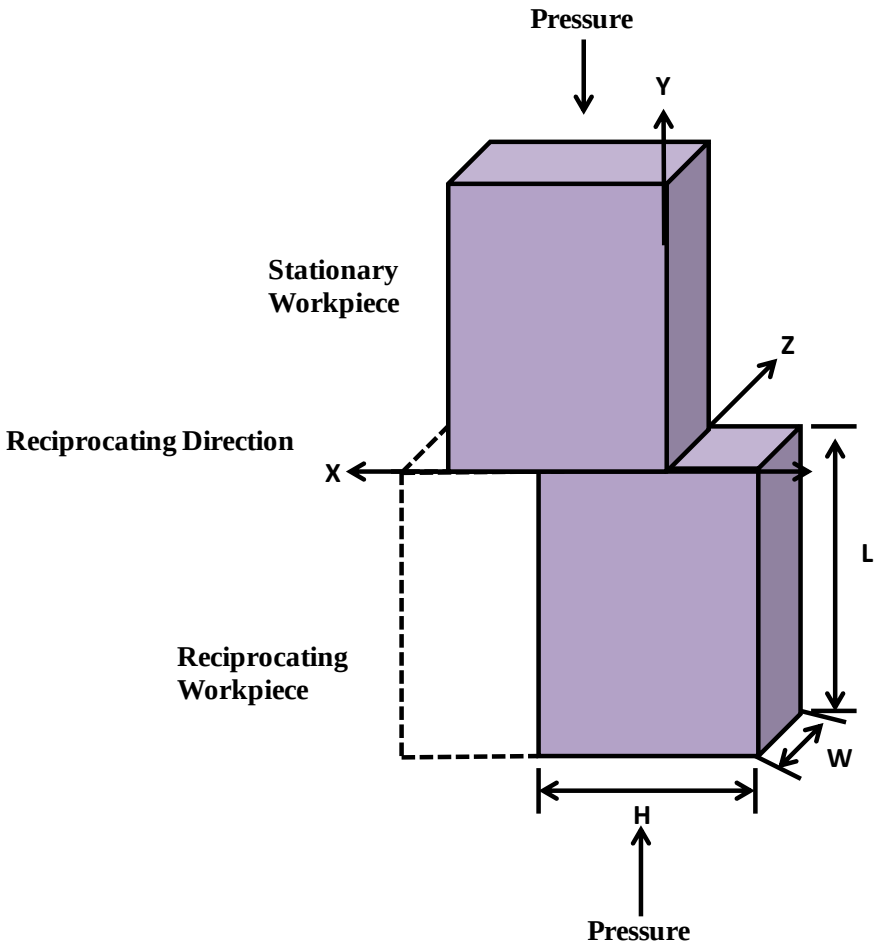

Figure 2-16: Basic principle of linear friction welding process.

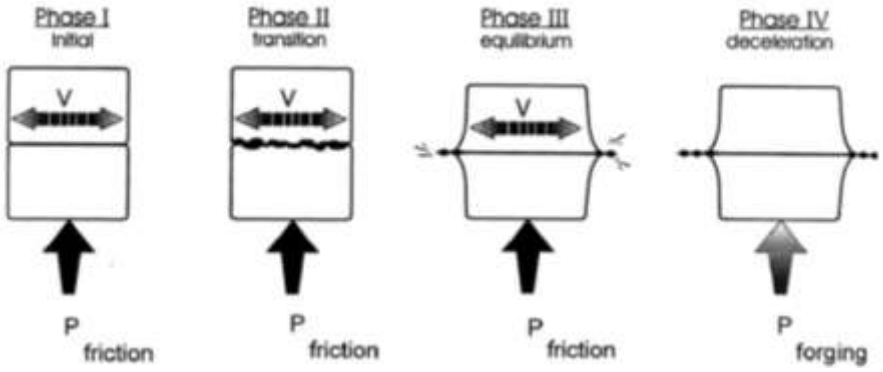

Figure 2- 17: The four phases that characterize linear friction welding.

Reprinted with permission from Elsevier [77] (April 17, 2012).

Phase IV: The relative motion between the work pieces is stopped abruptly and a compressive pressure applied to consolidate the weld.

Since the development of the linear friction welding process, it has been used successfully on Al-Fe-V-Si alloy 8009 [76], Ti6Al4V [77-80], polycrystalline nickel-base IN 718 [81].

2.8.4 Friction Stir Welding

The Welding Institute, a British research and technology organization in 1961, invented friction stir welding [82]. This technique utilizes frictional heating to achieve coalescence of the work pieces through interface deformation, heat, and solid state diffusion [83-85]. Despite that the material being welded heats up during the joining process, its temperature does not exceed the melting temperature. Therefore, the friction stir-welded joint produced has a microstructure entirely different from the dendritic microstructure typical of fusion-welded joints and also devoid of fusion weld defects. Although sound joints can be produced using conventional fusion welding processes, the microstructure of the material welded is altered completely and this can lead to degradation in the mechanical property of the material. Details of the friction stir welding process are available in the literature [86]. In friction stir welding, a non-consumable, cylindrical spin tool with a specially designed rotating tool is plunged into the abutting edges of the sheets or plates to be welded. Once the rotating tool has entered, frictional heat is generated and plastic deformation of the material takes place. The tool is then traversed along the desired bond line when the critical temperature and flow stress is reached. Metal flows to the back of the pin tool where it is extruded and forged behind

the tool, coalescing and cooling under hydrostatic pressure. Figure 2-18 shows a schematic diagram of the friction stir welding process.

Friction stir welding and inertia friction welding differ from each other by the mode in which frictional heat is generated. In friction stir welding, a rotating tool pin is used to generate frictional heat unlike in inertia friction welding where frictional heat is produced by the rubbing action of the work pieces to be joined in contact with each other. The most important variables to consider during friction stir welding in order to produce a high integrity defect-free weld are the traverse speed, the spindle speed and the depth of penetration. Successful welds of aluminium, lead, magnesium, steel and copper have been made using a non-consumable pin tool [90-92].

2.9 Significance of Friction Welding Processes

From a scientific point of view, friction welding is completely devoid of any fusion zone thus the welding process occurs below the sub-solidus temperature of the material although Ola et al have observed liquation of phases during linear friction welding [130]. This implies that cracking normally associated with fusion zone is precluded. Despite that HAZ forms during friction welding, HAZ cracking which is normally observed in fusion welds can also be avoided if friction welding parameters are carefully selected during welding. This has significantly led to using friction welding processes to join materials that are particularly susceptible to cracking during conventional welding.

It has been observed that dissimilar metals that could otherwise not have been joined using other welding processes due to the formation of eutectic microconstituents that render them less efficient in service environments could easily be joined using friction

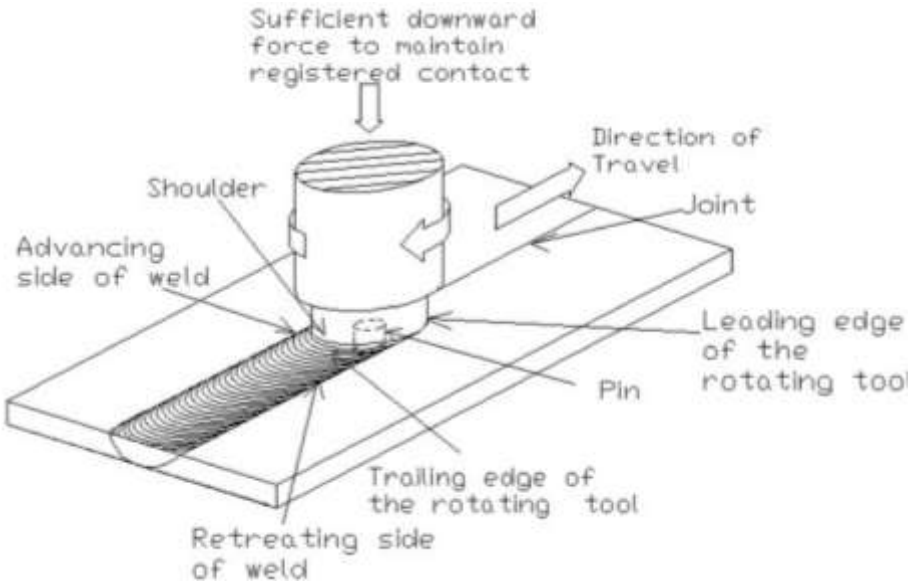

Figure 2- 18: Illustration of friction stir welding

Source: "Industrial Robot: An International Journal" by Cook et al [135]. Reprinted with permission from the Rights Assistant from Emerald Group Publishing Limited (April 20, 2012).

welding processes [93]. Several combinations of metals are also joined faster due to the relatively shorter times required to carry out most friction welding processes. Rolls-Royce has basically employed friction welding processes to join most of its components in the aerospace industry. These include aeroengine components such as disc-to-disc, disc-to-shaft and shaft-to-flange combinations [94]. Nickel base alloys which are generally considered difficult to weld by conventional fusion welding process, due to their high susceptibility to fusion zone cracking, have also been successfully joined using friction welding processes. Inertia friction welding was successfully used to join Waspaloy, a Nickel base superalloy [95]. On the other hand, linear friction welding which is also a promising joining method is currently being exploited with the aim of making it more effective and efficient in the industrial sector, especially in the aerospace industry for joining those components that are not axially symmetric, for example turbine blades and disks.

Another efficient method of joining known as hybrid welding which combines two different welding methods to achieve coalescence of materials is also gaining much recognition in the aerospace industry. A discussion on hybrid welding is presented next.

2.10 Hybrid Welding

For economic reasons, new materials are continually developed for new applications in various sectors of engineering applications, that include offshore, automotive, aerospace etc, has led to the development of new production technologies. One of these technologies is hybrid welding which is being patronized by most manufacturers due to a wider gap bridgeability, enhanced process stability and higher welding speed offered by

the process. Hybrid welding is a joining method that combines two different welding processes to join a material. They are classified by the type of heat sources used and their relative arrangement with each other. A discussion on one of the most widely used hybrid welding combination, hybrid laser-arc welding, is presented next.

2.10.1 Hybrid Laser-Arc Welding

This technique of joining combines laser and arc welding processes to provide advantages not found in using either of these two processes independently. Theoretically, the beam from any laser source (CO2, Nd:YAG, diode, Yb fibre, Yb:YAG disk etc) can be combined with any arc welding process (MIG, TIG, SAW, plasma). However the commonest combination used is the hybrid laser-MIG and laser-TIG. The capacity to increase the weld bead penetration, width and welding speed, which in most cases is difficult to achieve using either laser or arc welding independently, can be achieved by combining the two processes with optimized parameter settings. A typical feature produced by arc welding process is the wide process zone which results in a wide bead. Studies on fabricated lap-welded joints by laser welding and hybrid laser-arc welding showed that bead width increases with gap width using laser-arc hybrid welding, while the bead width remains almost unchanged using laser welding even when the gap width is increased. This is attributed to the additional molten metal supplied from the arc coupled with the molten pool filling the gap which is formed by the laser. Tensile shear tests performed on hybrid welded and laser welded joints have showed that welds produced by hybrid welding are relatively stronger than laser welds. The welds produced by hybrid welding failed in the base metal while all of the laser-welded joints fractured in the weld

[96]. Also zinc-coated steel plates have proven to be difficult to weld using laser welding. Since the melting point of zinc is significantly lower than the melting point of iron, laser welding of this coated steel resulted in the evaporation of zinc and led to the formation of pores in the weld metal. On the other hand, hybrid welding of the zinc coated steel plates suppressed the formation of these blowholes or pores. It was suggested that during hybrid welding, the filler metal provided by the arc filled the pores that would have been created by zinc vapour escaping from the weld metal. Also, in laser-arc hybrid welding, the laser precedes the arc. This implies that adequate amount of time would have also been allowed for zinc vapour to escape from the weld hence precluding the formation of holes in the weld. Furthermore, using arc welding alone to join materials also comes with its associated problems. Hybrid welding was not only useful in solving the problems associated with laser welding but also arc welding. A problem that is common to arc welding is the uneven beads produced due to the unstable nature of the arc when the welding speed is increased. Hybrid welding on the other hand provides uniform beads when the welding speed is increased since droplet transfer from the wire takes place in a very short cycle. A study was conducted on the speed limit required to form a uniform bead using arc welding and hybrid welding processes. It was observed that the welding speed limit for forming uniform beads using laser-arc hybrid welding process is at least seven times higher than that for arc welding. This implies that more efficient use of time will be made by increasing the welding speed while obtaining a uniform weld bead using laser-arc welding process. Hybrid welding has been extended to join nickel base superalloys. Successful welds of Inconel 600 were made using laser-FSW Hybrid welding [101]. Different combinations of arc and laser can be achieved in various process

arrangements to solve specific joining problems. Nevertheless, the nature of these combinations places a higher demand on technology development and process optimization.

2.11 Objectives of this Research

A major limitation of joining difficult to weld nickel base superalloys, such as IN 738, by conventional fusion welding methods is their susceptibility to heat affected zone (HAZ) grain boundary liquation cracking. The cause of this type of cracking is attributed to the liquation of micro-constituents, subsequent wetting of grain boundaries and de-cohesion along one of the solid-liquid interfaces when on-cooling tensile stresses overcome the local strength of the liquated boundary. Crack-free welding of nickel base superalloys can be achieved by using exclusive solid state joining methods such as friction welding processes. Technological advancements in welding have led to the development of a novel process called linear friction welding process, a variant of friction welding, which is used in recent applications in the conservative aerospace industry for joining crack susceptible alloys such as IN738.

The main process parameters on which the quality of the weld joint produced by linear friction welding is dependent upon include amplitude, frequency, and forge pressure. However, availability of information about the influence of these process parameters on the quality and microstructure of linear friction welded nickel base alloys is limited although some work has been done on titanium and ferrous alloys [108, 102]. Therefore, the objective of this research was:

- To study the effect of one of the very important process parameter that is the forging pressure on the microstructure of linear friction welded IN 738 superalloy.

2.12 Scope of the Research Project

Cast IN 738 superalloy plates, provided by Hitchiner Manufacturing were used in this study. 17.7 mm X 12.8 mm X 11.1 mm specimens were linear friction welded using three forging pressures at the Aerospace Manufacturing Technology Centre of the National Council of Canada's Institute for Aerospace Research in Montréal (NRC). The microstructures of the welds were characterized by optical and scanning electron microscopy, x-ray energy dispersive analysis, electron back scattered diffraction, and orientation imaging microscopy.

CHAPTER 3

Materials and Experimental Procedure

3.1 Materials Preparation

Cast IN 738LC with a nominal composition, as shown in table 3-1, was received from the Hitchiner Manufacturing Co. Inc. in the form of plates with dimensions 238 mm × 58 mm × 14 mm in length, width and thickness, respectively. Specimens of 17.7 mm long × 12.8 mm wide × 11.1 mm thick were machined from the as-received cast plates by using a Hansvedt Model DS-2 travelling wire Electro-Discharge Machine (EDM). The specimens prepared for linear friction welding were given a standard solution heat treatment at 1120^{o}C for 2 hours in an argon-controlled atmosphere and subsequently air cooled. Surface grinding of the solution heat treated specimens was performed to rid it of any oxides that formed on the surface before welding at the Aerospace Manufacturing Technology Centre of the National Council of Canada's Institute for Aerospace Research in Montréal (NRC). Linear friction welded (LFWed) specimens were sectioned axially perpendicular to the weld interface using the EDM. Standard metallographic techniques were used to prepare the specimens for microscopy studies. In order to reveal the microstructure of the linear friction welded specimens, the specimens were electrolytically etched in 12mL H_3PO_4 + 40mL HNO_3 + 48mL HCl.

3.2 Linear Friction Welding (LFW)

Linear friction welding of the solution heat treated specimens was performed using a Linear Friction Welding Process Development System situated at NRC, Canada. The

Table 3-1: Composition of cast IN 738 used in the study

Element	Weight Percent (wt %)
Aluminium	3.46
Titanium	3.47
Tantalum	1.69
Chromium	15.84
Cobalt	8.5
Carbon	0.11
Tungsten	2.48
Niobium	0.92
Iron	0.07
Zirconium	0.04
Manganese	0.01
Silicon	0.01
Sulphur	0.01
Boron	0.012
Nickel	Balance

welding was carried out with varying pressures P, 2.5P and 4P. The actual values of the forge pressures are proprietary to NRC and will not be divulged in this discussion. Other variables including amplitude and the frequency, of values 2mm and 100HZ respectively, were kept constant. The LFW machine comprises of two hydraulic actuators, namely the in-plane actuator and the forge actuator. The lower work piece is inserted in the in-plane actuator which oscillates it in the horizontal direction. The forge actuator applies a download force via the fixed upper work piece to consolidate the joint during the last stage of the process.

3.3 Gleeble Thermo-Mechanical Simulation

Gleeble thermo-mechanical physical simulation was performed to study the effect of strain on the solution heat treated (SHT) material in order to gain a better understanding of the microstructural development during the LFW process. The simulation was performed by using the Gleeble-1500D Thermo-Mechanical Simulation Machine in the Department of Mechanical and Manufacturing Engineering at the University of Manitoba. IN 738 Gleeble specimens of dimensions, 6mm diameter by 10mm length were heated at a rate of 150^{o}C/s to temperatures ranging from 1200^{o}C to 1270^{o}C under thermal cycle alone, as well as with imposed strain to study the effect of forge pressure on the microstructure formed during linear friction welding. In order to measure the temperature during the simulation, thermocouples were spot welded on each cylindrical specimen at the mid section of its length. Gleeble simulated specimens were sectioned at the position of the spot welds and prepared by standard metallographic techniques for microscopy studies.

3.4 Microscopy

Microstructural studies of the linear friction welded specimen, solution heat treated specimen and Gleeble simulated specimens were carried out using the ZEISS Axiovert 25 inverted reflected-light optical microscope equipped with a CLEMEX vision 3.0 image analyzer developed by Clemex Technologies Inc., Longueuil, Canada and JEOL JSM-5900 scanning electron microscope equipped with an Oxford (Oxford Instruments, Oxford, United Kingdom) ultrathin window energy-dispersive spectrometer (EDS) and Inca analyzing software. Re-crystallized grains in welded specimens were investigated by carrying out electron backscatter diffraction (EBSD) based orientation mapping using an HKL Nordlys (EBSD) detector (a product of Oxford Instruments) for EBSD acquisition, which is attached to a PHILIPS XL 30 SEM. The Electron Probe Microanalyzer (EPMA), Cameca SX 100 located at the Department of Geological Sciences was used to perform quantitative analysis of oxides that formed on the weld line during linear friction welding of IN 738.

3.5 Microhardness

Microhardness measurements were taken across the weld joints at an interval of 0.4 mm from the weld line of the linear friction welded specimens with a load of 300 grams using the Buehler microhardness tester.

CHAPTER 4

Results and Discussion

In this chapter, the results of an investigation on the effect of forging pressure on the microstructural response of linear friction welded IN 738 is presented. The findings are presented and discussed in three sections:

4.1 Microstructure of the solution heat treated (SHT) material prior to linear friction welding.

4.2 Microstructure of the linear friction welded specimens.

4.3 The evolution of microstructure in IN 738 due to increased forging pressure during linear friction welding.

4.1 Microstructure of the solution heat treated (SHT) material prior to linear friction welding

Figure 4-1 shows the microstructure of the pre-weld solution heat treated material. The microstructure after this solution heat treatment shows a bimodal distribution of the main strengthening phase in the material consisting of primary γ' precipitates ranging from about 0.4 to 0.8 μm and fine spherical secondary γ' precipitates of about 0.1μm diameter in size (figure 4-1a). Cast solidified products which include MC carbide and γ - γ' eutectic phases were observed to have survived in the material after solution heat treatment (figure 4-1b). This microstructure is consistent with that reported by other investigators on SHT IN 738 material [100, 137].

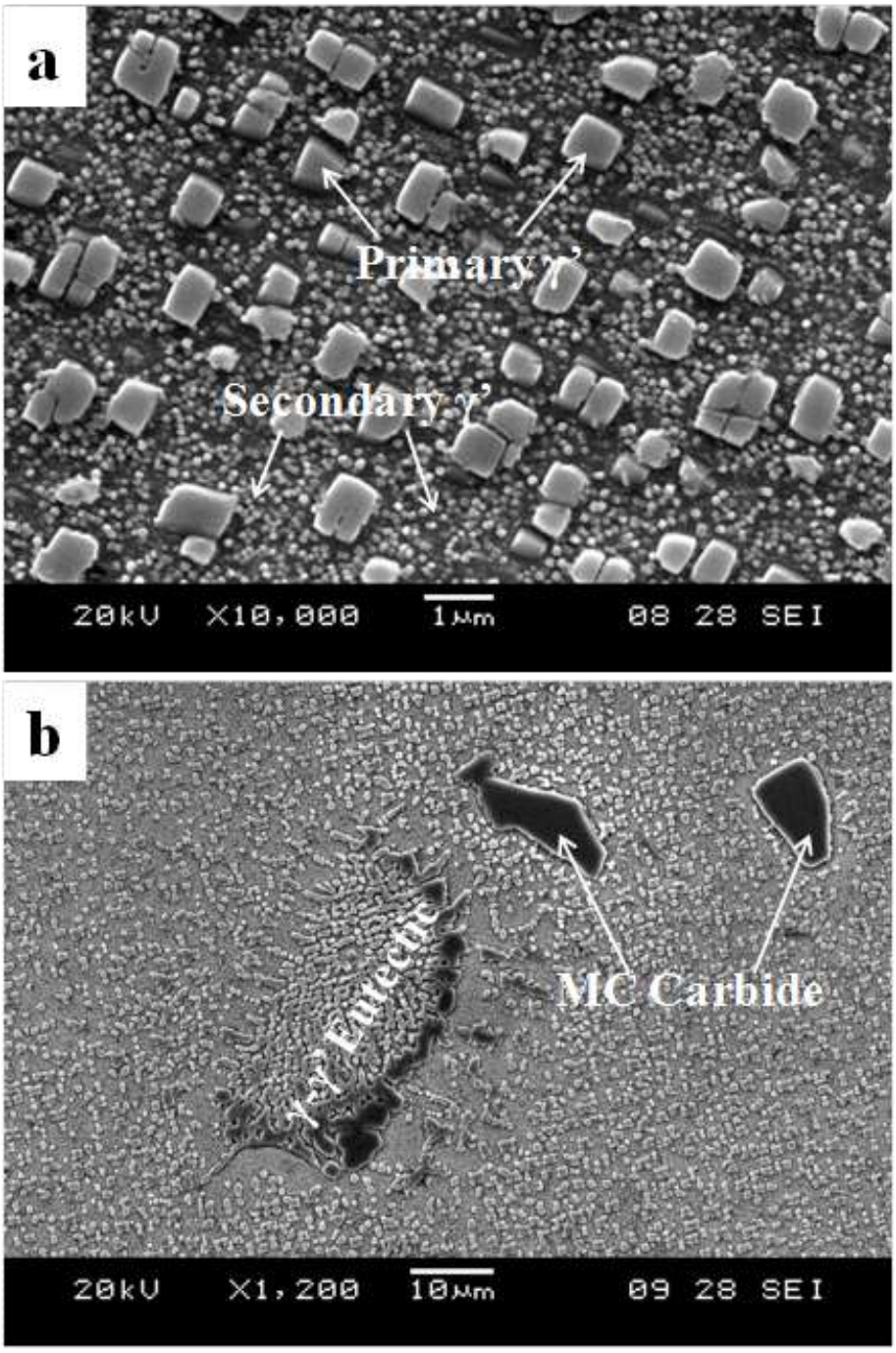

Figure 4-1: (a) SEM micrographs of solution-heat-treated (SHT) IN 738 showing (a) primary and secondary γ' precipitates (b) MC carbide and γ - γ' eutectic phases

4.2 Microstructure of Linear Friction Welded Specimens

Microstructural examination of the linear friction welded IN 738 joints by optical and scanning electron microscopy showed the joints to be devoid of cracking as opposed to cracking normally observed in conventional fusion welds. Figure 4-2 shows a general overview of the linear friction welded joints. The general overview of the linear friction welded joints showed three distinct regions. They include: weld zone (WZ), thermo-mechanically affected zone (TMAZ) and the heat affected zone (HAZ).

4.2.1 Weld Zone Microstructure of Linear Friction Welded Joints

Figure 4-3 represents SEM micrographs of the weld joints showing the weld zone regions of linear friction welded specimens with forge pressures of P, 2.5P and 4P. Complete dissolution of both primary and secondary γ' precipitates occurred in the weld zone regions of the welded specimens. In general, materials adjacent to the weld interface are affected in the same manner regardless of which work piece was oscillated or kept stationary during the joining process [113]. For the specimen welded with a forge pressure of P, the weld zone region extended about 300μm from the weld line into both sides of the base metal (figure 4-2a). Further increase in the forge pressure to 2.5P resulted in a narrower weld zone region of about 200μm (figure 4-2b). The specimen which was welded with the highest forge pressure of 4P, exhibited the smallest weld zone size of about 100μm, extending from the weld line into both sides of the base metal. This showed that as the forge pressure was increased, the weld zone became narrower.

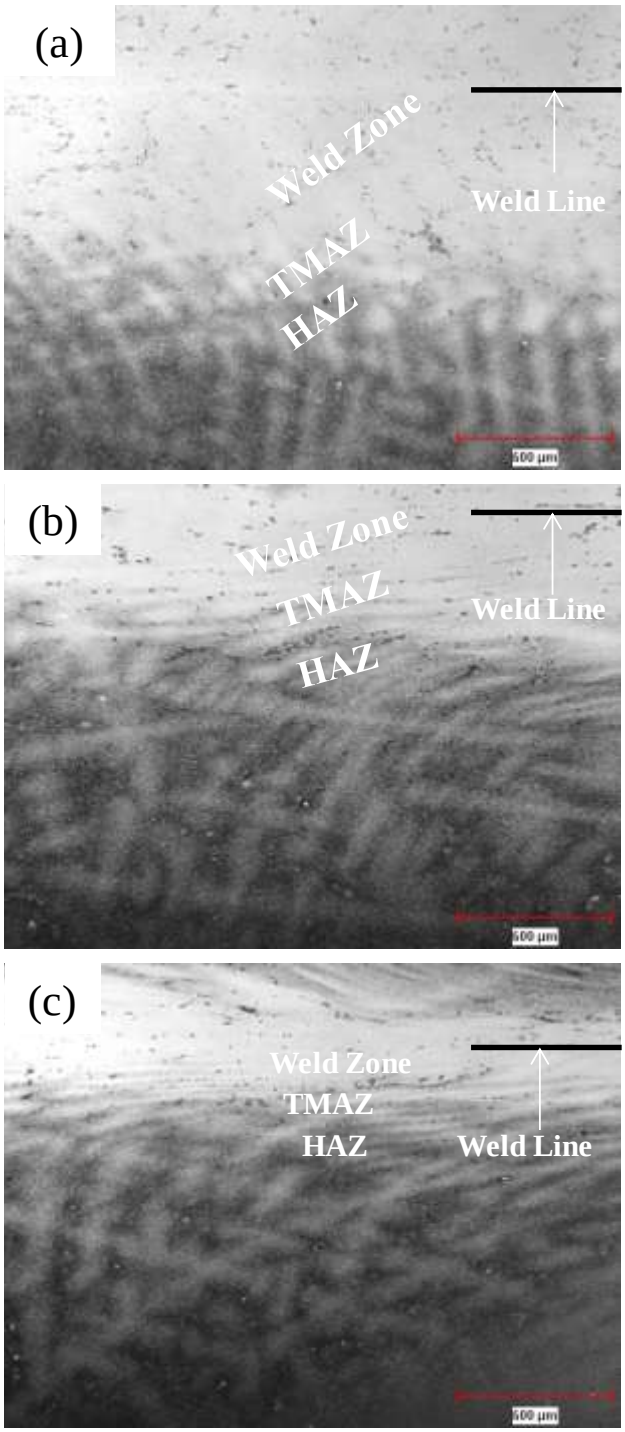

Figure 4-2: Optical micrographs showing WZ, TMAZ and HAZ regions of specimens joined with forge pressures of (a) P (b) 2.5P (c) 4P

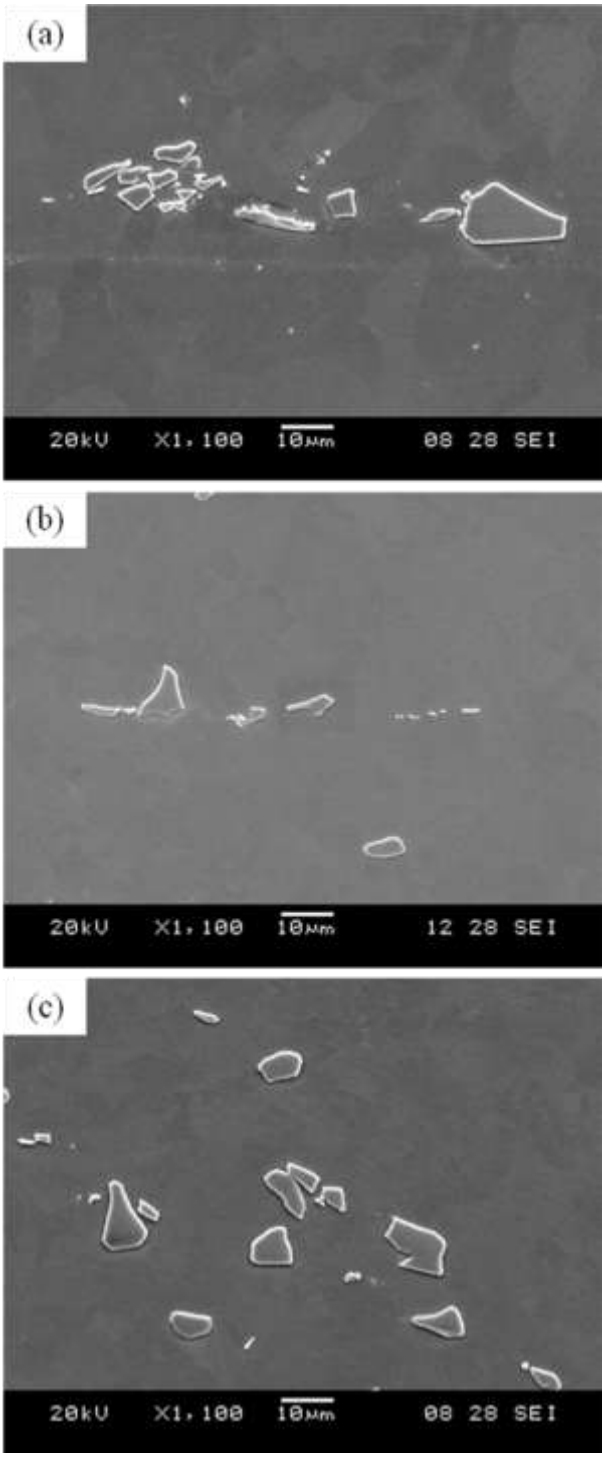

Figure 4-3: SEM micrographs showing complete dissolution of primary and secondary γ' precipitates in the WZ of linear friction welded specimens with forging pressures of (a) P (b) 2.5P and (c) 4P

This observation has perpetually been attributed to more material being expelled out of the weld interface as the forge pressure is increased during linear friction welding of other alloys [109]. Moreover, this may not only be the case as it has been showed in this work that the peak temperature reached during linear friction welding could be playing role in the reduction in size of the weld zone region as the forging pressure was increased. It was observed that the peak temperature decreased with increasing forge pressure. The explanation which supports the reduction in the weld zone in relation to the peak temperature reached in the welded specimens is described in detail in section 4.3.4.

Due to the thermo-mechanical nature of the LFW process, new grains were formed in the WZ and TMAZ regions of the linear friction welded specimens. The LFWed specimens were further characterized based on the observed re-crystallized grains in the weld joint. It was found that in the weld zone regions, the observed re-crystallized grains were uniformly distributed while re-crystallization was localized along prior grain boundaries in the TMAZ (figure 4-4). A discussion on the TMAZ and HAZ regions of the linear friction welded specimens is presented next.

4.2.2 Microstructure of the TMAZ and HAZ Regions of the Linear Friction Welded Specimens

The TMAZ is the region located beyond the weld zone regions of the linear friction welded specimens. The TMAZ was characterized by complete dissolution of gamma prime precipitates. The TMAZ region of the welded specimens extended beyond the weld zone regions and was also characterized by complete dissolution of both primary and

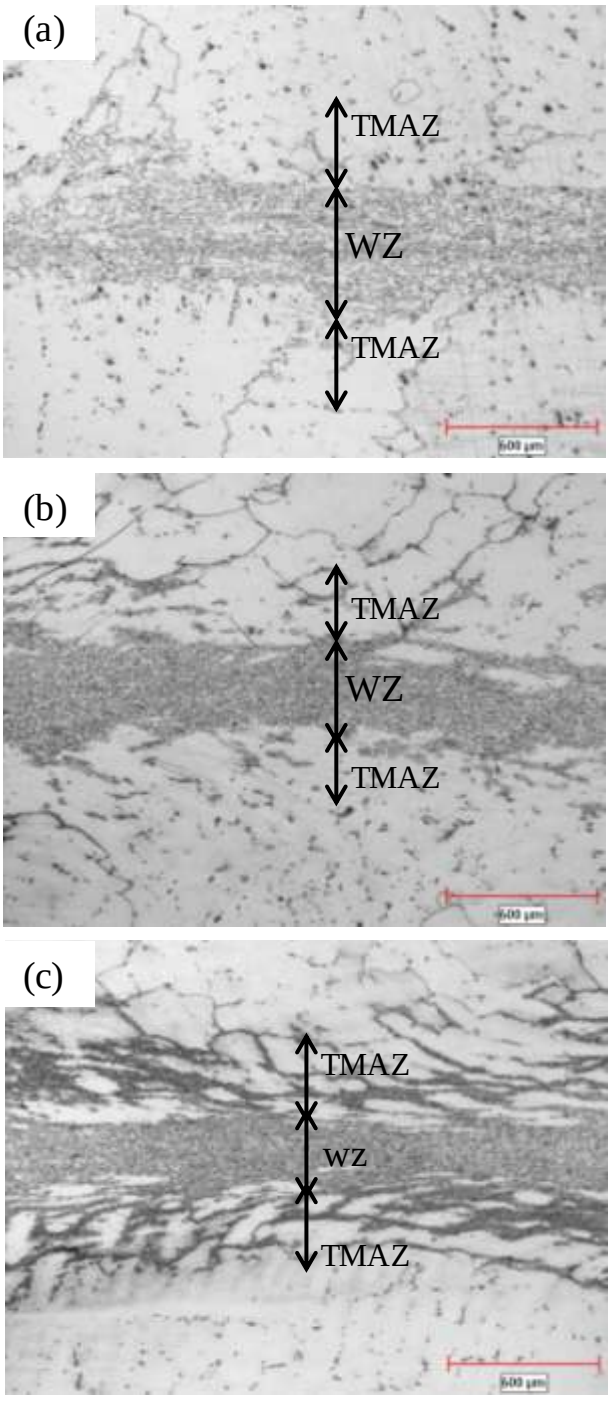

Figure 4-4: Optical micrographs showing re-crystallized grains across linear friction welded specimens with (a) P (b) 2.5P and (c) 4P pressures.

and secondary γ’ particles. Beyond the TMAZ is the heat affected zone (HAZ). In the HAZ region of the welded specimens, complete dissolution of secondary γ’ precipitate particles and partial dissolution of primary γ’ precipitate particles occurred while MC carbides and γ-γ’ eutectics remained. Previous study has shown through Gleeble simulation that compressive strain can assist in the dissolution of γ’ particles [8]. The heat affected zone experienced marginal strain coupled with a relatively lower peak temperature compared to the WZ and TMAZ. Hence the observance of partially dissolved γ’ particles in the HAZ region can be related to insufficient strain induced in the HAZ region coupled with the lower temperature reached in the HAZ. The strain imposed on the specimen during linear friction welding decreases from the weld line into the base metal region. Similarly, the temperature reduces from the weld zone towards the base metal due to heat being conducted away from the weld zone region into the base metal, which could have also influenced the dissolution of the γ’ precipitates. Liquation occurred during linear friction welding, and the consequent result was the formation of eutectics in the TMAZ region of the linear friction welded specimens. A discussion on the microstructural changes in linear friction welded IN 738 superalloy joined with varying forge pressures is discussed next.

4.3 The Evolution of Microstructure in IN 738 due to Increased Forging during Linear Friction Welding

Microstructural changes that occurred during linear friction welding of IN 738 include liquation, re-crystallization and oxidation. The effect of increased forging pressure on these microstructural changes is presented next.

4.3.1 Liquation Related Microstructural Changes in Linear Friction Welded IN 738 Superalloy due to Increased Forging Pressure

To assess the effect of forging pressure on the liquation related microstructure of linear friction welded IN 738, the microstructures of welded specimens with forging pressures of P, 2.5P and 4P were studied. γ-γ' re-solidified eutectic products were observed in LFWed IN 738 specimens, due to liquation that occurred during the joining process. The amount of these re-solidified eutectic products appears to decrease with increasing forge pressure. In addition, oxides, which could detrimentally affect the weld integrity of the LFWed specimens, were observed along the weld line in the welded specimens. These oxides were observed to reduce significantly with increasing forge pressure. A detailed discussion on the phenomena responsible for these microstructural behaviours due to increased forging pressure of LFWed IN 738 superalloy is systematically elucidated in subsequent sections.

4.3.2 Constitutional Liquation during Linear Friction Welding of IN 738 Superalloy

γ' precipitate particles can survive to temperatures above their equilibrium solvus due to rapid heating during the contact phase of linear friction welding. Consequently, γ' precipitate particles can react with the γ matrix through a non-equilibrium eutectic-type reaction to produce liquid by a phenomenon called constitutional liquation which was first reported by Pepe and Savage [34]. The susceptibility of an A_xB_y–type second phase to constitutional liquation can be linked to its dissolution behaviour, in that complete dissolution before reaching the eutectic temperature will hinder the occurrence of liquation. The main strengthening phase of IN 738, which is the γ' precipitate, is reported

to undergo solid-state dissolution during linear friction welding [133]. During the linear friction welding process, the dissolution behaviour of γ' precipitates is anticipated to deviate from equilibrium due to the rapid thermal cycling involved. Based on the initial particle size and heating rate, γ' precipitate particles can survive to temperatures above their solvus as well as the γ- γ' eutectic temperature reaction temperatures of the alloy, due to limited integrated time available for homogenization by diffusion process during rapid heating. The implication of this is that liquid will be produced below the bulk solidus of the alloy due to constitutional liquation of the γ' precipitates. Evidence of liquation was observed in the TMAZ region of welded specimen with a forge pressure of P. Figure 4-5 shows re-solidified eutectic phases in the TMAZ region of the specimen welded with a forge pressure of P. Generally these eutectic products have a lower melting temperature compared to the bulk melting temperature of the alloy. As a result, they may cause incipient melting since they can preferentially melt below the bulk melting temperature of the alloy in service. Incipient melting, which is peculiar to eutectics, renders them undesirable since they can detrimentally affect the mechanical properties of the alloy. The pre-conditions necessary for liquation cracking to occur include grain boundary liquation (a continuous film of liquid) and the existence of tensile stresses which will cause de-cohesion along the relatively weak wetted grain boundary. These two primary factors were not fully complemented in the TMAZ region of the welded specimens. In linear friction welding, one of the two pre-conditions necessary for liquation cracking to occur is satisfied that is the occurrence of grain boundary liquation. Contrary to tensile stresses in fusion welds, compressive stresses are imposed on the work pieces during linear friction welding and may cause liquation cracks to close.

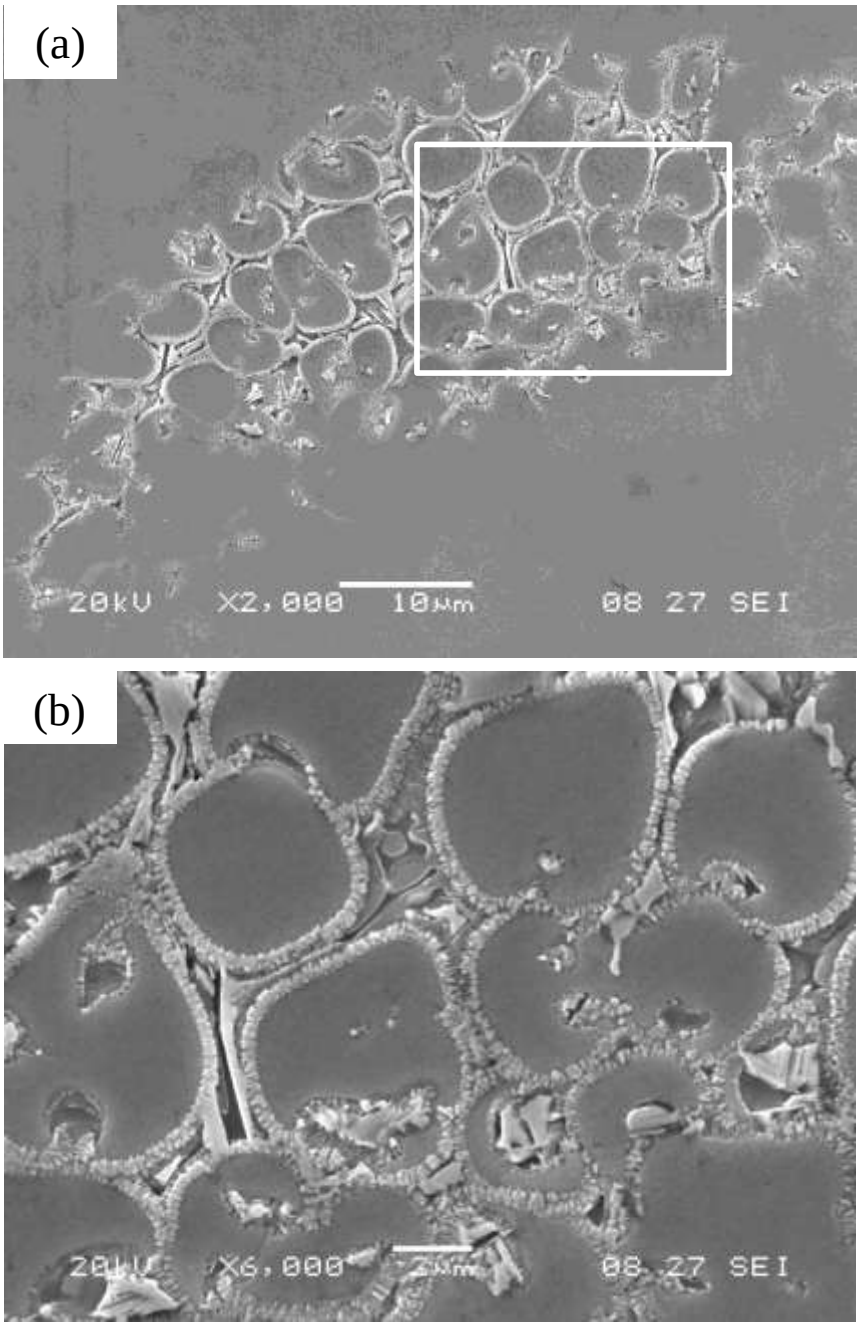

Figure 4-5: SEM micrograph showing (a) liquation in the TMAZ in the specimen welded with P pressure (b) high magnification micrograph showing eutectics and re-solidified in the rectangular region in (a)

Similarly, evidence of liquation was observed in the TMAZ region of the linear friction welded specimen with a forge pressure of 2.5P (figure 4-6). Comparatively, the amount of eutectics observed in the specimen linear friction welded with a forge pressure of 2.5P was smaller than the amount of eutectics observed in the TMAZ region of the welded specimen with a forge pressure of P, which suggests that the forge pressure applied during linear friction welding influenced the amount of eutectics that formed in the TMAZ of LFWed specimens. Detailed observation of the joint microstructure of the LFWed specimen with a forge pressure of 4P showed no trace of any re-solidified products or eutectics in the WZ or TMAZ region as shown in figure 4-7. This result implies that, the amount of re-solidified γ- γ' eutectics observed in the TMAZ regions of the linear friction welded specimens decreased with a corresponding increase in the forge pressure. Essentially, increased pressure during linear friction welding aided in the rapid re-solidification of interdendritic liquid which eventually reduced the formation of re-solidified γ- γ' eutectics in the TMAZ.

Gleeble specimens were processed under rapid heating conditions in order to study in detail the effect of compressive strain on the re-solidification of liquid.

4.3.3 Effect of Forging Pressure on the Solidification of Interdendritic Liquid

The rapid solidification of interdendritic liquid due to imposed compressive strain during linear friction welding was studied using Gleeble simulation. The total time used during linear friction welding of IN 738 is less than 10 seconds. Moreover, the peak temperature reached in the thermo-mechanically affected zone region of IN 738 during linear friction welding has been shown to be not less than 1230^{o}C [8]. Gleeble specimens were rapidly

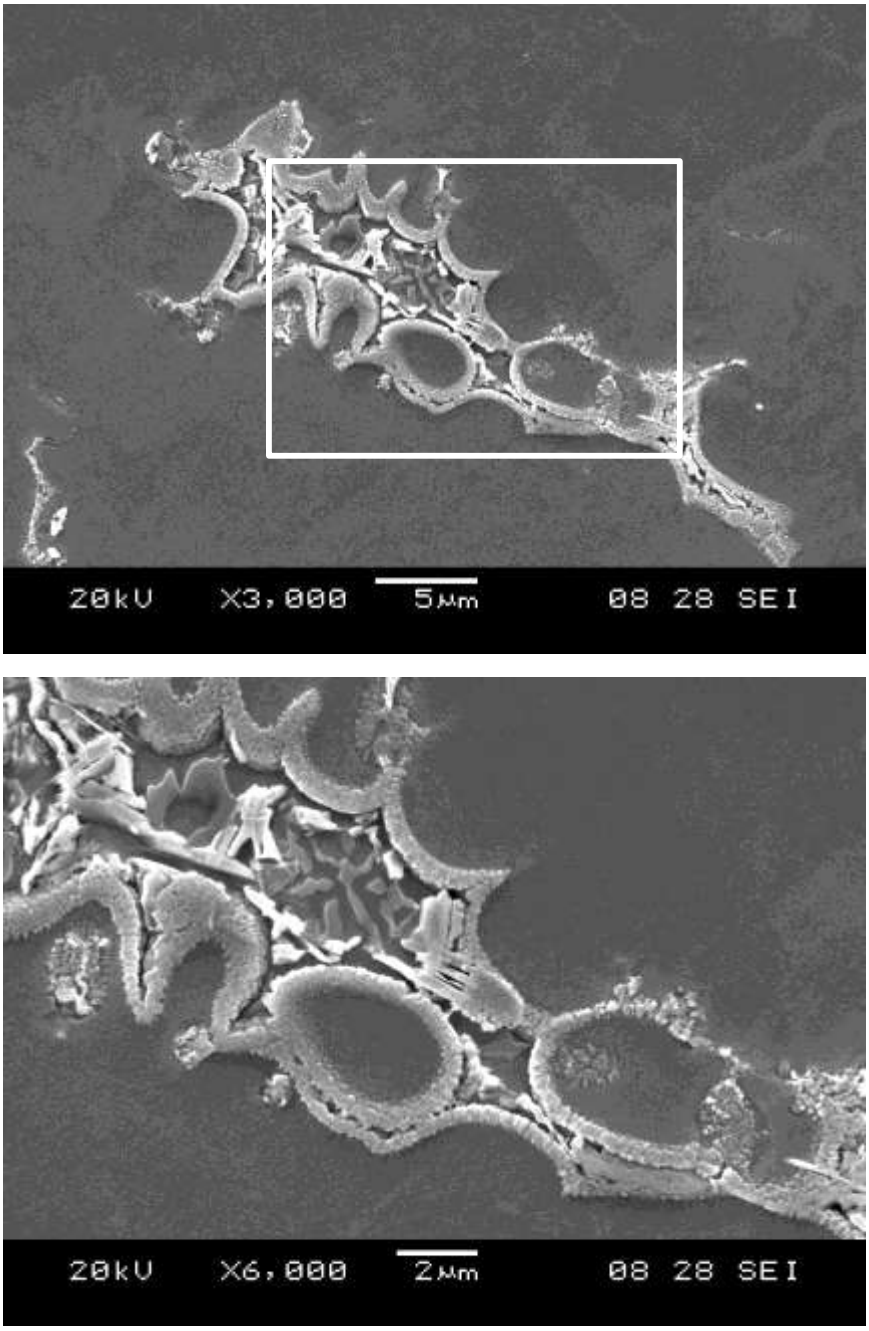

Figure 4-6: SEM micrograph showing (a) liquation in the TMAZ in the specimen welded with 2.5P pressure (b) high magnification micrograph showing re-solidified eutectic products in the rectangular region in (a)

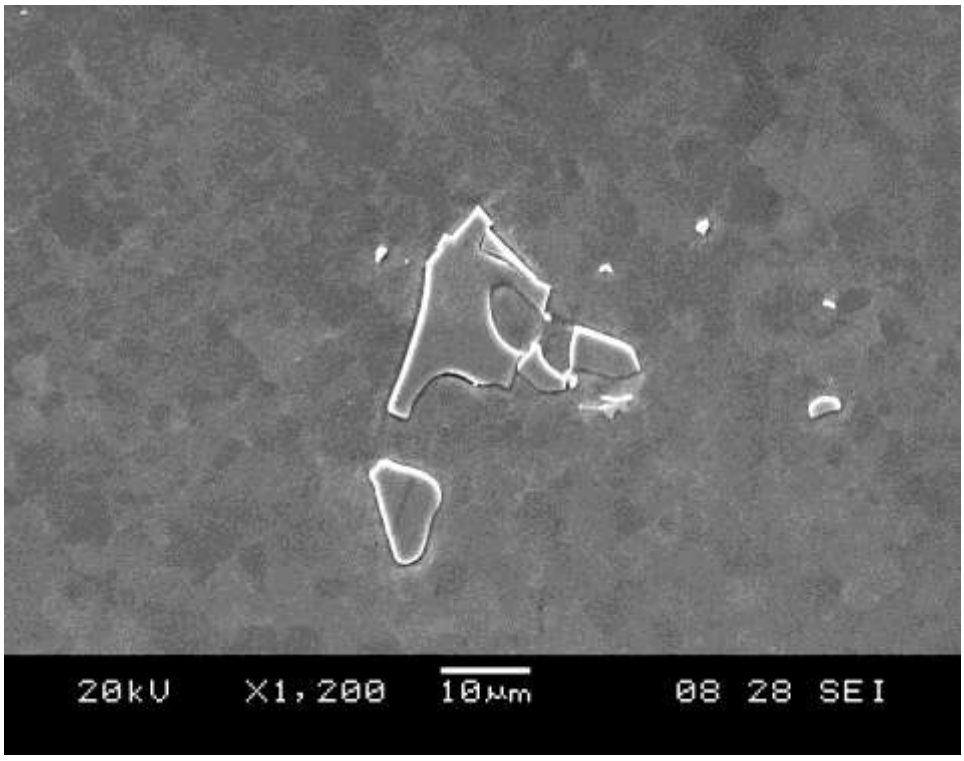

Figure 4-7: SEM micrographs showing the TMAZ region of specimen welded with 4P pressure and devoid of eutectics

heated to 1230^{o}C at a rate of 150^{o}C/sec, held for 2.5 seconds and air cooled. Another specimen was heated at a rate of 150^{o}C/sec to 1230^{o}C and held for 0.5 seconds and a compressive force applied for 2 seconds to achieve a length reduction of 25%. Extensive liquation was observed in the Gleeble simulated specimen under thermal cycle alone (figure 4-8a). In contrast, there was no indication of re-solidified eutectic products in the microstructure of the Gleeble simulated specimen under strain. It can be observed that the imposed compressive strain assisted in rapid re-solidification of interdendritic liquid (figure 4-8b). Figure 4-9 shows SEM micrographs of Gleeble-simulated specimens under thermal cycle and strain, heated at the same peak temperature of 1230^{o}C, while held for 10.5 seconds instead of 2.5 seconds. It is observed that the imposed strain was effective in rapidly re-solidifying the liquid by enhanced back-diffusion (figure 4-9b). It should be noted that remarkable intragranular liquation occurred at 1230^{o}C even after holding for 0.5 seconds prior to applying compressive strain as shown in figure 4-10**.**

It is notable that a thermal gradient develops across the linear friction welded joint such that the temperature decreases away from the weld zone region towards the heat affected zone region. A relatively higher temperature will favour the formation of a large amount of liquid. This suggests that the largest amount of liquid produced in the linear friction welded specimen will be in the weld zone region. However, re-solidified eutectic products were not observed in the weld zone regions of the linear friction welded specimens. It is also notable that a strain gradient exists across the weld joint due to the compressive force applied during the linear friction welding process. This strain variation across the LFWed joint is such that the strain induced in the material decreases away from the WZ region towards the TMAZ region further into the HAZ and eventually into

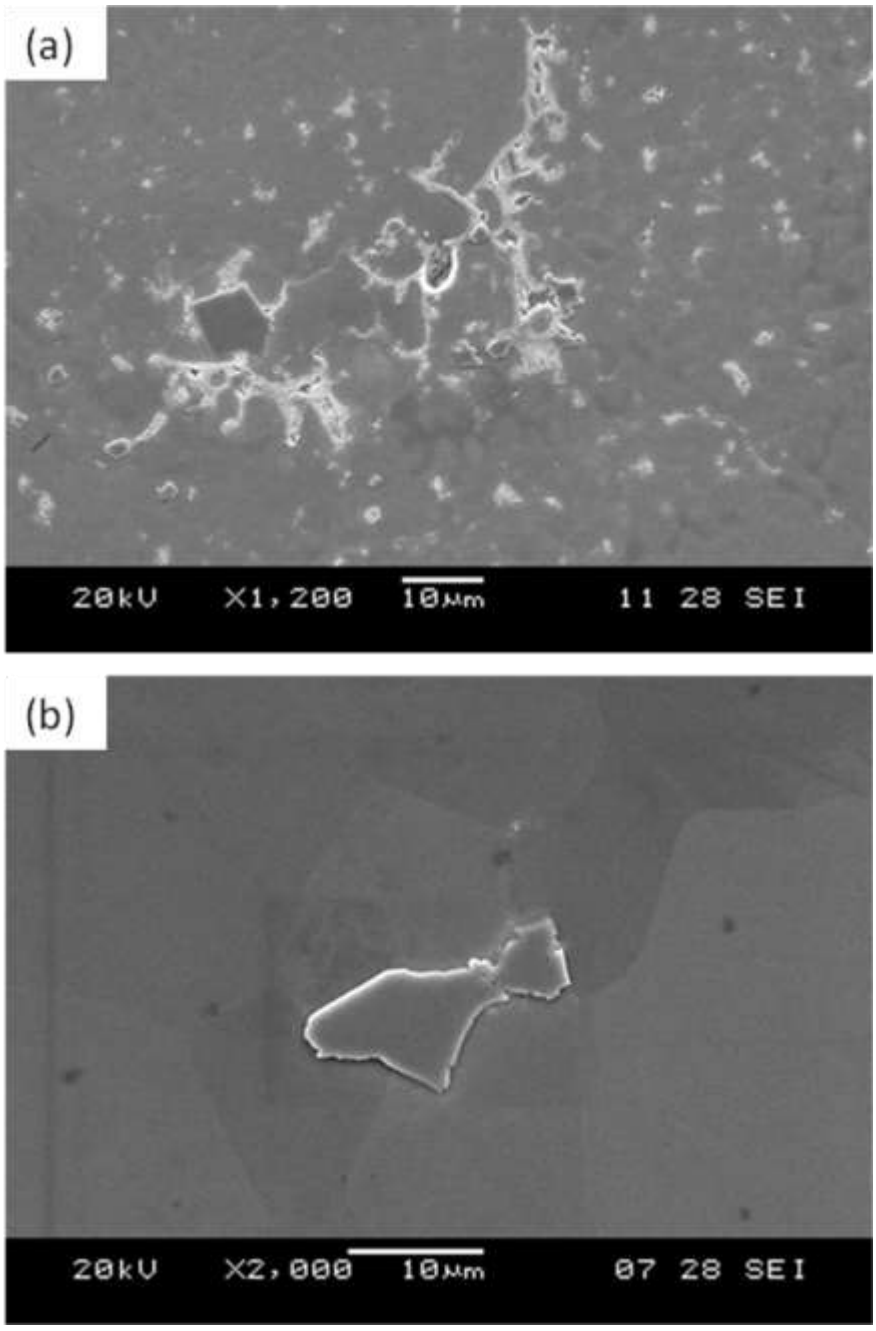

Figure 4-8: SEM micrograph showing extensive liquation in the Gleeble simulated specimen (a) heated at 150^{o}C/sec to 1230^{o}C and held for 2.5 (b) heated at 150^{o}C/sec to 1230^{o}C and strained to achieve a length reduction of 25%

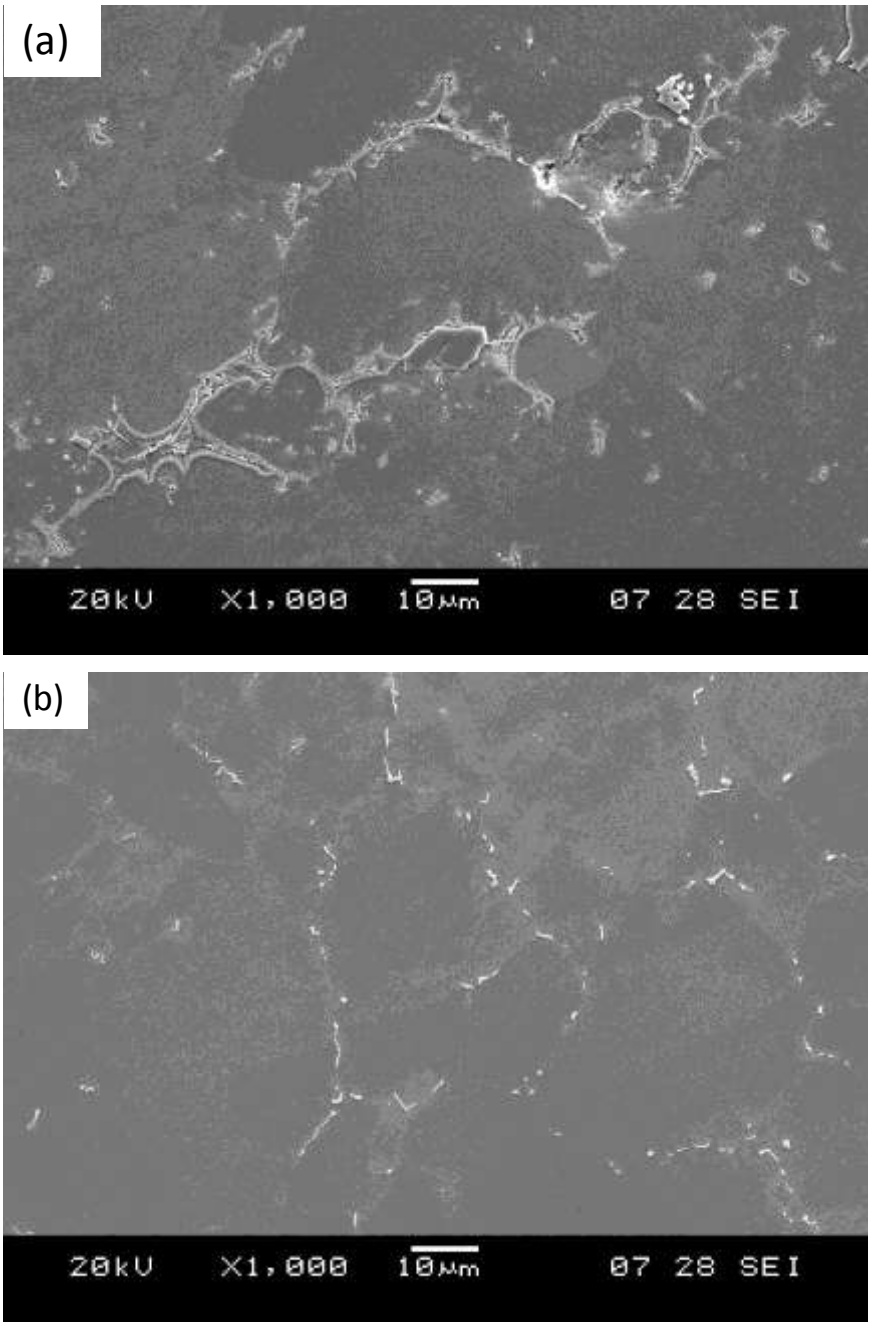

Figure 4-9: Gleeble simulated specimen heated at 150^{o}C/sec and held for 10.5 sec at 1230^{o}C followed by air cooling; showing (a) intergranular re-solidified products under thermal cycle alone (b) absence of re-solidified products when 25% length reduction was imposed

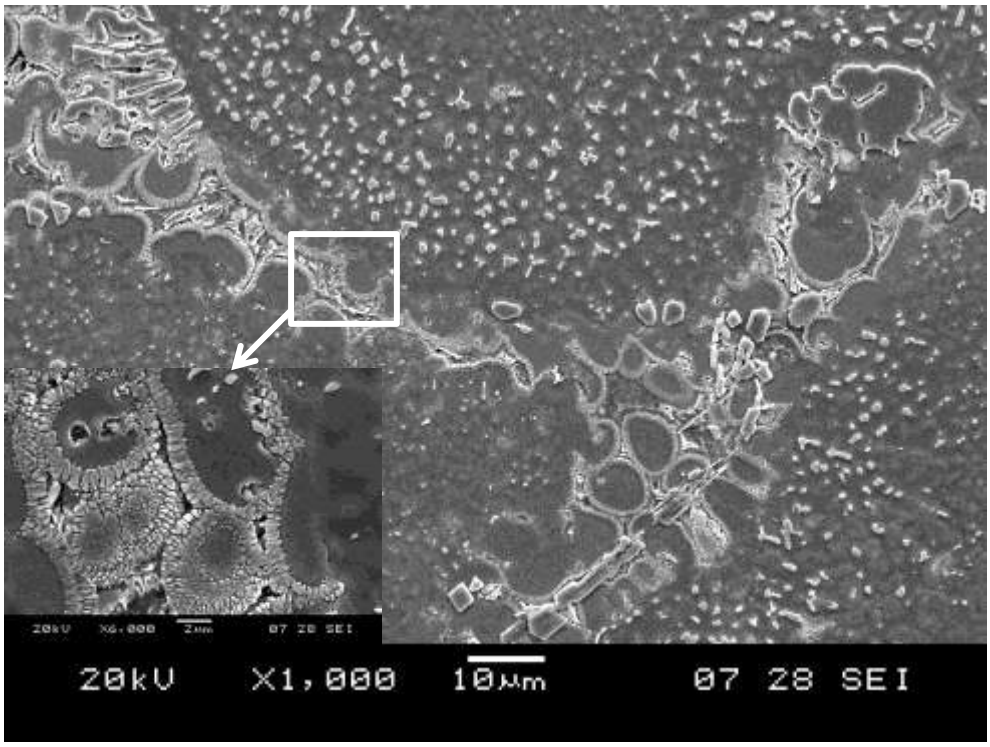

Figure 4-10: SEM micrograph showing extensive liquation in the Gleeble simulated specimen heated at 150^{o}C/sec to 1230^{o}C and held for 0.5 sec with inset showing a high magnification of re-solidified products

the base metal. This means that the microstructure in the TMAZ region experienced a lesser degree of strain as compared to the weld zone region. Hence, the re-solidification of interdendritic liquid would have been more effective in the WZ region than in the TMAZ region due to the effect of imposed stress. The explanation for this form of behaviour, with regards to the nil observance of eutectics in the weld zone region, can be related to a relatively higher strain induced in the weld zone region which ensured efficient rapid re-solidification of interdendritic liquid than in the TMAZ. It is known that meta-stable liquid solidification, as is the case during linear friction welding, is a diffusion dependent process which involves the diffusion of solute atoms. Fick's first law, which is related to diffusion, is stated mathematically as:

$$J = -D\frac{dc}{dx} \quad \text{(4.1)}$$

where J is the flux, D is the diffusivity or diffusion coefficient, and dc/dx is the concentration gradient.

The kinetics that affect the diffusion process are dependent on the temperature and the concentration gradient. The Arrhenius equation, which shows the relationship between the diffusivity and temperature, is given as:

$$D = D_O \exp\left(\frac{-Q}{KT}\right) \quad \text{(4.2)}$$

where Q is the activation energy, D_o is the pre-exponential factor, K is the gas constant and T is the absolute temperature. In most alloys, solute diffusion can occur through lattice diffusion, pipe diffusion through dislocations, grain boundaries, surface defects etc [114]. In principle, during plastic deformation of an alloy, solute atoms diffuse mainly within the matrix through lattice diffusion and pipe diffusion. Pipe diffusion of solute atoms can be enhanced by the movement of solute atoms via dislocation cores. It is

known that plastic deformation of an alloy introduces dislocations into the system. In essence, high temperature plastic deformation, will result in a drastic increase in the dislocation density, which in turn will facilitate the movement of solute atoms via dislocation cores. Recent study has shown that high temperature plastic deformation can also lead to the production of vacancies in metals [131]. Lattice diffusion mechanism of substitutional atoms is based on vacancy formation and migration. Hence, the production of excess vacancies will enhance solute diffusion. The following relation was developed for the deformation-induced supersaturated vacancy-enhanced solute diffusion coefficient D_i^{V} and the excess vacancies created through plastic deformation [127];

$$D_{\mathrm{i}}^{\mathrm{V}} = D_{\mathrm{i}}^{\mathrm{th}} \frac{(C_{\mathrm{v}}^{\mathrm{th}} + C_{\mathrm{v}}^{\mathrm{ex}})}{C_{\mathrm{V}}^{\mathrm{th}}} \quad \text{.....(4.3)}$$

where $D_{\mathrm{i}}^{\mathrm{th}}$ is the thermal diffusion coefficient, $C_{\mathrm{v}}^{\mathrm{th}}$ is the thermal equilibrium vacancy and $C_{\mathrm{v}}^{\mathrm{ex}}$ is the deformation-induced excess vacancy.

Similarly, the pipe diffusivity is also given by the relation:

$$D_{\mathrm{i}}^{\mathrm{P}} = D_{\mathrm{i}}^{\mathrm{th}} \exp\left(\frac{Q_{\mathrm{th}} - Q_{\mathrm{p}}}{kT}\right) \quad \text{.....(4.4)}$$

where Q_{p} is the activation energy for pipe diffusion, Q_{th} is the lattice activation energy. However, the overall deformation-enhanced solute diffusivity D_i^{T} which is a function of the pipe diffusivity and deformation-induced supersaturated vacancy-enhanced solute diffusion coefficient is given by [138]:

$$D_{\mathrm{i}}^{\mathrm{T}} = D_{\mathrm{i}}^{\mathrm{v}} \mathrm{x}\,(1-\mathrm{g}) + D_{\mathrm{i}}^{\mathrm{p}} \mathrm{x}\,\mathrm{g} \quad \text{.....(4.5)}$$

where g is ratio of solute atoms associated with the dislocation, which can diffuse via the dislocation core. This implies that a higher magnitude of deformation will result in a

larger amount of vacancies and dislocation cores which can enhance solute diffusion. Since the specimen welded with a forge pressure of 4P experienced the largest amount of deformation, it can be assumed that solute diffusion would have been most enhanced and as a result, the rapid re-solidification of interdendritic liquid most favoured. Cowern et al and other investigators [106, 130] have shown that applying compressive pressure can generally enhance atomic diffusion. For vacancy-assisted diffusion, the Arrhenius equation can be expanded as [139]:

$$D = \frac{1}{6} d^2 Z v \exp\left[\frac{(\Delta S_f + \Delta S_m)}{k}\right] \exp\left[\frac{-(\Delta H_f + \Delta H_m)}{kT}\right] \text{.....(4.6)}$$

where, d is the inter-atomic distance, Z is the coordination number, v is the vibrational frequency of an atom along its reaction path, ΔS_f and ΔS_m are the vacancy formation and migration entropies respectively, and ΔH_f and ΔH_m are the vacancy formation and migration enthalpies respectively. The first exponent and the parameters before it represent D_o in equation 2.2 whereas $(\Delta H_f + \Delta H_m)$ of the second exponent represents the activation energy, Q. Since the activation energy can be influenced by pressure, it can be inferred that the diffusivity is also dependent on pressure. A relationship was developed between the activation energy per unit strain, Q, and the diffusion coefficients without strain, D (relax) and under strain D (strain), and is expressed by the following equation [106]:

$$D\ (strain) = D\ (relax) \exp\left(\frac{-Q'}{kT} s\right) \text{..... (4.7)}$$

where k is a constant, s is the strain (negative for compression and positive for tension). From equation 4.7, it is evident that atomic diffusion can indeed be enhanced by

compressive strain. Therefore, the compressive force induced during linear friction welding will essentially aid the rapid re-solidification of liquid.

Another noticeable phenomenon that was observed during linear friction welding is re-crystallization. This observation provides substantial information about the variation in weld temperature with forging pressure during linear friction welding. Next is a discussion on the re-crystallization analysis obtained by carrying out electron backscatter diffraction based orientation mapping.

4.3.4 Effect of Forging Pressure on Weld Temperature during Linear Friction Welding

Due to the thermo-mechanical nature of the linear friction welding process, dynamic re-crystallization occurred during the joining process. Re-crystallization is a solid-state phenomenon that involves the production of new stress free grains through nucleation and growth processes. Dynamic re-crystallization is used to improve the mechanical properties of several alloys through the production of fine grains in materials. Generally, the factors, which affect dynamic re-crystallization, include strain rate, temperature, time and the magnitude of strain. Among these factors, it has been reported that high strain and low temperature are best suited for achieving finer grains in metals [118-125].

In order to perform a detailed analysis of the re-crystallized grains, electron backscatter diffraction based orientation imaging microscopy was performed. A representative example of the EBSD map in the weld zone of the specimen linear friction welded with a forge pressure of P is shown in figure 4-11. As stated earlier, and shown in the EBSD map of the welded specimen with a forge pressure of P (figure 4-11), the weld zone

region extended about 300μm from the weld line into the base metal on both sides of the weld line. In the weld joint of the linear friction welded specimen with a forge pressure of 2.5P, the weld zone extended about 200μm from the weld line into both sides of the base metal as shown in the EBSD map **(**figure 4-12**)**. This indicates that the weld zone region became narrower when the forge pressure was increased from P to 2.5P such that the specimen welded with the highest pressure, 4P had a weld zone of about 100μm, as shown in the EBSD map (figure 4-13). Figure 4-14 shows a plot of the average grain size against forge pressure of the linear friction welded specimens. It can be seen that as the forge pressure was increased, the average re-crystallized grain size decreased. This can be linked to the reduction in the weld zone regions as the forge pressure was increased during linear friction welding.

Grain growth is usually favoured at high temperature. If the forge pressures were kept constant while the peak temperatures attained in the specimens were varied, then the specimen with the highest peak temperature will record the largest grain size since grain growth would have been more favourable. Since, the average re-crystallized grain size decreased with increasing forge pressure, it can be deduced that the peak temperature reached during linear friction welding decreased as the forge pressure was increased. This is consistent with findings which revealed, that the weld temperature decreases as forging pressure increases during linear friction welding [109,126]. An increase in the peak temperature will warrant the production of a large amount of liquid. In relation to the linear friction welded specimens, it can be deduced that the peak temperature was highest in the specimen linear friction welded with a forge pressure of P. Hence, the linear friction welded specimen with the highest forge pressure 4P, would have experienced the

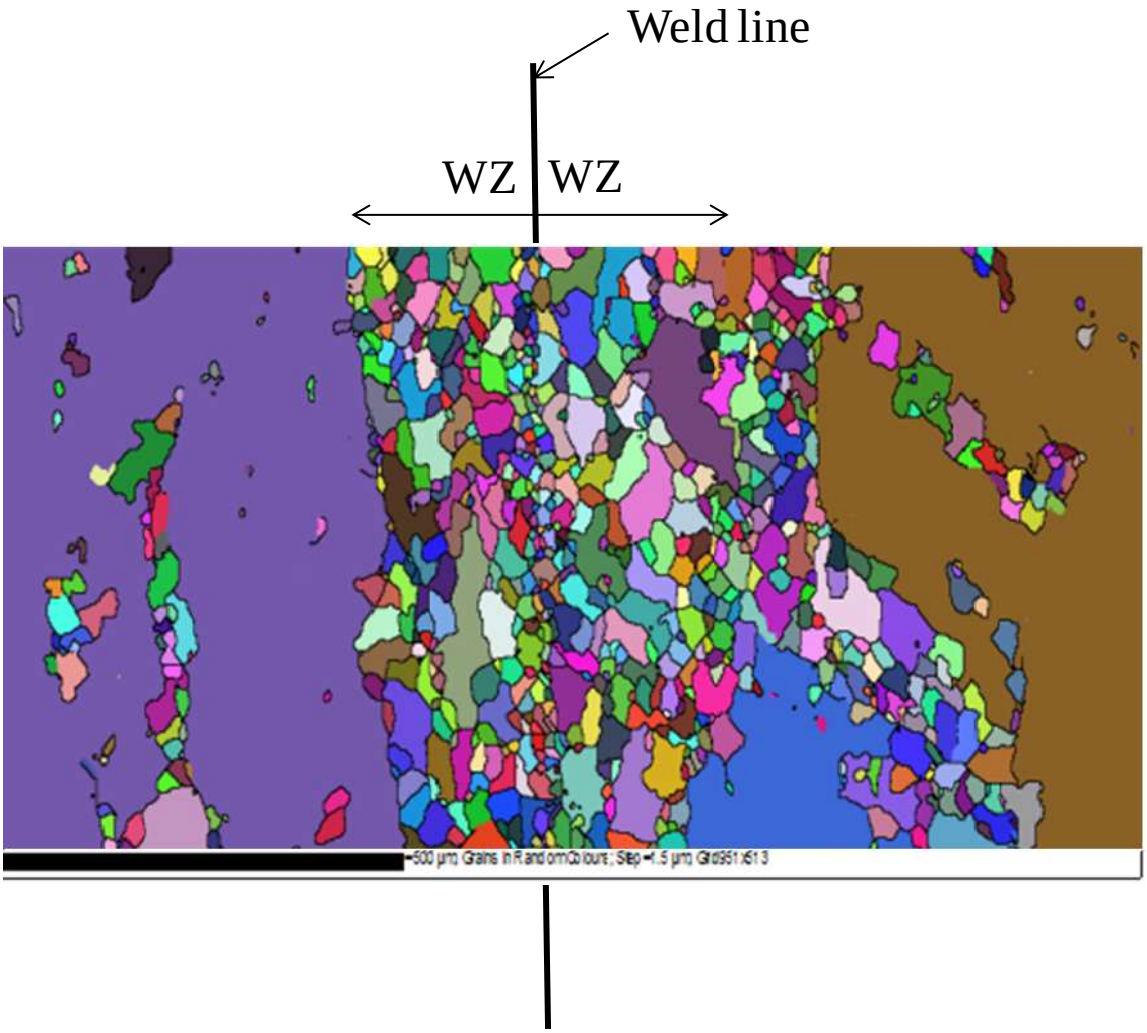

Figure 4- 11: EBSD map showing re-crystallized grains across the WZ and TMAZ regions of specimen linear friction welded with P pressure.

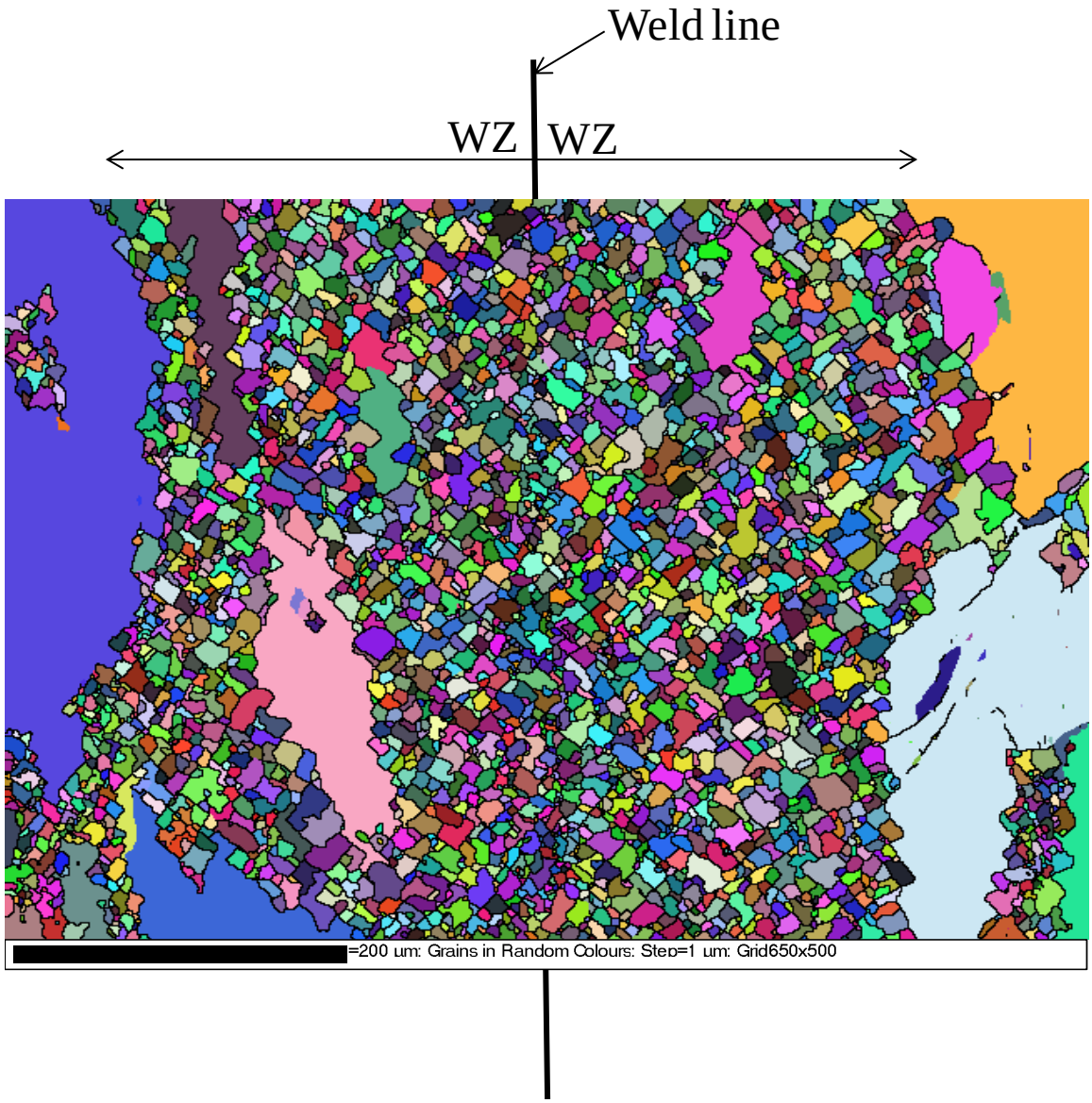

Figure 4-12: EBSD map showing re-crystallized grains across the WZ and TMAZ regions of linear friction welded specimen with 2.5P.

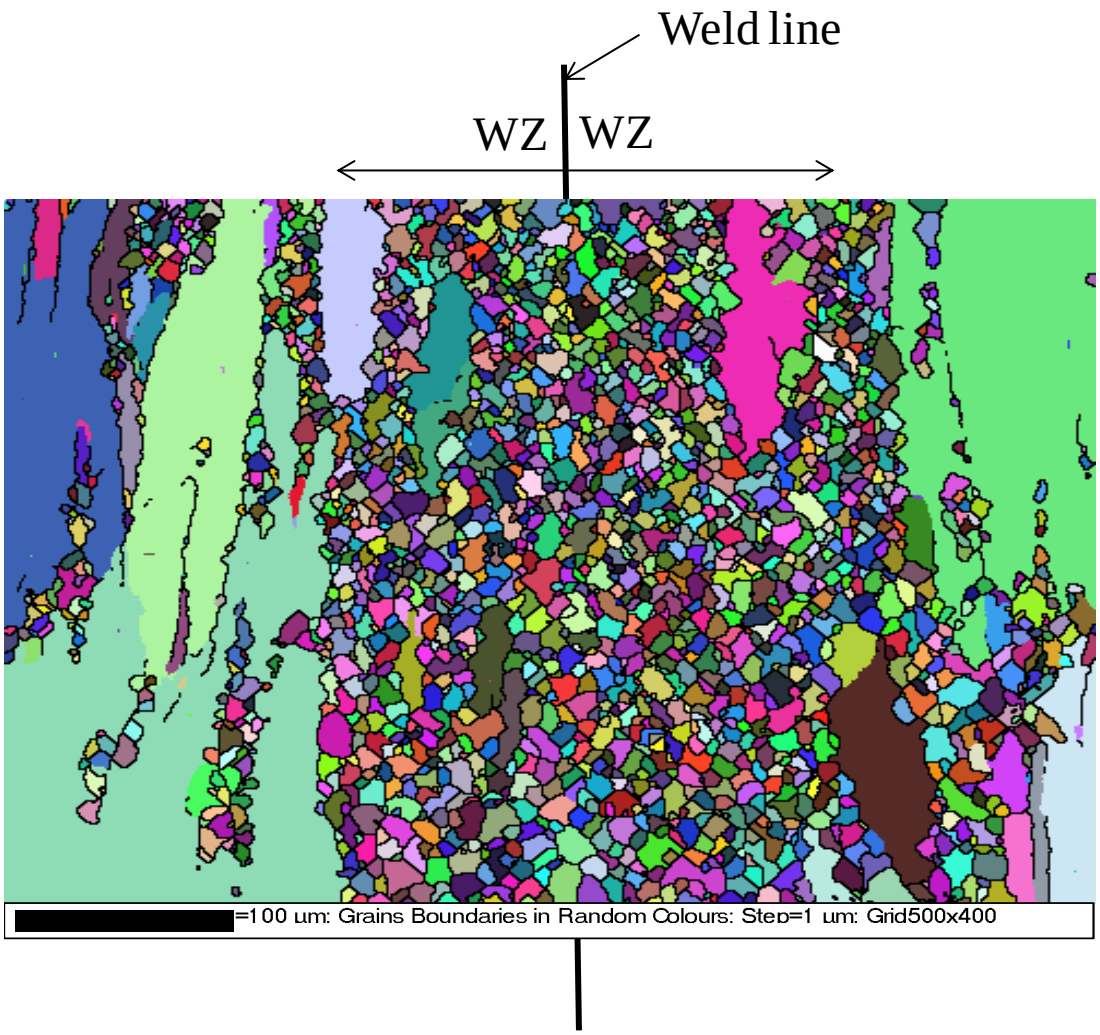

Figure 4-13: EBSD map showing the re-crystallized region across the WZ and TMAZ region of specimen linear friction welded with 4P pressure.

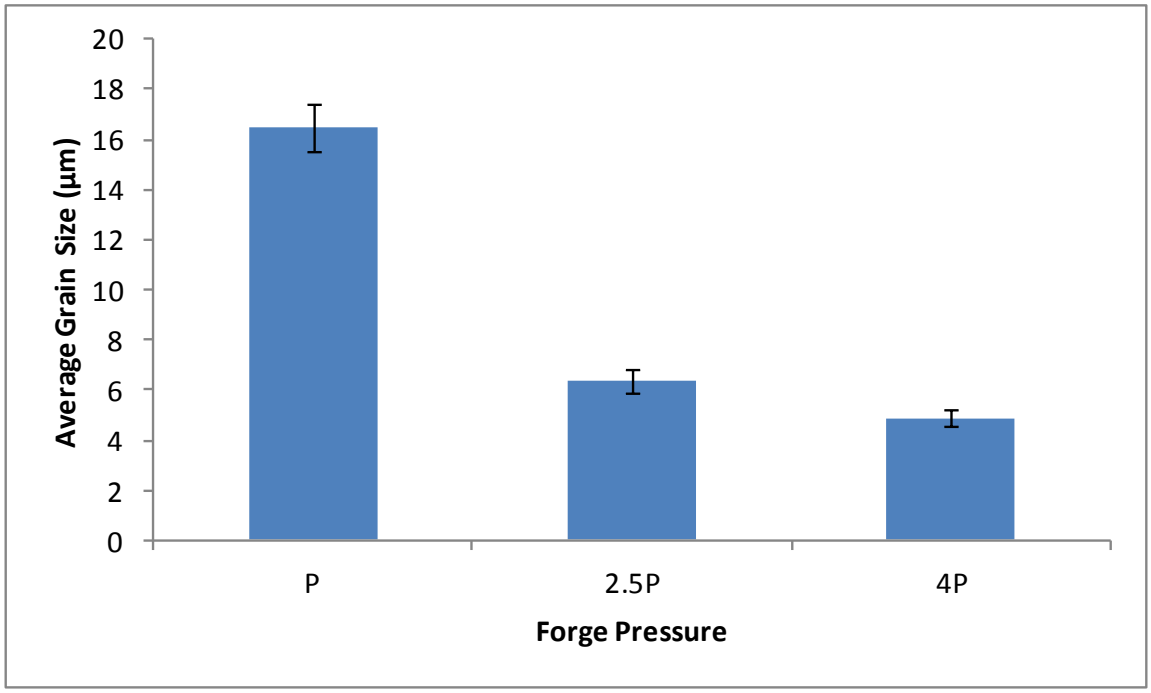

Figure 4-14: Bar chart showing the average re-crystallized grain size with forge pressure.

least peak temperature during joining. As a result, the amount of liquid that formed during joining of the specimens could have decreased with increasing forge pressure. This implies that the extent of liquation that could have occurred during linear friction welding of specimen joined with a forge pressure of 4P would significantly be less compared to the extent of liquation that would have occurred in the specimen joined with a forge pressure of P. As discussed earlier, the amount of liquid produced thus likely reduced as the forge pressure was increased. In addition, the rapidity with which liquid would solidify will increase with increasing forge pressure due to strain enhanced diffusion. This implies that the conditions required to enhance the elimination of re-solidified eutectics was dominant in the linear friction welded specimen with the highest forge pressure, 4P. As a result, no eutectics were observed in the microstructure of the specimen joined with a forge pressure of 4P. This explanation correlates with why the amount of eutectics decreased with increased forging pressure during linear friction welding.

The microhardness measurements across the weld joints of the LFWed specimens provide additional insight into the reduction of the amount of eutectics as the forge pressure was increased. The result of the microhardness measurements is presented next.

4.3.5 Hardness Test Measurements

Hardness measurements were taken across the weld joints of the linear friction welded specimens. It was observed that the hardness increased in the weld zone and thermo-mechanically affected zone regions than in the base metal region of the linear friction welded specimens. The trend in change in hardness in the weld joint was also observed in

a linear friction welded IN 738 specimen [100]. In general, it is known that a re-precipitation of ultra fine gamma prime particles takes place during cooling after a complete dissolution of gamma prime particles occurs in IN 738 [18]. Ultra-fine gamma prime particles can cause an increase in hardness of the material and may be responsible for the increased hardness in the WZ and TMAZ regions of LFWed specimens. This observation is in agreement with a previous research on dissimilar inertia friction welding of two Ni-based superalloys IN 718 and RR1000, where they reported an increase in hardness to be caused by the re-precipitation of very fine tertiary γ' particles during weld cooling of RR1000 [129]. Figure 4-15 compares hardness measurements taken at regular intervals within 0.4 mm from the weld line of the linear friction welded specimens. The results showed that the hardness increased with increasing forge pressure in the regions where complete dissolution of γ' particles was observed. As earlier stated, the amount of re-solidified eutectics decreased in the TMAZ of the linear friction welded specimens as the forge pressure increased such that no re-solidified eutectics were observed in the weld microstructure of the linear friction welded specimen with a forge pressure of 4P. The re-solidified eutectics formed by the re-solidification of interdendritic liquid produced by non-equilibrium reactions between the γ' particles and γ matrix. This implies that the re-solidified eutectics were formed from γ' forming elements. Since the amount of eutectics reduced as the forge pressure was increased, it is possible that more γ' forming elements, that would have been used in the formation of these eutectics, were in turn utilized in forming ultra fine γ' particles which increased the hardness in the WZ and TMAZ. Hence, the volume fraction of the very fine γ' particles would be higher in the TMAZ regions of the linear friction welded specimens as the forge pressure is increased.

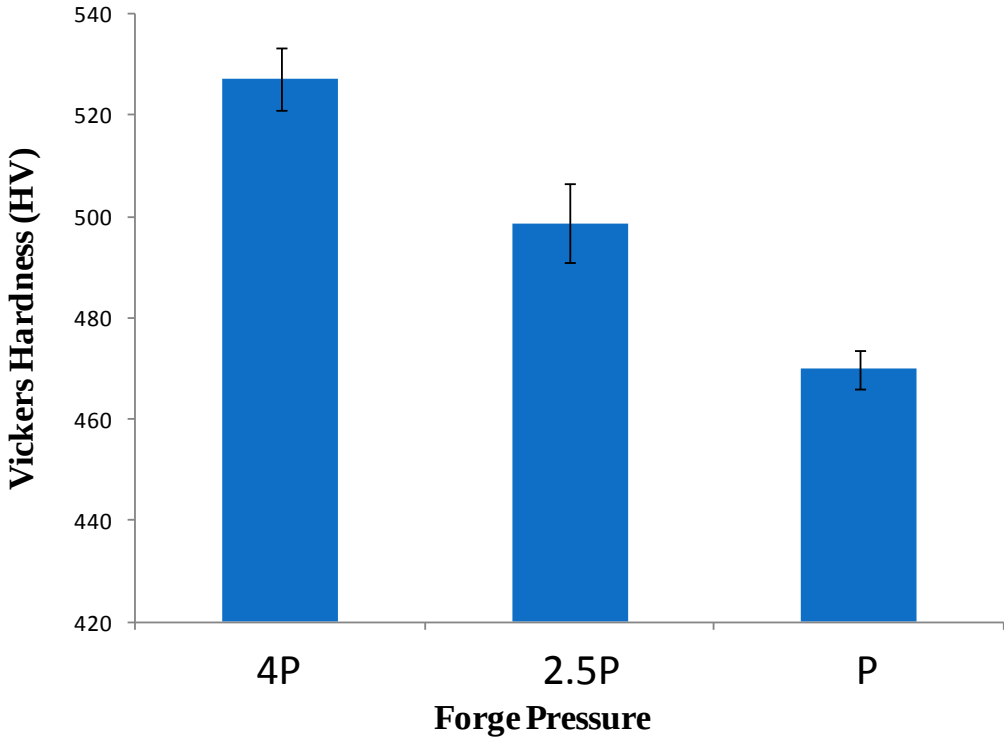

Figure 4-15: Hardness results taken in the weld zone regions of the linear friction welded specimens.

Liquation cracking is generally considered to be a phenomenon that does not occur during friction welding. On the contrary, cracks associated with re-solidification products were observed during linear friction welding and the factors, which contributed to this observation is discussed next.

4.3.6 Liquation Related Cracking during Linear Friction Welding

The process of linear friction welding involves the rubbing of two work pieces against each other in order to produce frictional heat. At the last stage of the joining process, a forging pressure is applied to consolidate the work pieces. During the equilibrium phase of the linear friction welding process, axial shortening starts as a result of plasticised layer being expelled from the weld interface. The expelled plasticised layer forms a flash at the periphery of the joints, which normally appears to have exfoliated from each other. Figure 4-16 shows an optical micrograph of the flash formed as result of plasticised material being forced out of the interface during linear friction welding with a forging pressure of 2.5P. Detailed microstructural study revealed some of the cracks in the flash region to be associated with re-solidified products (figure 4-17). The preponderance of compressive stresses at the weld joint region of the linear friction welded specimens, due to the compressive strain induced in the weld joint as a result of the forging pressure applied during the terminal stage of the joining process, aided in the preclusion of cracks in the weld region. In contrast, tensile stresses are usually induced in the flash region of the linear friction welded specimen. Numerical simulation of the stress distribution in a material under compressive axial loading, analogous to the forging pressure imposed during linear friction welding, has revealed that most of the material is subjected to

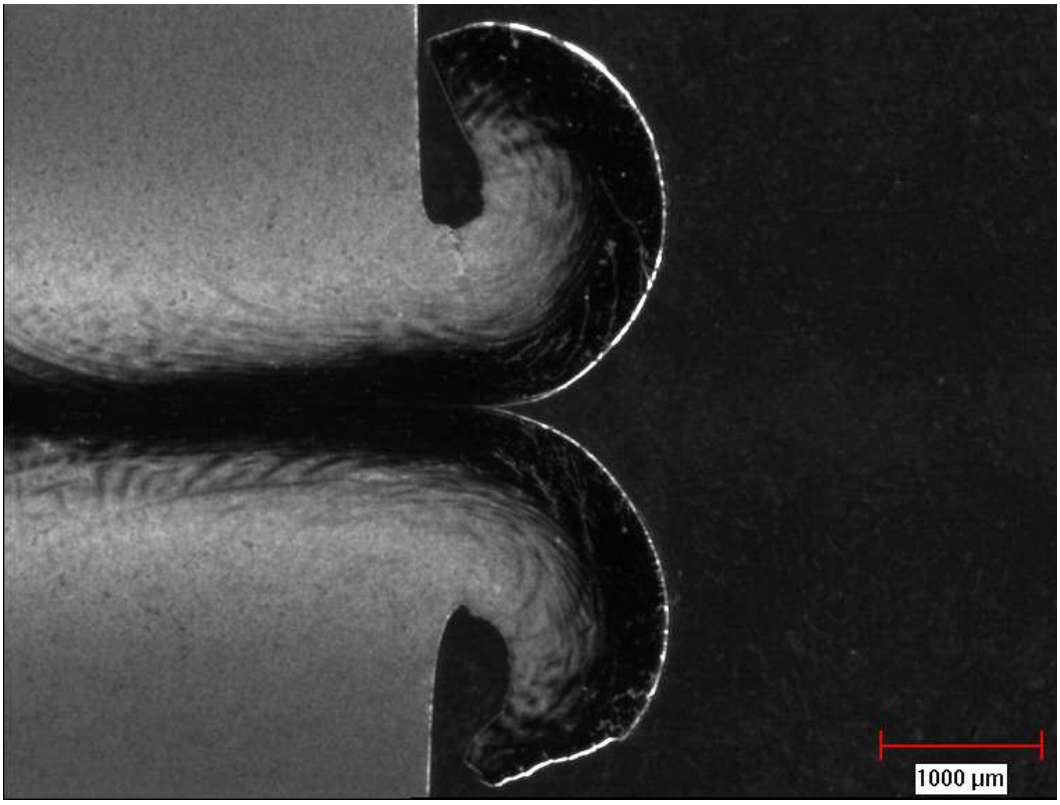

Figure 4-16: Shows an optical micrograph of flash formed of the linear friction welded specimen with 2.5P pressure.

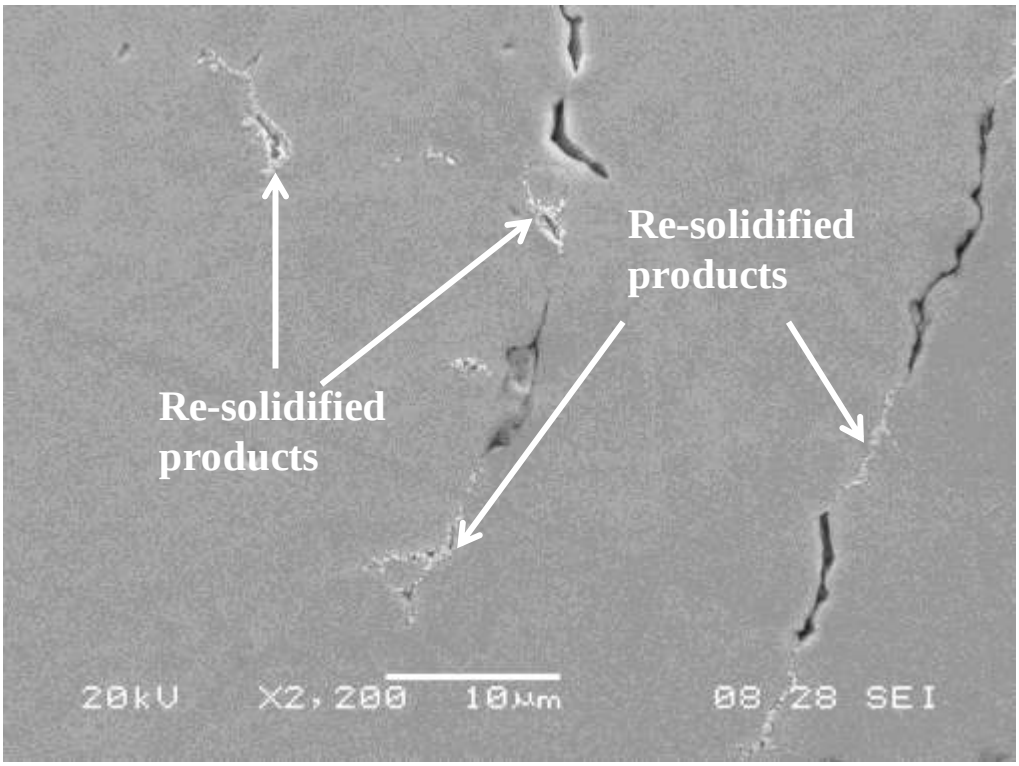

Figure 4-17: Liquation in the flash region of the linear friction welded specimen with 2.5P pressure.

compressive stresses, while tensile stress is mainly concentrated in regions extruded away from the joint [132]. The observance of cracks associated with re-solidified products in the flash region suggests that the conditions required for the occurrence of liquation cracking, both metallurgical and mechanical, may have been satisfied in the flash region. These conditions include sufficient wetting of the grain boundaries by liquid and occurrence of tensile stresses along liquated grain boundaries, and resulted in de-cohesion along one of the solid-liquid interface. Albeit the occurrence of cracking in the flash, it must be emphasized that the flash will be grounded off and may not pose any problems in practical applications of the service component.

Even though cracking did not occur in the weld zone region, another detrimental feature observed, was oxidation along the weld line of linear friction welded specimens. A discussion on oxidation during linear friction welding of IN 738 is presented next.

4.3.7 Weld Line Oxidation during Linear Friction Welding of IN 738 Superalloy

Notwithstanding, the strain induced rapid solidification of the liquated phases, continuously distributed oxide formed along the weld line of the linear friction welded specimens with forging pressure of P and 2.5P. These oxides were observed at about 2000μm to 3000μm away from the middle of the weld line towards the periphery of the LFWed specimens. The morphology as well as the SEM/EDS spectra of the oxide on the weld line of the linear friction welded specimen with a pressure of P is shown in figure 4-18. Electron probe microanalysis of the continuous phase oxide which formed along the weld line revealed that it was mainly rich in aluminium (Table 4-1). In order to understand the type of oxidation that occurred on the weld line of IN 738 during linear

friction welding, Gleeble specimens physically simulated under atmospheric condition were carefully studied. Two main types of oxide scale, based on morphology and chemical composition were observed in the Gleeble simulated specimens. The type 1 oxide scale was composed of a discontinuous Al rich inner oxide layer, an intermediate oxide layer comprising of Cr and Ti, and a nickel-base outer layer (figure 4-19a). On the other hand, the second type of oxide scale, type 2, basically consisted of one layer of oxide phase, which was an Al-base oxide, as shown in figure 4-21.

The type 1 oxide scale was noticed on the surface of all the Gleeble simulated specimens and also on an IN 738 sample that was heated to 1230^{o}C in an ordinary laboratory furnace and held for 5 minutes in air (figure 4-19b). The type 2 oxide scale was solely observed on the surface of those Gleeble specimens in which significant melting occurred during rapid heating to peak temperatures. One of the several cases was at 1270^{o}C, where the application of compressive load resulted in squeezing out of liquid that re-solidified with a new dendritic structure, as shown in figure 4-20. The surface of the expelled liquid exposed to the atmosphere was subsequently oxidized to produce the type 2 oxide scale before the liquid became solidified.

In the present work, the type 1 oxide scale was not observed in the linear friction welded IN 738 with a forge pressure of P. Instead, the continuous Al-base oxide film that formed along the weld line was similar in morphology and composition to the type 2 oxide scale that was solely identified with liquation in the Gleeble-simulated specimens, suggesting that the oxides observed at the weld line of the linear friction welded IN 738 samples with a forge pressure of P and 2.5P formed by a liquid phase reaction. Figure 4-22 shows EDS spectra of the weld line oxide and the oxide which formed on the surface of liquid

Table 4-1: Chemical composition of continuous aluminium-rich oxide film on the weld line of IN 738 superalloy, determined by EPMA-WDS.

Element	Oxide Comp. Wt% (IN 738)
Cr	2.50
Co	0.31
Mo	0.09
W	0.22
Al	39.11
Ti	13.18
Zr	0.08
Hf	_
Re	_
Nb	0.93
O	42.27
Ta	1.78
Ni	2.43

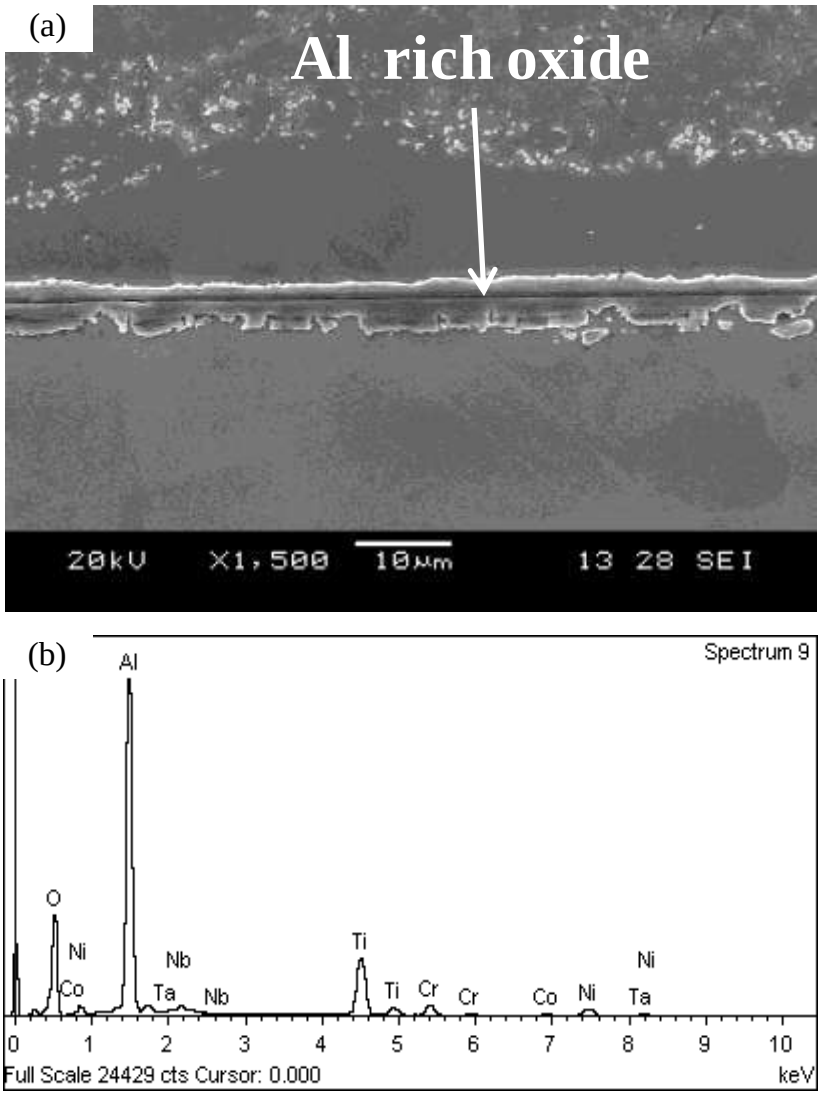

Figure 4-18: (a) SEM image and (b) EDS spectrum of Al-rich oxide on the weld line of IN 738 superalloy linear friction welded with forging pressure of P.

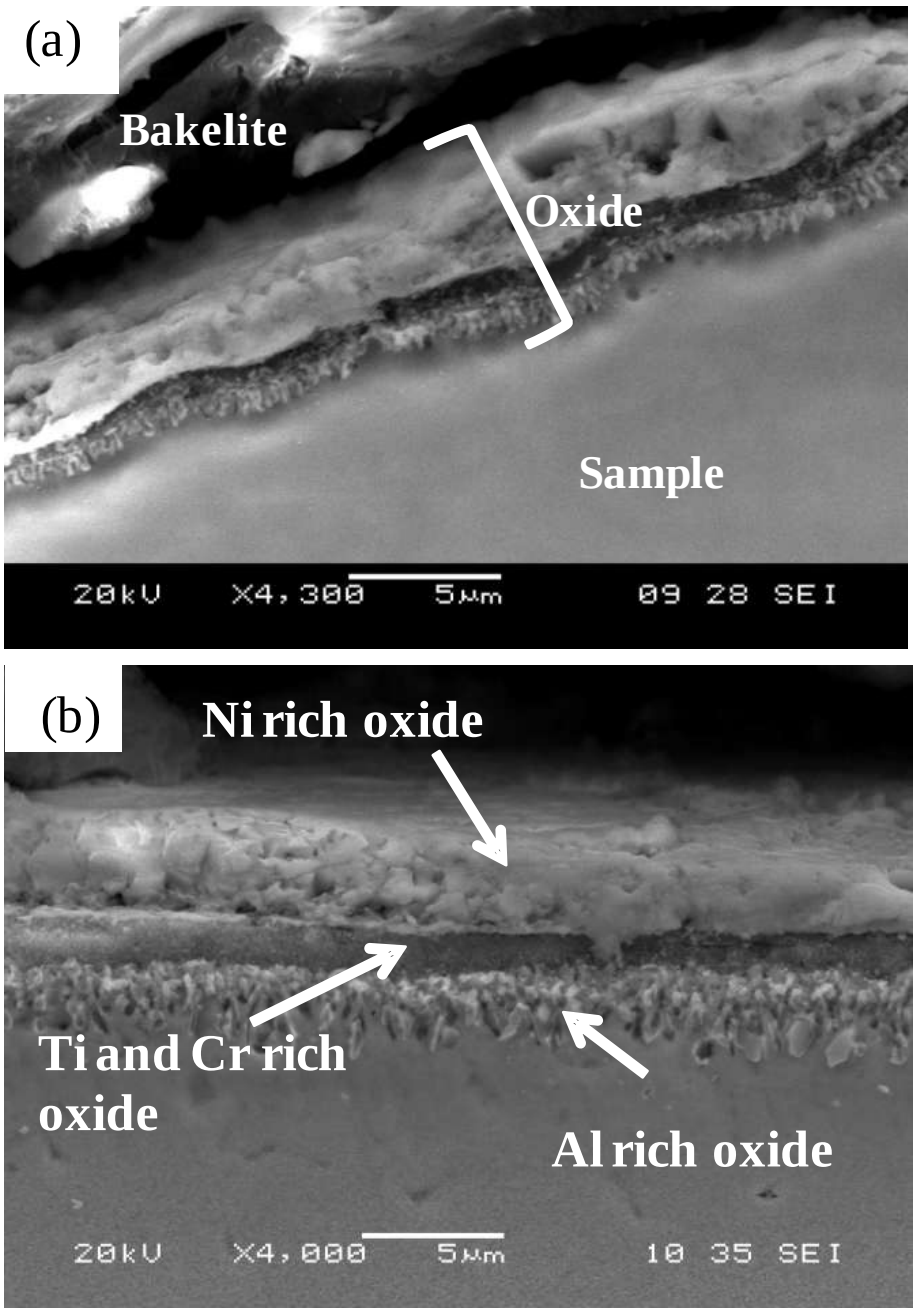

Figure 4-19: SEM micrographs showing the morphologies of oxide that formed on (a) Gleeble oxidized at 1230^{o}C for 2.5 seconds (a) IN 738 sample oxidized at 1230^{o}C in an ordinary laboratory furnace

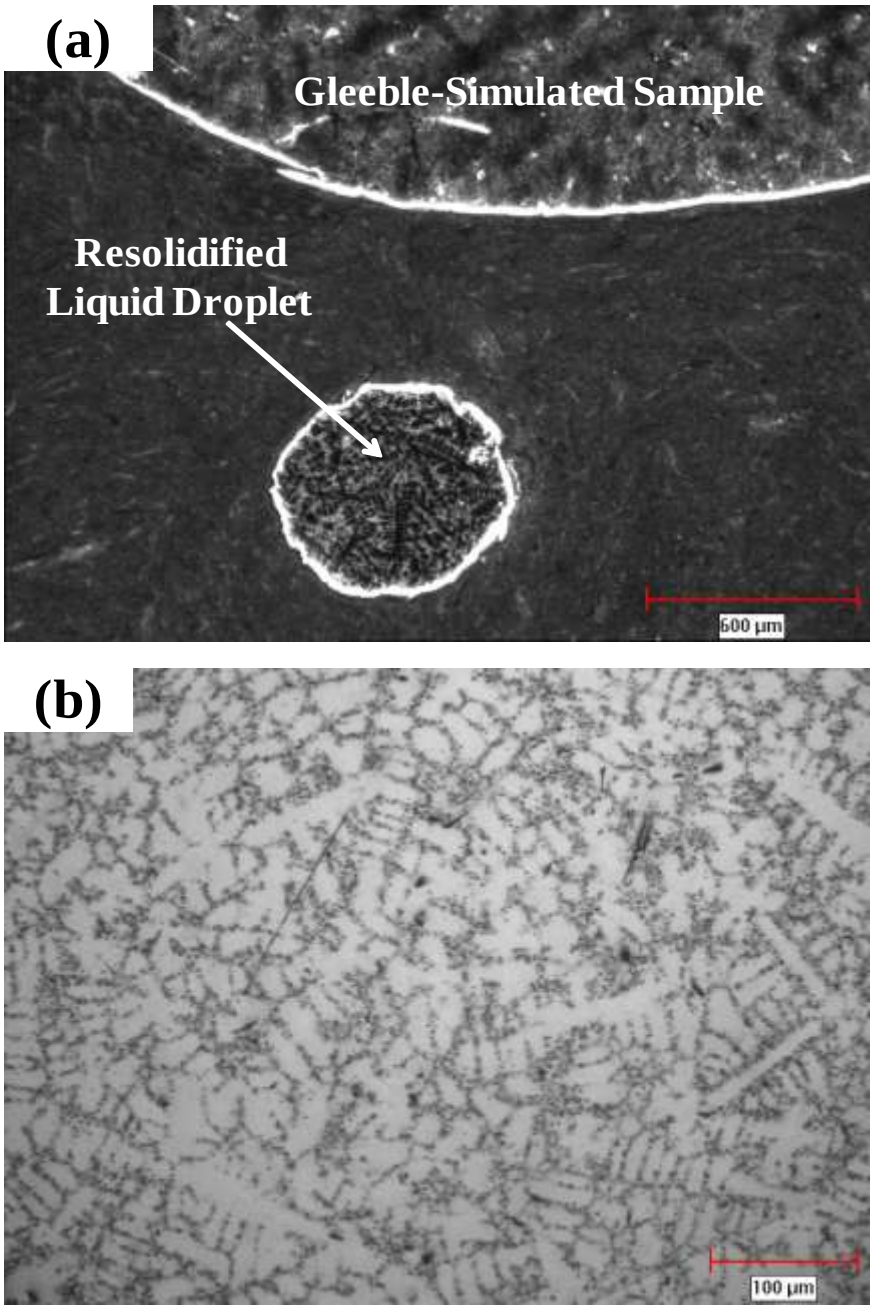

Figure 4-20: Optical micrographs of a Gleeble simulated specimen rapidly heated to 1270^{o}C and held for 2.5 seconds, with 20 pct strain at peak temperature showing (a) re-solidified expelled liquid droplet (b) new dendritic structure

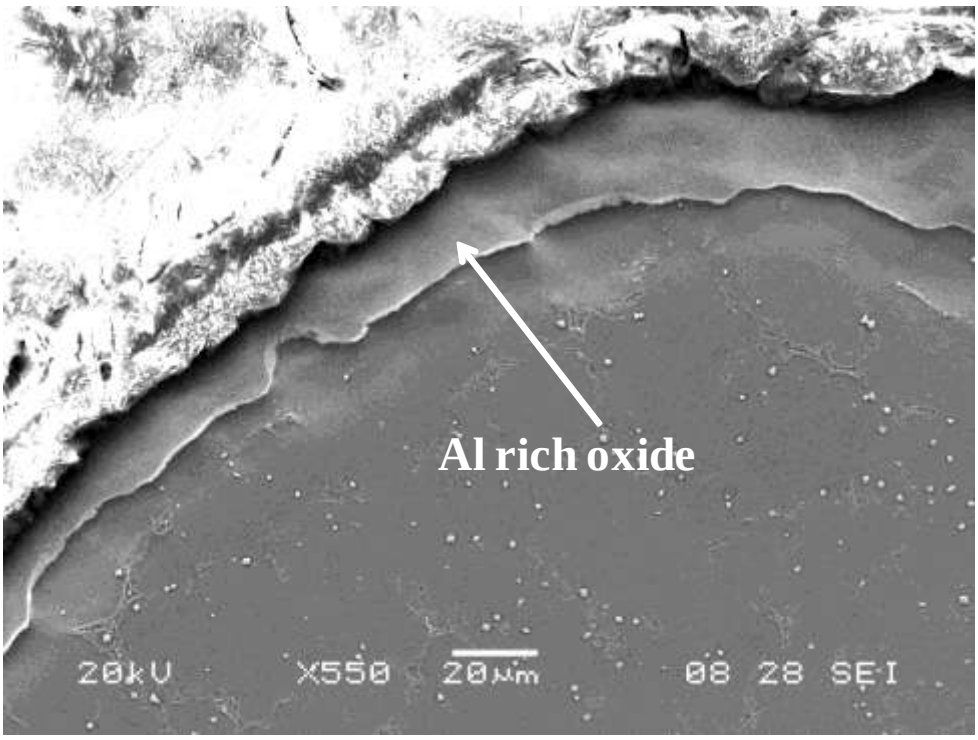

Figure 4-21: SEM micrograph showing Al rich oxide layer on liquid

droplet. As discussed earlier, liquation does occur during linear friction welding. Some of the liquid in contact with oxygen at the mating surfaces of the work pieces appeared to have reacted with oxygen to produce the continuous aluminium-rich oxide film along the weld line of the linear friction welded specimen. Formation of continuous oxide films during linear friction welding was reported to be detrimental to the mechanical properties of nickel base superalloys [5], [6]. As a consequence, the observed Al-rich continuous phase oxide along the weld line of the linear friction welded IN 738 superalloy could negatively affect the mechanical integrity of the weld joint. Any factor that can minimize or preclude the formation of continuous oxide films would improve the efficiency of using LFW for the joining of IN 738. A practically feasible method of eliminating liquid phase oxidation during linear friction welding is discussed next.

4.3.8 Elimination of Liquid Phase Oxidation during LFW

Microstructural developments during LFW of IN 738 is strongly dependent on the compressive stress that is normally applied during the terminal stage of the welding process. The imposed stress induces compressive strain in the weld joint such that the highest strain is experienced at regions closest to the weld line and decreases as the distance from the weld line increase. As seen in this work, re-solidification eutectic products that formed during cooling from the welding peak temperatures were confined to the TMAZ, which is situated beyond the WZ regions away from the weld line. As discussed earlier, the weld zone of the welded work pieces were essentially free from re-solidified eutectic products. This aberrant microstructural behaviour can be related to the strain-induced rapid solidification of liquid in the WZ during LFW. The liquid produced in the WZ during LFW can be rapidly solidified due to the high strain experienced in this

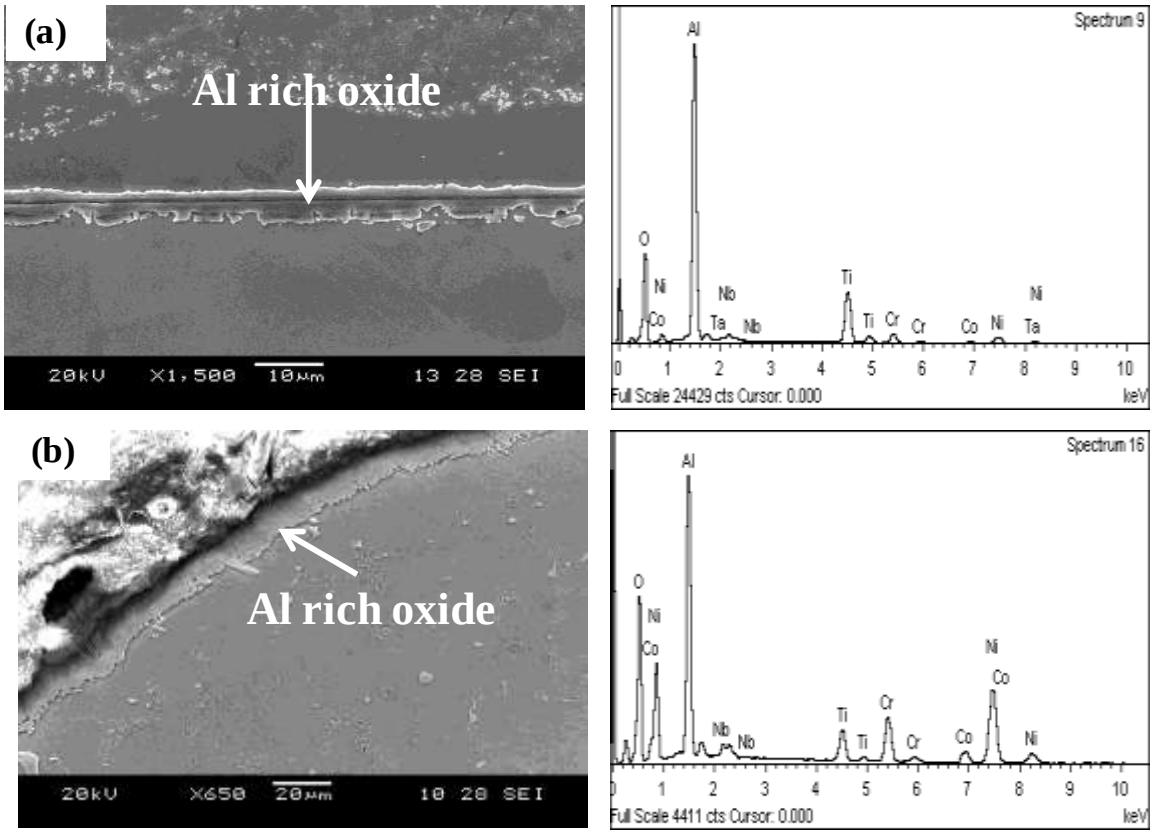

Figure 4-22: EDS semi-quantitative analysis of (a) oxides on the weld line of linear friction welded specimen (b) oxides on the liquefied droplet oxides in air

region during the forging stage, such that no residual liquid remains to be transformed into the eutectic products during cooling from the welding temperatures. Therefore, the TMAZ that experienced marginal compressive strain during forging contained the re-solidification eutectic products. SEM micrographs of weld lines of the linear friction welded IN 738 that were welded with forging pressures of 2.5P and 4P are presented in figures 4-23 (a) and (b), respectively. Increasing the forging pressure from P to 2.5P resulted in a significant reduction in oxidation, while the oxides were completely eliminated in the material welded with a forging pressure of 4P. The increased forging pressure produced an enhanced re-solidification of the liquid, which resulted in the welds that were free of oxides.

In addition, it has also been shown that increased pressure during linear friction welding will result in the reduction of the peak temperature. This implies that the amount of liquid that would have been produced in the linear friction welded specimen joined with a relatively higher pressure will be less compared to the amount of liquid that would have formed in the specimens that were linear friction welded with lower forge pressures. In essence, the combination of lower amount of liquid and increased driving force for re-solidification of liquid will be more favoured as the forging pressure is increased. Therefore, an important benefit of increasing forge pressure during LFW is reduction in the thick and continuous weld line oxide film produced by liquid phase oxidation, which can result in improved mechanical properties of linear friction welded materials.

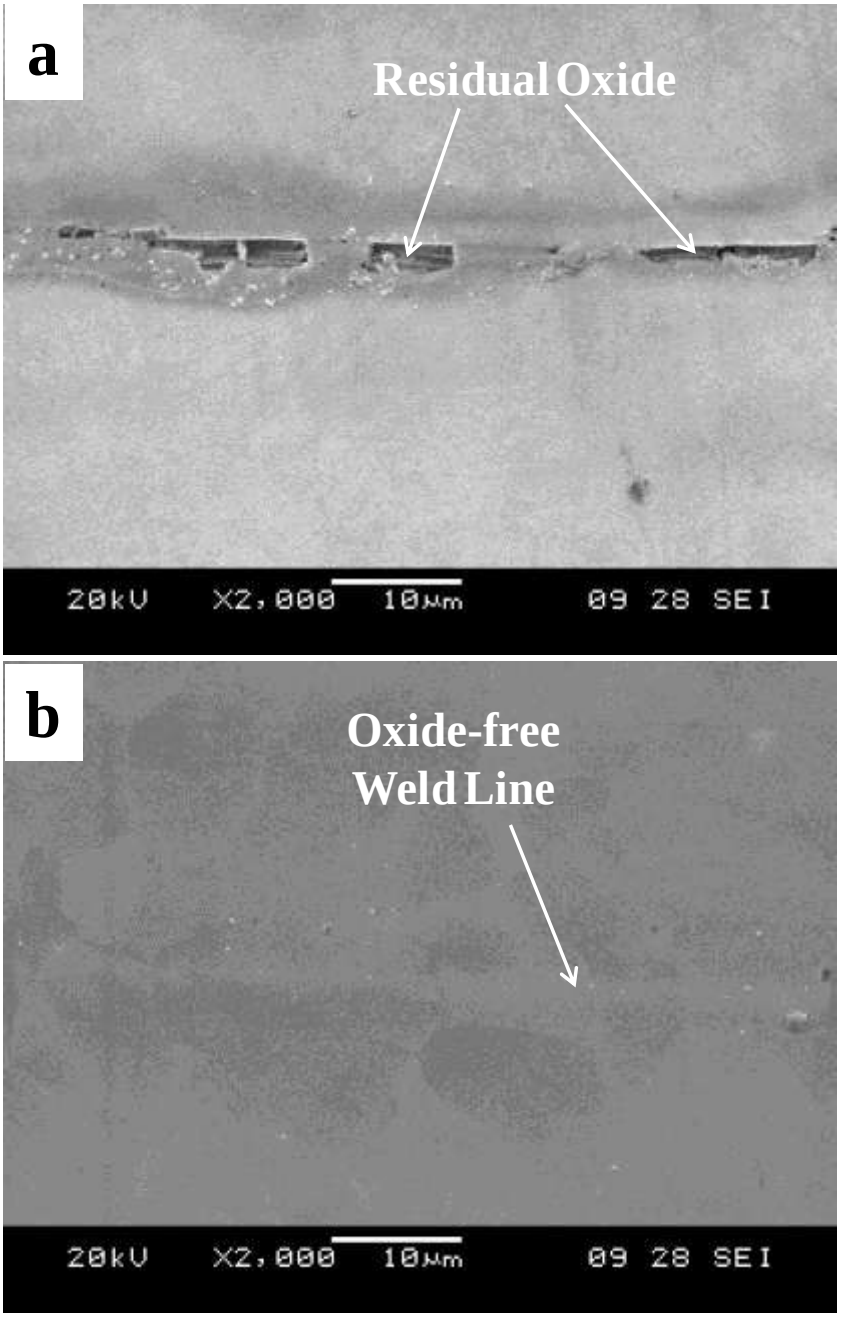

Figure 4-23: SEM micrographs of linear friction welded IN 738 materials, showing (a) residual oxide on the weld line of the material welded with 2.5 P (b) oxide-free weld line in the material welded with 4 P

CHAPTER 5

Summary and Conclusions

Microstructural analysis of linear friction welded IN 738 superalloy with varying forge pressures of P, 2.5P and 4P was carried out. The microstructural evolution of the linear friction welded specimens was greatly influenced by the forging pressure. Gleeble simulation was also performed to adequately understand the microstructural changes that occurred while varying the forge pressure during linear friction welding. The results of this research are summarized as follows:

1. Linear friction welding of IN 738, which is difficult to weld by conventional methods due to its high propensity to liquation cracking, produced sound joints free from cracks.
2. Due to the non-equilibrium eutectic type liquation reaction between γ' precipitate particles, which is the main strengthening phase of the alloy, and the γ matrix of the alloy, liquation occurred during linear friction welding of IN 738.
3. Deleterious re-solidified eutectic products were observed in the TMAZ of the linear friction welded specimens but not in the WZ regions, even though the temperature experienced in the WZ was higher than in the TMAZ region. This observation is related to the higher compressive strain induced in the WZ which assisted in the rapid solidification of liquid.
4. Increase in the forging pressure resulted in a reduction in the amount of harmful eutectics such that the microstructure of the LFWed specimen with a forge pressure of 4P was completely devoid of eutectics. This is attributed to the forging

pressure which aided in the rapid solidification of liquid. Gleeble simulation performed, further supported the finding that, compressive strain assisted the rapid solidification of liquid.

5. In the past, it was assumed LFW is a solid state joining process and liquation cracking did not occur, however, cracking associated with re-solidified products was observed, in the flash region that likely experienced tensile stress when the grain boundaries were liquated.
6. Continuously distributed Al rich oxides were observed on the weld line of the linear friction welded specimens with forging pressures of P and 2.5P. These oxides were ascertained to form by liquid phase reactions during linear friction welding. This suggests that the mode by which oxides are eliminated during linear friction welding is not solely by extrusion.
7. Increased forging pressure resulted in a significant reduction in the amount of oxides formed on the weld line such that the linear friction welded specimen with a forging pressure of 4P had no oxides on its weld line. This is attributed to a combination of;

   (i) lower amount of liquid due to the reduction in peak temperature

   (ii) increase in the imposed strain which aids rapid re-solidification of liquid that otherwise would have been exposed to atmosphere to form oxide along the weld line.
8. Linear friction welding of IN 738 superalloy with a forging pressure of 4P produced a desired microstructure free of deleterious eutectics, which could detrimentally affect the mechanical property of the alloy, and a sound joint devoid

completely of oxides which could affect the weld integrity of the LFWed specimen. Therefore, this information is indispensable and will be very useful in optimizing the forge pressure during linear friction welding of other nickel base superalloys with chemical composition similar to that of IN 738.

CHAPTER 6

Suggestions for Future Work

1. Mechanical testing should be performed on the welded as well as the parent material in order to determine the strength of the joint in relation to the parent material.
2. The effect of other process parameters, such as the frequency and amplitude on the microstructure of IN 738 during linear friction welding should be performed in order to evaluate the microstructural response of the alloy to the other process parameters.
3. Microstructure of the WZ, TMAZ and HAZ need to be examined by transmission electron microscopy to study the deformation lattice-defects, recrystallization process, and presence of very fine γ' particles.

References

[1] M. Prager and C. S. Shira, Weld. Res. Council Bull., 128, 1968, p.1.

[2] O. A. Ojo, N. L. Richards, and M. C. Chaturvedi, Metall. Mater. Trans. A, 2006, vol. 37A, p. 321.

[3] A. Ojo, N. L. Richards, and M. C. Chaturvedi, Mater. Sci. Technol., 2004, vol. 20, p. 1027.

[4] A. N. Davies, Exploiting Friction Welding in Production, The Welding Institute, Cambridge, United Kingdom, 1979, p. 20.

[5] M. Karadge, M. Preuss, P. J. Withers, and S. Bray, Mater. Sci. Eng. A, 491, 2008, p. 446.

[6] C. Mary and M. Jahazi, Adv. Eng. Mater. 10, 2008, p. 573.

[7] A. Vairis and M. Frost, Wear, vol. 217, 1998, p.117.

[8] O. T. Ola, O. A. Ojo. P. Wanjara, and M. C. Chaturvedi, Metall. and Mater. Trans. A., 42A, 2011, p. 3764.

[9] E. F. Bradley, Superalloys: A technical Guide, ASM International, Metals Park, OH, 1988.

[10] Alloy IN 738, A Technical Data, INCO, New York, 1-11.

[11] W. F. Smith, Structure and Properties of Engineering Alloys, 2nd Edition, New York: McGraw-Hill, c1993, p. 504.

[12] C. T. Sims, N. S. Stoloff, W. C. Hagel (Editors), Superalloys II, High Temperature Materials for Aerospace and Industrial Power, A Wiley-Interscience publication, 1987, p.104.

[13] J. M. Larson, Metallurgical Trans., Vol. 7A, 1976, p. 1497.

[14] D. S. Paul and S. J. Duvall, Trans. ASM, Vol. 62, 1969, p. 611.

[15] H. R. Zhang, O. A. Ojo, M. C. Chaturverdi, Scripta Mater., Vol. 58, 2008, p.167.

[16] D. A. Canonico, W. F. Savage, W. J. Werner, G. M. Goodwin, Welding Research Council, 1965, p. 68.

[17] J. W. Schultz, University of Michigan, Uni. Microfilms, Ann Arbor, PhD Thesis, 1965.

[18] O. A. Ojo, PhD Thesis, University of Manitoba, 2004.

[19] W. Hoffelner, E. Kny, R. Stickler, W. J. McCall, The Effect of Aging Treatment on the Microstructure of the Ni-base Superalloy IN 738, Z. Werkstofftech Vol. 10, 1979, p. 84.

[20] R. Sallemark, Progress Report 2 Cost 50 Programme Sweden, 1975.

[21] J. S. Zhang, Z. Q. Hu, Y. Murata, M. Morinaga, N. Yukawa, Metall. Mater. Trans., Vol. 24A, 1993, p. 2443.

[22] R. Rosenthal, D. R. F. West, Mater. Sci. Technol., Vol. 15, 1999, p. 1387.

[23] ESAB welding and cutting products, " A Full Line of Submerged Arc Flux and Wire for every Application, Industry and Environment".

[24] R. A. Lindberg, N. R. Braton, " Welding and Other Joining Processes", Allyn and Bacon, Inc., 1976.

[25] G. J. Davies, J. G. Garland, Int. Metall. Rev., Vol. 20, 1975, p. 83.

[26] D. C. G. Lees, J. Inst. Metals, Vol. 72, 1946, p.343.

[27] A. R. E. Singer, P. H. Jennings, J. Inst. Metals, Vol. 73, 1947, p. 273.

[28] M. J. Cieslak, Cracking Phenomena Associated with Welding, ASM Handbook: Welding Brazing and Soldering, Vol. 6, 1993, p.88.

[29] K. Nakata, F. Matsuda, Trans JWRI, Vol. 24, 1995, p.23.

[30] K. Easterling, "Introduction to the Physical Metallurgy of Welding", 2nd Edition, Copyright Butterworth-Heinemann, 1992.

[31] M.J. Cieslak, Cracking Phenomena Associated with Welding, ASM Handbook: Welding Brazing and Soldering, vol. 6, 1993, p.88.

[32] R. G. Baker, Philosophical Transactions of the Royal Society of London, Series A, Mathematical and Physical Sciences, Vol.1307, 1976, p. 207.

[33] M. C. Chaturvedi, Materials Science Forum, vols. 546-549, 2007, p. 1163.

[34] J. J. Pepe and W. F. Savage, Welding J., Vol. 46, 1967, p.411.

[35] W. A. Owczarski, D. S. Duvall and C. P. Sullivan, Weld. J., Vol. 46, 1967, p. 423s.

[36] B. Weiss, G. E. Grotke and R. Stickler, Weld. J., Vol. 49, 1970, p. 471s.

[37] J. A. Brooks, Weld. J., Vol. 53, 1974, p. 517.

[38] R. Nakkalil, N. L. Richards and M. C. Chaturvedi, Metall. Mater. Trans. A, Vol. 24A, 1993, p. 1169.

[39] B. Radhakrishnan and R. G. Thompson, Metall. Mater. Trans. A, Vol. 24A, 1993, p. 104.

[40] K. R. Vishwakarma, M. C. Chaturvedi, in E.A. Loria (Ed.), Superallloys 718, 625, 706 and Derivatives 2005, The Minerals, Metals and Materials Society, 2005, p.637.

[41] M. C. Chaturvedi, Materials Science Forum, vols. 546-549, 2007, p. 1163.

[42] O. A. Ojo, N. L. Richards, M. C. Chaturvedi, Mater. Sci. Technol. Vol. 20, 2004, p. 1027.

[43] O. A. Ojo, N. L. Richards, M. C. Chaturvedi, Metall. Mater. Transac. A, 37A, 2006, p.421.

[44] M. McLean, A. Strang, Metals Technol., Vol. 11, 1984, p. 454.

[45] E. D. Hondros, M. P. Seah, in R. W. Chan (Ed): Physical Metallurgy, 3rd edition, North Holland, Amsterdam, 1984.

[46] M. P. Seah, E. D. Hondros, Proc. R. Soc., Vol. 335A, 1973, p. 191.

[47] D. McLean, in Grain Boundaries in Metals, Clarendon Press, Oxford, 1957.

[48] J. H. Westbrook, K. T. Aust, Acta Metall., Vol. 11, 1963, p. 1115.

[49] K. T. Aust, R. E. Hanneman, P. Nissen, J. H. Westbrook, Acta Metall, Vol. 16, 1968, p. 291.

[50] R. L. Eadie, K. T. Aust, Scripta Metall., Vol. 4, 1970, p.461.

[51] K. T. Aust, Canadian Metallurgical Q., Vol. 13 (1), 1974, p. 133.

[52] D. C. Paine, G. C. Weatherly, K. T. Aust, J. Mater. Sci., Vol.21, 1986, p.5257.

[53] L. Karlson, H. Horden, Acta Metall. Vol. 36, 1988, p. 13.

[54] L. Karlson, Acta Metall. Vol. 36, 1988, p. 25.

[55] L. Karlson, H. Horden, Acta Metall. Vol. 36, 1988, p. 13.

[56] W. Chen, M. C. Chaturvedi, Metall. Mater. Trans. A. Vol. @9A, 1998, p. 743.

[57] J. A. Quimby, Friction Welding: Present-Past-Future, ASTME Creative Mfg Seminar, Technical paper No SP65-90, April 1965.

[58] V. I. Vill, Friction Welding of Metals, translated and published by the American Welding Society, 1962.

[59] M. J.Donachie and S. J. Donachie, Superalloys: A Technical Guide, 2nd Edition, ASM International, 2002, p. 31.

[60] D. E. Spindler, "Inertial Friction Welding", Manufacturing Technology, Inc., South Bend, IN 46628 USA, 1978.

[61] M. Preuss, J. W. L. Pang, P. J. Withers, G. J. Baxter, Metall. Mater. Trans. A, Vol. 33A, 2002, p. 3215.

[62] M. Soucail, A. Moal, L. Naze, E. Massoni, C. Levaillant, Y. Bienvenu, Superalloys 1992, The Minerals, Metals and Materials Society, 1992, p. 847.

[63] K. H. G. Schmitt-Thomas, R. Siede, The International Conference of Quality and Reliability in Welding, Hangshou, China, 1984, p.D-8-1.

[64] "Inertia Welding: Simple in Principle and Application", Welding and Metal Fabrication, Vol. 47(8), 1979, p.585.

[65] K. S. Moetensen, C. G. Jensen, L. C. Conrad, F. Losee, Welding Research Supplement, p.268-s.

[66] A. S. Bahrani, JOM-2 (Joining of Metals), Helsingor, Denmark, 15-18 Apr., 1984, p. 98.

[67] F. D. Duffin, A. S. Bahrani, Wear, Vol. 26, 1973, p.53.

[68] M. Cocks, J. Appl. Physics, Vol. 35, 1964, p. 1807.

[69] S. Sundaresan K. G. K. Murti, Materials Forum, Vol. 17, 1993, p. 301.

[70] K. G. K. Murti, S. Sundaresan, Metal Construction, 1993, p. 331.

[71] S. V. Lalam, G. M. Reddy, T. Mohandas, M. Kamaraj, B. S. Murty, Mater. Sci. Technol., Vol. 25(7), 2009, p.851.

[72] S. A. Saregin, A. S. Saregin, V. P. Sabantsev. Svar. Proiz, 1979, No. 11, p. 22

[73] I. O.Khansanov, N. I. Formin, Welding International, Vol. 6(11), 1992, p. 890.

[74] F. D. Duffin, A. S. Bahrani, Metal Construction, 1967, p.267.

[75] Y.-C. Kim, A. Fuji, Sci. and Technol. of Welding and Joining, Vol. 7(3), 2002, p. 149.

[76] H. H. Koo, W. A. Baeslack III, Materials Characterization, Vol. 28, 1992, p. 157

[77] A. Vairis, M. Frost, Mat. Sci. A 271, 1999, p. 477

[78] A. Vairis, M. Frost, Mater. Sci. Eng. A, Vol. 217, 1991, p. 27

[79] P. Wanjara, C. Booth-Morrison, E. Hsu, M. Jahazi, Proceedings of the 7th International Conference on Trends in Welding Research, Georgia USA, May 16-2-, 2005, p. 35

[80] M. Karadge, P. Frenkel, A. Steuwer, C. Lovell, S. Bray, P. J. Withers, M. Preuss, Joining of Advanced and Speciality Materials, Mater. Sci. and Technol. (MS&T) 2006: Product Manufacturing, p. 35.

[81] C. Mary, M. Jahazi, Advanced Engineering Materials, Vol. 10(6), 2008, p. 573.

[82] W. M. Thomas et al, International Patent Application Number PCT/GB92/02203 and GB Patent Application Number 9125978.8 (December 1991), U. S. Patent Number 5, 460,317.

[83] C. Dawes and W. Thomas, TWI Bulletin 6, 124, Nov./Dec. 1995.

[84] M. Ellis and M. Stragwood, TWI Bulletin 6, 138, Nov./Dec 1995.

[85] C. J. Dawes and W. M. Thomas, Welding Journal, 75 (30), 41, 1996.

[86] B. J. Drucap, W. J. Arbegast, Society of Automotive Engineers, Inc., Paper 1999-01-3432, 1999.

[87] W. J. Arbegast, Society of Automotive Engineers, Inc., Paper 1999-01-3432, 1999.

[88] W. J. Arbegast, P. J. Hartley, Proceedings of the 5th International Conference on Trends in Welding Research, Pine Mountain, GA, June 1-5, 1998, p. 541.

[89] W. M. Thomas and E. D. Nicholas, "Friction Stir Welding for the Transportation Industries", Materials and Design, Vol.18, 1997, p. 269.s

[90] E.D. Nicholas, The 6th International Conference of Aluminium Alloys, ICAA-6, July 5-10. 1998. Toyohashi, Japan.

[91] C. J. Dawes, Bulletin Vol. 41 No. 4, July/August, 2000, p.51.

[92] A. P. Reynolds, T. U. Seidel, M. Simmonsen, 1st symposium on Friction Stir Welding, 14-16 June 1999, Rockwell Science Centre, Thousand Oaks, California, USA.

[93] "Inertia Welding: Simple in Principle and Application", Welding and Metal Fabrication, Vol. 47(80, 1979, p. 585.

[94] A. N. Davies, "Friction Welding in Aerospace Manufacture", in : Exploiting Friction Welding in Production, written The Welding Institute, 1979,p.20.

[95] J. R. Doyle et al, Pratt and Whitney, AWS National Fall Meeting, 6-9 October 1969; also in Welding Journal, Vol. 48(11), 1969, p.514s.

[96] M. Ono, Y. Shinbo, A. Yoshitake, M. Ohmura, "Development of Laser-Arc Hybrid Welding", NKK Technical Review, No. 26, 2002.

[97] T. J. Ma, W. Y. Li, Q. Z. Xue, Y. Zhang, J. L. Li, and S. Q. Yang, Mater. Sci. Forum, 2008, Vols. 580-582, pp. 405-408.

[98] V. I. Vill, "Friction Welding of Metals", New York, American Welding Society, 1962.

[99] R. Maurya and J. Kauzlarich, “Bonding apparatus-friction welding by reciprocal motion”, Patent nos.US3420428-A, DE1552871-A, CA844858-A, 1969.

[100] O. T. Ola, “Microstructural Analysis of Linear Friction Welded Joint in Nickel-Base Inconel 738 Superalloy”, University of Manitoba, 2010.

[101] K. H. Song, T. Tsumara and K. Nakata., “Development of Microstructure and Mechanical Properties in Laser-FSW Hybrid Welded Inconel 600”, Materials Transactions, Vol. 50, no. 7, 2009, pp. 1832-1837.

[102] M. Militzer, W. P. Sun, J. J. Jonas, Acta Metall. Mater. 42, 1994, p. 133.

[103] K. Murty, K. Detemple, O. Kanert, J. Dehosson, Metall. Mater. Trans. A29, 1998, p. 153.

[104] E. W. Hart, Acta Metall. 5, 1957, p. 597.

[105] P. E. Armstrong, W. V. Green, O. D. Sherby, E. G. Zukas, Acta Metall. 21, 1973, p. 1319.

[106] N. E. B. Cowern, P. C. Zalm, P. Van der Sluis, D. J. Graventeijn, W. B. de Boer, Phys. Rev. Lett. Vol. 72, 1994, p.2585.

[107] O. T. Ola, O. A. Ojo. P. Wanjara, and M. C. Chaturvedi, Metall. and Mater. Trans. A, published online November 10, 2011.

[108] J.E. R. Ospina, M.Sc. Thesis, University of Manchester, UK, 2006.

[109] J. Romero, M. M. Atallah, M. Preuss, M. Karadge, S. E. Bray, Acta. Mat. Vol. 57, 2009, P. 5582.

[110] W. Y. Li, T. J. Ma, S. Q. Yang, Q. Z. Xu, Y. Zhand, J. L. Li, H. L. Liao, Materials Letters, Vol. 62, 2008, p. 293.

[111] E. D. Nicholas: 3rd International SAMPE Metals Conference, Oct. 1992, p. M450.

[112] P. Wanjara and M. Jahazi, Metal. and Mater. Trans. A. Vol. 36A, August 2005, p. 2149.

[113] A. Chamanfar, M. Jahazi, J. Gholipour, P. Wanjara and S. Yue, Metal. and Mater. Trans. A, Vol. 42A, March 2011, p. 729.

[114] H. Mehrer, "Diffusion in Solids", Berlin, Springer, 2007.

[115] S. Kuo, Welding Metallurgy, 2nd ed., Wiley & Sons Inc., Hoboken, 2003, p. 9.

[116] M. E. Nunn: 1st Int. Conf. on Innovation and Integration in Aero-space Sciences, Queen's University, Belfast, Northern Ireland, United Kingdom, 2005.

[117] O. T. Ola, O. A. Ojo, P. Wanjara and M. C. Chaturvedi, Philosophical Magazine Letters, 2011, Vol. 91, P.140-149.

[118] Y. Saito, N. Tsuji, H. Utsunomiya, T. Sakai, Acta Mater. Vol. 47, 1999, p. 579.

[119] A. Belyakov, T. Sakai, H. Miura, R. Kaibyshev, Scr. Mater., Vol. 42, 2000, p. 319.

[120] A. Belyakov, T. Sakai, H. Miura, Mater Sci. Eng., A Struct. Mater.: Prop. Microstruct. Process, Vols. 319-321, 2001, p. 867.

[121] N. Tsuji, Y. Ito, Y. Saito, Y. Minamino, Scr. Mater., Vol. 47, 2002, p. 893.

[122] R. Z. Valiev, R. K. Isalamgliev, I. V. Alexadrov, Prog. Mater. Scie, Vol. 45, 2000, p. 103.

[123] N. Tsuji, Y. Saito, S. H. Lee, Y. Minamino, Sci. Technol. Adv. Mater., Vol. 5, 2003, p.338.

[124] N. Tsuji, Y. Saito, H. Utsunomiya, S. Tanigawa, Scr. Mater. Vol. 40, 1999, p.795.

[125] D. H. Shin, R. Ueji, Y. Minamino, Y. Saito, Scr. Mater. Vol. 46, 2002, p. 305.

[126] R. Turner, J. –C. Gebelin, R. M. Ward, R. C. Reed, Acta Materialia, Vol. 59, 2011, p. 3792.

[127] S.-H. Song, X.-M. Chen, L.-Q. Weng, Mater. Sci. Eng. A., Vol. 528, 2011, p. 7196.

[128] I. Weiss, P. J. Alvaradot, G. Fitzsimons, A. J. DeArdo, Scripta Metallurgica, Vol. 17, 1983, p. 693.

[129] F. Daus, H. Y. Li, G. Baxter, S. Bray, P. Bowen, Mater. Sci. and Technol., Vol. 23, 2007, p. 1424.

[130] O. T. Ola, O. A. Ojo. P. Wanjara, and M. C. Chaturvedi, Philosophical Magazine Lettters, Vol. 91, 2011, p. 140.

[131] T. Watanabe and S. Karashima, Phys. Stat. Sol., vol. 42, 1970, p. 749.

[132] F. Ju, Z. Xa, B. J. Diak, O. A. Ojo, W.D. MacDonald, and M. Niewezas, Magnesium Science and Technology- Automotive Lightweighting, Detroit, MI, Apr., 2008, p.14.

[133] M. Soucail and Y. Bienvenu, Mater. Sci. Eng. A., vol. 220, 1996, p. 215.

[134] J. Cadek, M. Pahutova and P. Rys, Phys. Stat. Sol., vol. 36, 1969, p. 345.

[135] H. Kuscu, I. Becenen, M. Sahin, "Evaluation of temperature and properties at interface of AISI 1040 steels joined by friction welding", Assembly Automation, Vol. 28 Iss: 4, 2008, p.308.

[136] G. E. Cook, R. Crawford, D. E. Clark, A. M. Strauss, "Robotic friction stir welding", Industrial Robot: An International Journal, Vol. 31 Iss: 1, 2004, p.55.

[137] R. K. Sidhu, O. A. Ojo and M.C. Chaturvedi, Metal. and Mater. Trans. A, Vol. 38A, March 2007, p. 858.

[138] P. E. Armstrong, W. V. Green, O. D. Sherby, E. G. Zukas, Acta. Metall.. Vol. 21, 1973, 1319.

[139] A. K. Jena, M.C. Chaturvedi, in: Brendan M. Stewart (Ed), Phase transformation in Materials, Prentice-Hall Inc, 1992, p.91.

[140] K. K. Wang, Wen Lin, Weld J., Vol. 53, 1974, p.233s